Master Thesis

TU Delft
Delft University of Technology

Particulate COD Capture in an Aerobic Granular Sludge Bed

Shiyu Tang

Oct. 14th, 2020

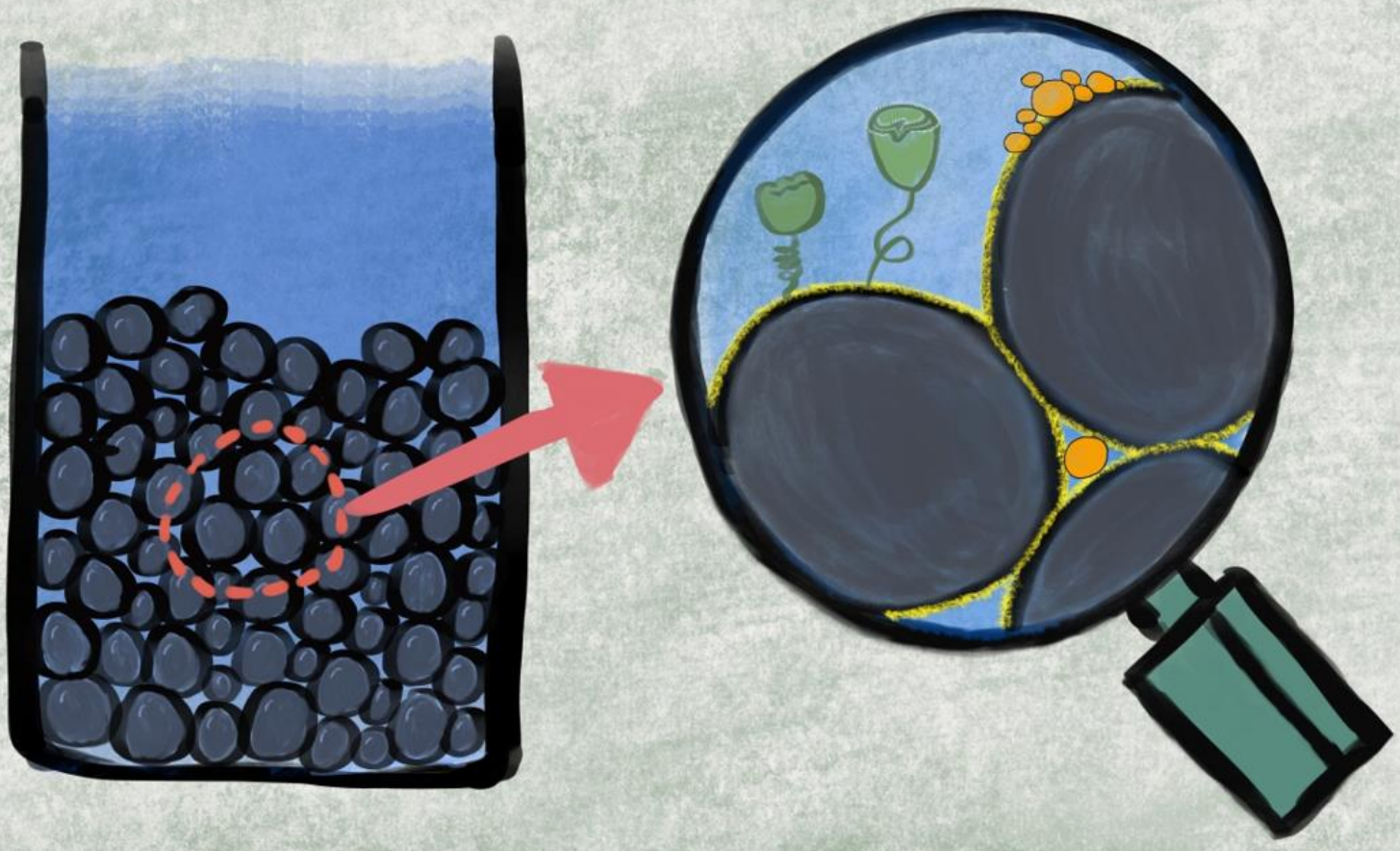

Particulate COD Capture in an Aerobic Granular Sludge Bed

A thesis submitted to Delft University of Technology in partial fulfillment of the requirements for the degree of

Master of Science in Civil Engineering
Track of Water Management

by

Shiyu Tang

14 October 2020

Assessment Committee:

TU Delft	Prof.dr. Merle de Kreuk (Chair)
TU Delft	Prof.dr. Timo Heimovaara
TU Delft	ir. Lenno van den Berg

Shiyu Tang: *Particulate COD Capture in an Aerobic Granular Sludge Bed (2020)*

The work in this thesis was made in the:

Department of Sanitary Engineering
Faculty of Civil Engineering and Geosciences
Delft University of Technology

Supervisors: Prof.dr. Merle de Kreuk
Prof.dr. Timo Heimovaara
ir. Lenno van den Berg

ABSTRACT

Aerobic granular sludge (AGS) is a revolution in the water treatment field, since it enables to simultaneously remove carbon, nitrogen, and phosphorus. Recently, the AGS studies mostly focus on the formation of granules, and the factors that influence the AGS morphology, like temperature and substrate type. In domestic wastewater, 85 % of total chemical oxygen demand (COD) are particulate COD (PCOD), which are likely to be mostly captured in anaerobic phase in AGS systems. These particles can have a negative impact on granules' morphology. However, there are few studies about the AGS performance on particle capture in anaerobic phase. Hence, the major research objective was to investigate to what extent can particles in the influent be captured by the AGS bed in the anaerobic feeding period.

There were three possible mechanisms attributing to particle capture in the anaerobic phase, which were filtering effect, adsorption, and protozoa consumption. The contribution of protozoa was investigated with a theoretical approach. Furthermore, A model was built up for studying the influence of particle transport mechanism on particle capture. A lab-scale plug-flow experiment in a column was conducted for investigation of AGS bed performance on particles in different size ranges, and the influence of duration on particle capture.

The result of the laboratory work found that the particle capture efficiency was 95 %, 84 %, and 23 % for particles in the range of 45-100 μm, 10-45 μm, and 0.45-10 μm, respectively. The 1-10 μm particles were hard to be captured. Besides, the particle capture efficiency was constant with the duration of 2 hours. Anaerobic feeding duration will have limited influence on particle capture without negatively affecting the phosphorus and nitrogen removal. Towards to the role of protozoa, they are unlikely to contribute to wastewater particle capture and removal in anaerobic period. Additionally, the AGS system in anaerobic phase can act as granular filtration system and the filtration model can be applicable in AGS research. Overall, anaerobic phase most likely contributes little on particle removal for whole AGS system.

ACKNOWLEDGEMENTS

The master journey in Delft University of technology is near to the end. This year to me is special and challenging. My work is like playing with the puzzle. Every piece of necessary puzzle is not only difficult to find out, but also hard to put it in the right position. In this process, I fell into the cycle between tackling with stress and regaining confidence. Now the whole figure is almost completed.

This work would not have been possible without the help from a lot of people. Firstly, I am deeply indebted to my thesis committee. Prof. Merle de Kreuk, who is the chair of the thesis committee, always encouraged me when I lost confidence and gave me helpful suggestions on experiment design and report improvement. Her energetic personality infects me all the time. Thanks to Prof. Timo Heimovaara, who is my enlightener in programming language. Although I am still not so good at modelling, he indeed inspired me a lot in improving my programming skills and thinking ability. I also want to express my sincere gratitude to my daily supervisor, Lenno van den Berg. In the back of one year, he taught me a lot in almost every aspect referring to scientific research, such as experiment design, thesis writing, critical thinking and so on and so forth. He was always patient to guide me on the right way, and he also showed me a real look of scientific research.

I am also grateful to my classmates and my friends. They cared me, inspired me and accompanied me, especially during the tough quarantine time. We had enjoyed unforgettable nice moments. The memories with you are a precious treasure in my life.

Finally, I would like to express my deepest gratitude to my parents, who respect every decision I have made, and always support me when I feel depressed. They stand behind me with their unconditional love, which enables me to become brave to encounter ups and downs in my life.

I would like to refer one sentence to summarize this extraordinary year. “Tough days do not last, but tough people do.”

CONTENTS

LIST OF FIGURES

LIST OF TABLES

NOMENCLATURE

Symbol	Property	Unit
A_c	Capture cross section area per grain	m^2
A_h	Capture cross section area per unit bed volume	m^2
A_{cell}	Cell surface area	m^2
A_p	Projected area	m^2
A_s	Grain surface area	m^2
Ar	Archimedes number	-
C	Particle volume concentration in effluent	m^3/m^3
C_0	Initial particle volume concentration	m^3/m^3
C_1	Constant defined in Eq. (B 2)	-
C_2	Constant defined in Eq. (B 3)	-
d	Particle diameter	m
d_r	reactor inner diameter	m
dT	Time step	h
D	Grain diameter	m
DEP	Summation of e_d for each time step.	-
e	Porosity	-
e_0	Clean bed porosity	-
e_{dep}	Porosity taken up by deposited particles at this time step	-
g	Gravitational constant	m/s^2
ΔG^{01}	Gibbs free energy at standard conditions (1 M concentration of the reactants, 25 °C, pH 7)	kJ/mol
ΔG^0	Standard Gibbs free energy	kJ/mol
h	Layer height	m
h_b	Bed height	m
h_o	Outlet height	m
H	Bed height	m
ΔH	Headloss	m
K_F	Correction factor for the increased roughness caused by deposited particles	-
K_M	Correction factor for the shrinkage of the capture cross section at high shear stress	-
K_D	Diffusion coefficient	-
K_B	Boltzmann constant	J/K
N	Number of grains per unit area and depth h	-
p	Pressure	Pa

Q_c	Flow from which particles will be captured per unit area and depth h	m^3/h
R	Gas constant	$J \cdot K^{-1} \cdot mol^{-1}$
R’	Surface shear stress	N/m^2
Re	Reynolds number	-
R_{emf}	Reynolds number at minimum fluidization velocity	-
S	Specific area of grains	m^{-1}
Sc	Schmidt number	-
Sh	Sherwood number	-
t_f	Fluidization time	h
T	Temperature	K
u_y	Fluid velocity at a distance of y from the grain surface	m/h
v	Filtration velocity	m/h
v_s	Settling velocity	m/h
v_c	Calculated cell superficial velocity	m/h
v_{c_avg}	Calculated layer superficial velocity or average cell superficial velocity per layer	m/h
v_{cm}	Calibrated cell superficial velocity	m/h
v_f	minimum fluidization velocity	m/h
V_{tp}	Total volume of grains per unit area and depth h	m^3
V_p	Volume of a grain	m^3
V_{dp}	Volume of deposited particles	m^3
V_{cell}	Volume of a cell	m^3
V_f	Tap water volume used for fluidization	m^3
V_{in}	influent volume in the reactor	m^3
y	Distance from a grain surface	m
α	Angle of repose	°
ε_{mf}	Voidage at minimum fluidization	-
η	Coefficient of proton in the reaction	–
μ	Viscosity	Pa·s
ρ_{inorg}	Inorganic particle density	kg/m^3
ρ_L	Fluid density	kg/m^3
ρ_{org}	Organic particle density	kg/m^3
ρ_s	Solid (particle) density	kg/m^3
Φ	Sphericity	-

1 INTRODUCTION

1.1 BACKGROUND

Aerobic granular sludge (AGS) is a revolution in wastewater treatment which has been actively studied in recent years. The aerobic granules are aggregates of microbial origin with good settleability (De Kreuk, McSwain, et al., 2005). They are compact without the usage of carrier material and the minimum size of granules is set to be 0.2 mm (De Kreuk et al., 2007). The structure of aerobic granules is divided into layers which are the aerobic outer layer and the anoxic or anaerobic inner layer (Tay et al., 2002). This layered structure benefits different microorganisms coexisting in the granules like heterotrophs, nitrifiers, denitrifiers and polyphosphate-accumulating organisms (PAOs) (Gieseke et al., 2001; Pronk, Abbas, Al-Zuhairy, et al., 2015; Winkler et al., 2012). It gives rise to the simultaneously removal of COD, nitrogen, and phosphorus (De Kreuk, Heijnen, et al., 2005).

Recently, a lot of studies into AGS have been carried out. Initially, the granulation of AGS was achieved successfully in lab-scale sequencing batch reactors (SBR) with domestic sewage or synthetic wastewater (Beun et al., 1999; De Kreuk & van Loosdrecht, 2006). The SBR is operated in cycles including anaerobic feeding, aeration, settling, and discharge (De Kreuk & van Loosdrecht, 2006). Then, the AGS technology (Nereda® technology) was first applied to the industrial field and then further developed for domestic sewage treatment (Pronk, De Kreuk, et al., 2015). Besides, some research has been performed to investigate the effects of temperature (De Kreuk, Pronk, et al., 2005), oxygen concentration (Mosquera-Corral et al., 2005), and substrate (Pronk, Abbas, Al-Zuhairy, et al., 2015) on the formation or performance of AGS.

The substrate in wastewater can be characterized as dissolved readily biodegradable substrate and particulate slowly biodegradable substrate. The latter is hard to be treated by the compact-structure AGS due to its slow hydrolysis rate and particle size restriction (Beun et al., 1999; De Kreuk et al., 2010). These particulate substances should be hydrolyzed by the extracellular enzymes to soluble substrate before entering the aerobic granules (De Kreuk et al., 2010; Wang et al., 2014). In addition, the major fraction of COD in domestic wastewater is in particulate form which typically makes up around 85% of the total COD (Boltz & La Motta, 2007). Some studies relevant with AGS focused on the particulate substances, but they mostly paid attention to the influence of particulate substances on the performance and morphology of granules (De Kreuk et al., 2010; Wagner et al., 2015), and treated

effluent quality (Schwarzenbeck et al., 2004). In the research of De Kreuk et al. (2010) and Pronk, Abbas, Al-Zuhairy, et al. (2015), the influent composed of particulate substrate led to finger type structures. This structure occurs if there are substrate gradients near the granule surface. The substrate gradient means that the substrate concentration close to the granule surface is lower than the bulk liquid substrate concentration. The captured particulate substrate needs to be fermented in the anaerobic period or hydrolyzed in the aerobic period to easily biodegradable substances before feeding microorganisms. However, the anaerobic period is short for fermentation and the hydrolysis rate of these substrate is low (De Kreuk et al., 2010), leading to a substrate gradient on the granule surface in the aerobic period. The fast-growing microorganisms grow out of the granule surface towards the high substrate concentration, resulting in the finger type structure. The slow-growing microorganisms start to die off due to a lack of food. Therefore, particle capture on granules in feeding or anaerobic period is important for later operation in AGS system.

Nevertheless, there are only a few studies about particulate COD capture performance in anaerobic phase of AGS systems. Among the whole cycle in AGS systems, the particulate COD is removed by adsorption and protozoa consumption (De Kreuk et al., 2010; Pronk, De Kreuk, et al., 2015). Since the AGS bed looks like the granular filtration bed in anaerobic period, the particle capture mechanism in the granular filtration bed can also be similar to that happens in AGS bed during anaerobic phase. Particles should be transported to the granules before being captured (Jegatheesan & Vigneswaran, 2005). This process is controlled by different transport mechanisms, which is introduced in Paragraph 2.2. As shown in Figure 1.1, after particles are contacted with or closed to granule surfaces by the transport mechanism, three mechanisms can happen to capture or consume these particles. The particles can be captured by the filtering effect (Paragraph 2.3). Besides, the particles can be adsorbed by extracellular polymetric substances (EPS). The EPS adsorption can be one of attachment mechanisms, which is described in Paragraph 2.4. Additionally, the particles can be consumed by protozoa on granule surfaces (Paragraph 2.5). Therefore, the filtering effect, adsorption, and protozoa consumption can be particle capture mechanisms in anaerobic phase of AGS systems.

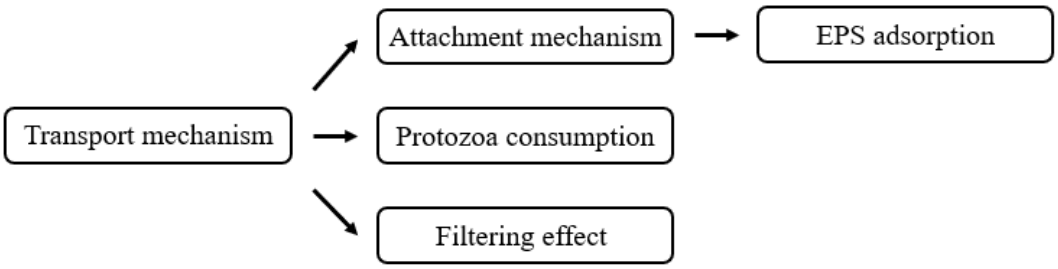

Figure 1.1: Particle capture process

1.2 KNOWLEDGE GAPS AND RESEARCH OBJECTIVE

According to the state of art illustrated in Paragraph 1.1, there are several knowledge gaps to be investigated:

1. AGS performance in anaerobic period in terms of particle capture of different size wastewater particles is unknown.
2. The wastewater particle capture mechanisms in anaerobic period are unknown.
3. The contribution of different particle capture mechanisms on overall particle capture in anaerobic period is unknown.
4. The influence of operation conditions on particle capture in anaerobic period is unknown.

Based on the stated knowledge gaps, the major research objective was to investigate to what extent can particles in the influent be captured by the AGS bed in the anaerobic feeding period.

1.3 RESEARCH QUESTIONS AND APPROACH

The following four research questions are formulated for meeting the main research objective stated in Paragraph 1.2.

1. What is the capture efficiency of particulate COD in different size ranges of wastewater particles?
2. Does the duration of the anaerobic feeding period influence the capture efficiency of small, medium and large wastewater particles?
3. Are the contributions of protozoa, the filtering effect, and adsorption significant for the capture of small, medium and large wastewater particles?
4. Can the performance of wastewater particle capture in aerobic granular sludge beds be described by granular filtration models?

The approach were applied to answer the research questions, which were literature review, theoretical research, laboratory research and model research.

Literature Review:

The literature review is presented in Paragraph 2. This was carried out for the understanding of particle capture process on AGS system and for the investigation of possible mechanisms (filtering effect, adsorption, and protozoa consumption) on particle capture in anaerobic phase.

Theoretical Research:

To investigate the contribution of protozoa on particle removal in anaerobic phase, the theoretical research was conducted. This theoretical research included the general introduction of protozoa, and the relation between protozoa and AGS systems (Paragraph 2.5.1 and 2.5.2). Additionally, the metabolisms of protozoans are also introduced in Paragraph 2.5.3. The procedure to estimate the potential contribution of protozoa to particle capture are presented in Paragraph 4.1. Lastly, the discussion for protozoa contribution are stated in Paragraph 5.1. The research question 3 could be partly answered after completing the theoretical research.

Laboratory Research:

It was expected that the research question 1 and 2 can be determined by the laboratory research. The core method for the laboratory research was the mass balance over the reactor during the anaerobic feeding period. The experimental set-up as well as the detailed experimental methods and materials are given in Paragraph 3.2.

To investigate the amount of COD released from aerobic granules, the plug-flow experiment was firstly carried out with tap water. After that, to achieve the research question 1, the plug-flow experiment was performed with domestic wastewater. Regarding to the research question 2, the plug-flow experiment was conducted with long feeding period (2 h) to study the influence of anaerobic duration. The particles in the domestic wastewater was classified into three size fractions. The particle capture efficiency for each fraction was analyzed based on the experimental data.

The results and discussions for the laboratory research are presented in Paragraph 4.2, 5.2 and 5.3, respectively.

Model Research:

To study the contribution of the transport mechanism on different size particles, the granular filtration model was built up. The detailed methods for the model are described in Paragraph 3.3. The model results are presented in Paragraph 4.3. The comparison of granular filtration beds and AGS systems, and the use of granular

filtration model in AGS systems are discussed in Paragraph 5.4 and 5.5, respectively. The research question 3 could be partly answered, the research question 4 could be answered by the model research.

2 LITERATURE REVIEW

2.1 GRANULAR FILTRATION

Generally, filtration is a particle removal process (Tien & Ramarao, 2011; Zamani & Maini, 2009). The granular filtration is typically applied in the water treatment field, in which water flows through granular filter media (sand, anthracite etc.) (Emelko et al., 2005). According to Ciuk Karlsson (2015), granular filtration is a combination of physical, chemical and biological process. Suspended solids can be retained on the grains through physical filtration (Hijnen et al., 2004; Tang et al., 2006). The chemical process or chemical transformation is relevant with the oxidation of iron, manganese, and ammonium etc. The presence of nutrients in the influent water stimulates the growth of microorganisms. These microorganisms generate EPS, leading to the formation of biofilm on the grain surfaces (Katznelson, 1989; Uhlinger & White, 1983). The biofilm at the surface of filtration bed is called mat or Schmutzdecke (Adin, 2003; Logsdon et al., 2002). As mentioned in Paragraph 2.4, EPS are capable of capturing organic matters. Furthermore, EPS can also change surface properties of granular filters, resulting in the changes of filtration performance. When it comes to type of granular filtration, it can be classified into slow sand filtration with filtration rate of less than 0.4 m/h, and rapid sand filtration with 5 to 25 m/h filtration rate (Au, 2005). There are various granular filter designs such as down-flow filter, up-flow filter, multi-layer filter and horizontal flow sand filter (Abdel-Shafy et al., 2014).

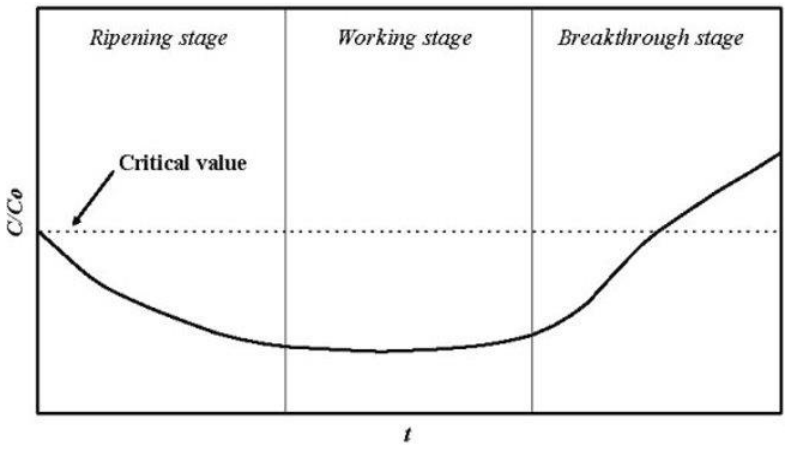

Figure 2.1: Typical curve showing filter performance over different filtration stages (Keir et al., 2009). C: effluent concentration; C_0: influent concentration

As displayed in Figure 2.1, the filtration process is divided into three stages, which are the ripening stage, the effective filtration stage (working stage), and the

breakthrough stage (Ginn Jr et al., 1992; Keir et al., 2009). In the beginning of the ripening stage, the filter in the granular filtration bed is clean. So the suspended solids in the influent directly deposit on the granular filters. The deposited particles can be regarded as collectors to capture other suspended solids in the influent. The filter efficiency or particle deposition increases due to the increasing surface area. In the effective filtration stage, the interstitial flow velocity rises, which is ascribed to the decreasing porosity. The high interstitial flow velocity has a negative effect on attachment and a positive effect on detachment of deposited particles. This does not result in bad filtration performance since the detached particles are removed by the grains in next layers. As time going on, some pores get clogged, resulting in even higher interstitial flow velocity in the open pores. This leads to the breakthrough stage, in which detachment keeps rising and attachment keeps decreasing. After that, preferential passages called wormholes start to form, which causes a remarkable increase in particle detachment and decrease in particle attachment. When the preferential route (wormholes) dominates the whole filtration bed, there is no attachment and detachment process, resulting from the exhaustion of filtration bed. In this case, the effluent particle concentration is the same as influent particle concentration, indicating the bad performance of granular filtration bed. Backwash needs to be applied for cleaning the bed.

As compared to the AGS system, the aerobic granules settle in the reactor in anaerobic phase, which is similar to the granular media in a granular filtration bed. The filtration bed is composed of inorganic grains like sands, and the aerobic granular sludge consist of the aggregates of microorganisms (De Kreuk et al., 2007). However, microorganisms also grow on the surface of sand grains and generate biofilms, resulting in the formation of EPS. As presented in Paragraph 2.4, aerobic granules are made of EPS. Similar to the function of EPS on aerobic granules, EPS in the biofilm have abilities to adsorb organic particles (Boltz & La Motta, 2007), leading to the same particle capture mechanism. The influent feeding direction in the granular filtration bed can be up-flow (Abdel-Shafy et al., 2014), which is the same as that in the AGS systems. Since the protozoa are retained in the granular filtration bed and the presence of nutrients in the influent (Hijnen et al., 2004), protozoa can potentially consume particles in the influent. Hence, AGS systems are very similar to granular filtration bed. The main differences are the filter media, operation processes, and EPS and protozoa distribution, which is discussed in Paragraph 5.4.

2.2 TRANSPORT MECHANISM

Particle removal by granular filtration beds consist of transport, attachment, and detachment process (Emelko et al., 2005). The transport mechanism enables influent particles to move across the streamlines and be close to the grain surface. Without the transport mechanism, many particles follow streamlines and flow out of the filtration bed. Transport mechanisms include straining, interception, inertia, sedimentation, diffusion and hydrodynamic action. The introduction of transport mechanisms is based on Jegatheesan and Vigneswaran (2005) and Keir et al. (2009).

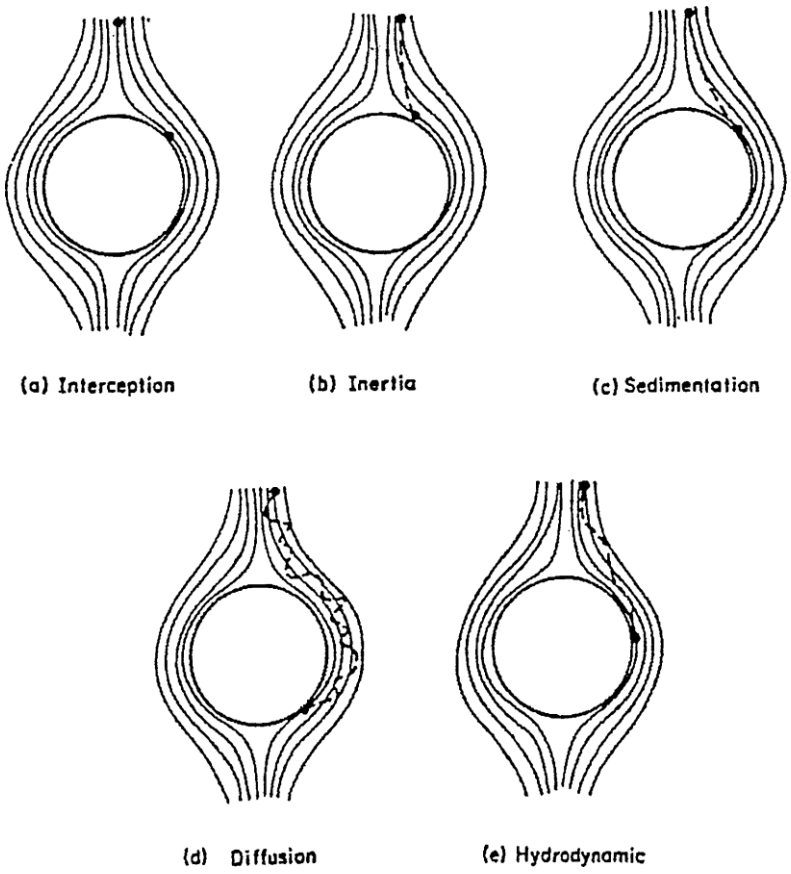

Figure 2.2: Transport mechanisms (Ives, 1970)

Interception

When the streamline leads particles close to the grains within the distance of particles' radius, these particles are captured by grains. This process is termed interception (Figure 2.2 (a)).

Inertia

As shown in Figure 2.2 (b), the streamline is straight before approaching the grains. To pass the grain, the streamline of influent flow must change direction and pass around the grain. In this case, if the inertia of the particle is big enough, it keeps the

trajectory of the previous streamline, leading to the collision between the grain and the particle.

Sedimentation

When the particle density is greater than water density, the particle will settle down following the direction of gravity (Figure 2.2 (c)). The degree of gravity effects for deviating the particle from streamlines depends on the relative orientation. The relative orientation is the difference between the streamline velocity vector and the gravitational velocity vector.

Diffusion

For particles less than 1 μm, the Brownian motion or random movement is observed (Figure 2.2 (d)), attributing to the thermal vibrations of water molecules. This process is called Brownian diffusion. The influence increases with decreasing particle size. For particle size larger than 1 μm, the Brownian diffusion is limited by fluid forces.

2.3 FILTERING EFFECT

After particles are transported to granule surfaces, some of these particles can be attached on granules by attachment mechanisms like EPS adsorption or consumed by protozoa. For the particles without being adsorbed or consumed, they just stay on granule surfaces. This particle capture way is termed as the filtering effect. The particles captured by the filtering effect loosely contact with granule surfaces.

2.4 ADSORPTION

In anaerobic phase, the domestic wastewater particles can be captured by adsorption to aerobic granules' surfaces through the presence of extracellular polymeric substances (EPS). According to Staudt et al. (2004) and Dong et al. (2017), the microorganism generate EPS to keep the microbial aggregate together. The EPS structure is diverse due to different environments (Nouha et al., 2018). EPS are made of complex high-molecular-weight mixture of polymers such as exopolysaccharides (PS), extracellular proteins (PN), humic acid and extracellular DNA (Dong et al., 2017; Sheng et al., 2010). The main components in EPS are PS and PN (Guo et al., 2012; Jorand et al., 1998). EPS divides into bound EPS, which is tightly bound with cells, and soluble EPS, which is dissolved in the liquid or loosely bound with cells (Nielsen & Jahn, 1999; Sheng et al., 2010). The flocs, biofilm, and granular sludge are mainly composed of EPS (Zhu et al., 2012). Additionally, there are abundant functional groups and binding sites in EPS, leading to the effective adsorption

ability on treating various wastewater (Liu et al., 2001). In the research of Boltz and La Motta (2007), EPS participated in the organic particle removal at the biofilm surface. Thus, EPS can adsorb particles in the domestic wastewater in the anaerobic phase of AGS systems.

Nouha et al. (2018) and Wang et al. (2012) reported that the particle adsorption by EPS was due to the surface interaction and the bridging effect (electrostatic interaction).

The surface interaction involves hydrophobic interaction and hydrophilic interaction, in which the interaction property is determined by EPS composition. According to Wang et al. (2012) and Zhu et al. (2012), the area composed of PS-based EPS is hydrophilic, which contains hydrophilic functional groups like carboxyl. The area of PN-based EPS is hydrophobic, which is formed by hydrophobic amino acids. In the research of Sheng et al. (2010), the co-existence of hydrophobic and hydrophilic functional groups in EPS shows amphoteric characteristic of EPS. In aerobic granular sludge, there is a controversy on the role of PN and PS. Some studies reported that the content of PS in EPS played an important role on the formation and stability of granules (Liu & Tay, 2002; Seviour et al., 2009; Tay et al., 2001). Others showed that the higher proportion of PN content in EPS not only contributed to the integrity of granules, but also increased the surface hydrophobicity (Xiong & Liu, 2013; L. Yan et al., 2019; Zhu et al., 2012). The hydrophobicity has benefits for organic pollutants' adsorption (Flemming et al., 2000; Späth et al., 1998).

The other mechanism belonging to adsorption is the bridge effect or electrostatic interaction. This is relevant with the charge interaction between EPS and adsorbent. There are negatively charged functional groups in EPS like carboxyl in PS and amino acids in PN (Wang et al., 2012). The charge of amino acids can be negative or positive, depending on their specific structure (Dignac et al., 1998; Sheng et al., 2010; Zhu et al., 2012). The charge and the zeta potential in EPS is generally negative (Esparza-Soto & Westerhoff, 2003; Liu & Fang, 2003; Subramanian et al., 2010; Wang et al., 2014), mainly due to the ionization of functional groups like carboxyl and phosphate in EPS (Liao et al., 2001; Liu & Fang, 2002). According to Lee and Richards (1971) and Wang et al. (2012), the charged functional groups in the protein influenced the protein structure, instead of affecting the electrostatic interaction between organic matters and EPS. The negative charges or the zeta potential of EPS highly depends on the solution pH (Sheng et al., 2008). At pH 3, EPS is positively charged, and the negative charge of EPS increase with increasing pH until reaching a relatively stable zeta potential at pH 9 (Ren et al., 2018; Z. Yan et al., 2019). The changes in charge and zeta potential in EPS with rising pH is relevant with the deprotonation of functional groups (hydroxyl, carboxyl, amino)

(Lin et al., 2016; Sheng et al., 2008). The negatively charged EPS can adsorb organic pollutants with positive charges (Esparza-Soto & Westerhoff, 2003). The negatively charged organic pollutants are repelled by the negatively charged EPS (Carlson & Silverstein, 1998; Mosquera-Corral et al., 2003). The repelling phenomenon can be mediated by the participation of polyvalent cations like Mg^{2+} and Ca^{2+} (Boltz & La Motta, 2007).

2.5 PROTOZOA CONSUMPTION

2.5.1 PROTOZOA CLASSIFICATION

2.5.1.1 BIOLOGICAL CLASSIFICATION

The protozoa are non-filamentous heterotrophic protists, which are single-cell eukaryotes with a membrane-bound nucleus (Bertrand et al., 2015; Britannica, 2019; Panno, 2014). They are represented by four major groups, which are Mastigophora (flagellates), Ciliophora (ciliates), Sarcodina (amebae) and Sporozoa. This classification is based on Britannica (2019) and Nielsen et al. (2017).

Mastigophora

The flagellated protozoa possess whip-like flagella used for moving and preying. Some flagellated protozoa can grow stalks, which enable them to attach to substrates. The protozoa with stalks are sessile protozoa, which cannot move as freely as the free-living protozoa. Although the sessile flagellates cannot move, the activities of flagella create water currents, which helps to bring food to these sessile flagellates (Ryan et al., 2019; Sleigh, 1964).

Ciliophora

Similar to flagellates, the ciliated protozoa have cilia for motions. The hair-like cilia cover around the body of the cells. In some species, the cilia around their ‘mouths’ is well-developed, but the cilia in other parts of the body is gone. Some ciliated protozoa can also develop a stalk, attaching to substrates. There are certain species lose all their cilia in adult stage and then develop stalks. After that, they cannot move around, to prevent overcrowded, they give birth to motile young generation. Then, their offspring can settle to other places before growing stalks.

Sarcodina

This kind of protozoa move with pseudopods. A pseudopod is a temporary foot-like structure extended during movements. The extension happens in the eukaryotic cell membrane. The Sarcodina are classified according to the type of pseudopods.

Sporozoa

Different from the aforementioned three classes of protozoa, the Sporozoa does not possess the motion organs like flagella, cilia or pseudopod. They carry endoparasites and other pathogens that cause disease.

2.5.1.2 METABOLIC CLASSIFICATION

According to their degree of oxygen dependence, the protozoans are classified into three groups: obligate aerobes, microaerophiles and anaerobes (Fenchel, 2014). Aerobic protozoans normally grow in high oxygen tensions (Fenchel, 2014). Microaerophilic protozoa are aerobes that prefer low oxygen tension, typically in the range of 1-20 %. Within this range they have high growth rates (Bernard & Fenchel, 1996; Fenchel, 2014; Hogg, 2013; Prescott et al., 1996). Under strict anaerobic conditions, they are incapable of growing (Fenchel et al., 1989). All anaerobic protozoa are sensitive to oxygen to some extent (Britannica, 2019; Fenchel & Finlay, 1991). For example, the protozoa *T. foetus* shows slow growth and the protozoa *D. ruminantium* can survive several hours under 1 % atmospheric saturated oxygen tension (atm. sat.) (Lloyd et al., 1982; Mack & Müller, 1978). Half of the cells of *Plagiopyla frontata* and *Metopus contortus* died within 10-20 h exposure to atmospheric oxygen tension. (Fenchel & Finlay, 1990).

2.5.2 PROTOZOA IN NEREDA

As shown in the literature about AGS, ciliated protozoa especially *Vorticella* spp., *Carchesium* spp. and *Epistylis* spp. were found in the AGS (De Kreuk et al., 2010; Li et al., 2013; Pronk, De Kreuk, et al., 2015; Schwarzenbeck et al., 2004). All of them have stalks, attaching to the granule surfaces (Plumb, 1997; Sun et al., 2011). The flagellates and free-living ciliates like *Pseudocohnilembus pusillus* and *metazoan-nematodes* were detected in AGS. But the flagellates were only present periodically with low numbers and the ciliates had much higher occurrence frequency and abundance than flagellates according to the measurements from Drzewicki et al. (2017). Thus, the ciliated protozoa are possibly the most common type of protozoa growing in AGS, compared to the remaining three kinds of protozoa.

The Nereda system is operated as a sequencing batch process. It contains three steps which are simultaneous feeding and effluent withdrawal period (anaerobic period), reaction period (aerobic period) and a settling/sludge withdrawal/idle period (Pronk, De Kreuk, et al., 2015). Although the literature about AGS mentioned that protozoa contributed to the particle removal, it is unclear what the contribution of protozoa is in each stage (anaerobic and aerobic). For example, based on AGS particle removal literature, it is unknown whether *Vorticella* spp. consume particles during the anaerobic or aerobic period. According to Priya et al. (2008), *Vorticella* spp.

was also detected in a biomethanation systems, under anaerobic conditions. According to Priya et al. (2019), *Vorticella* spp. were grouped in anaerobic protozoa and they were less sensitive to oxygen concentration at 1 % atm.sat. (0.1 mg/L) compared to some other anaerobic protozoa.

When it comes to the tolerance to oxygen, aerobic and microaerobic protozoans can work under high oxygen tensions. So they can work in reaction period, but they cannot grow under anaerobic condition. This means the aerobic and microaerobic protozoa cannot contribute to the particle removal under anaerobic period. To make sure the suitable living condition (aerobic or anaerobic) of *Vorticella* spp. in AGS, its metabolism should be investigated. But the research about its metabolism are few. In full-scale AGS reactor, the aerobic duration is five times longer than anaerobic duration. And the oxygen tension in the Nereda system is the atmospheric oxygen tension (21 %) with the DO of 1.8-2.5 mg/L during reaction/aeration period (Pronk, De Kreuk, et al., 2015). If *Vorticella* spp. in AGS are anaerobic protozoa, their growth should be negatively interfered by a long-time oxygen tension. Since the aerobic phase is very long, their growth rate in 1-hour anaerobic phase should be quite high to make the positive net growth population. It should be hard for them to survive for days in AGS system. However, De Kreuk et al. (2010), Li et al. (2013) and Pronk, De Kreuk, et al. (2015) show the presence of *Vorticella* spp. in both lab-scale and full-scale AGS reactor. The *Vorticella* spp. was also detected in activated sludge (AS) system (Madoni, 2011). Thus, it can be possible that the oxygen preference of *Vorticella* spp. depends on specific species. The *Vorticella* spp. in both AS and AGS systems are likely to belong to aerobic protozoa, and they can only contribute on particle capture and removal in aerobic period. To the aforementioned free-living ciliated protozoa like *Plagiopyla frontata* and *Metopus contortus* (Fenchel & Finlay, 1990) and other anaerobic protozoa, they are possible to hardly survive after several aerobic periods.

There are few literatures that mention the possible anaerobic protozoa living on AGS. Therefore, based on the detected high-number ciliated protozoa in AGS and discussions in previous paragraph, anaerobic ciliates can possibly not survive in the Nereda system.

2.5.3 METABOLISM OF ANAEROBIC PROTOZOA

The metabolism of anaerobic protozoa is different from that of aerobic protozoa. Compared to aerobes, the anaerobic protozoa do not possess the mitochondria. Therefore, the only thing in common between aerobes and anaerobes' metabolic processes is glycolysis, which converts carbohydrates to pyruvate and happens in cytosol. Then, anaerobes utilize substrate-level phosphorylation to generate energy

or adenosine triphosphate (ATP), instead of using the Krebs cycle and the electron transport chain (Britannica, 2019; Muller, 1988).

There are two main metabolic pathways for anaerobic protozoa, which are hydrogen production pathway and ethanol production pathway.

2.5.3.1 HYDROGEN PRODUCTION PATHWAY

Many anaerobic protozoans have one special organelle which is called hydrogenosome. It is enveloped by a double-layer membrane. The hydrogen production pathway mainly produces hydrogen, acetate and carbon dioxide (Britannica, 2019; Lindmark & Müller, 1973; Muller, 1988). Part of the hydrogen formation metabolic process is shown in Figure 2.3. this process happens firstly in the cytosol for glycolysis and then in the hydrogenosome. After glycolysis, pyruvate is catalyzed to acetyl-CoA which is then converted to acetate. After that, in order to reoxidize ferredoxin, the anaerobic protozoa form hydrogen by means of transferring electrons to protons. The hydrogen generation process cannot be carried out by organisms without hydrogenosomes. (Britannica, 2019; Muller, 1988).

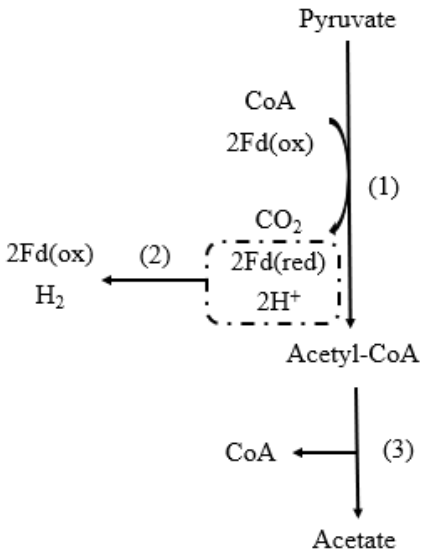

Figure 2.3: Fermentation of carbohydrates with hydrogen formation. The scheme displayed is from the stage of pyruvate to end products, the enzyme involved are (1) pyruvate: ferredoxin oxidoreductase, (2) ferredoxin-dependent hydrogenase, (3) acetate thiokinase.

The hydrogen generation pathway is depressed by higher hydrogen partial pressures, so keeping hydrogen partial pressure in a low value is important. Methanogens are essential to remove hydrogen produced by protozoans (Fenchel & Finlay, 2010; Hino, 1983; Kengen et al., 2009; Morgavi et al., 2010). They have been proven to live with some anaerobic protozoa such as *Plagiopyla* and *Metopus* during lab-scale

cultivation (Goosen et al., 1988; Van Bruggen et al., 1986). The presence of methanogens in lab-scale reactor has been reported in Pronk, Abbas, Al-Zuhairy, et al. (2015). According to Pronk, Abbas, Kleerebezem, et al. (2015), the presence of methanogens was controlled by the anaerobic solid retention time (SRT) during AGS formation process. The AGS was incubated in a lab-scale bioreactor and fed with methanol and acetate. The methanogens converted methanol to methane, but the growth of methanogens and the methane emission were prevented by shortening the anaerobic SRT from 17 to 8 days. The total average SRT decreased from 51 to 24 days. The cycle contained 60 min anaerobic phase, 112 min aerobic phase, 3 min settling and 5 min effluent discharging period. The anaerobic phase took up 33 % of the cycle time. According to Pronk, De Kreuk, et al. (2015), the SRT in Nereda system was 20-38 days and the anaerobic period took up 15 % of total cycle time. Thus, the anaerobic SRT was 3-6 days, which was lower than 8 days. The methanogens were unlikely to be present in full-scale AGS system.

Additionally, the position of methanogens needs to be near the protozoa to consume produced hydrogen in time. This means methanogens should also be on granule surfaces. But the methanogens are strictly anaerobic bacteria (Peters et al., 1995), which cannot keep alive on granule surfaces after several long-time aerobic periods.

2.5.3.2 ETHANOL PRODUCTION PATHWAY

The other metabolism is the ethanol production pathway. Part of the ethanol-formation metabolic process is shown in Figure 2.4. There are two ways to generate ethanol. For both ways, the first step is glycolysis (Embden-Meyerhof pathway). After that, there are two pathways to generate ethanol. The difference between these two pathways is the way to produce acetaldehyde. The acetaldehyde can be produced directly from pyruvate. In the other pathway, the pyruvate is firstly oxidized to acetyl-CoA, which then is converted to acetaldehyde. After that, ethanol is generated from acetaldehyde. Besides, acetate is formed as well from acetyl-CoA. (Boumba et al., 2008; Burdette & Zeikus, 1994; Muller, 1988)

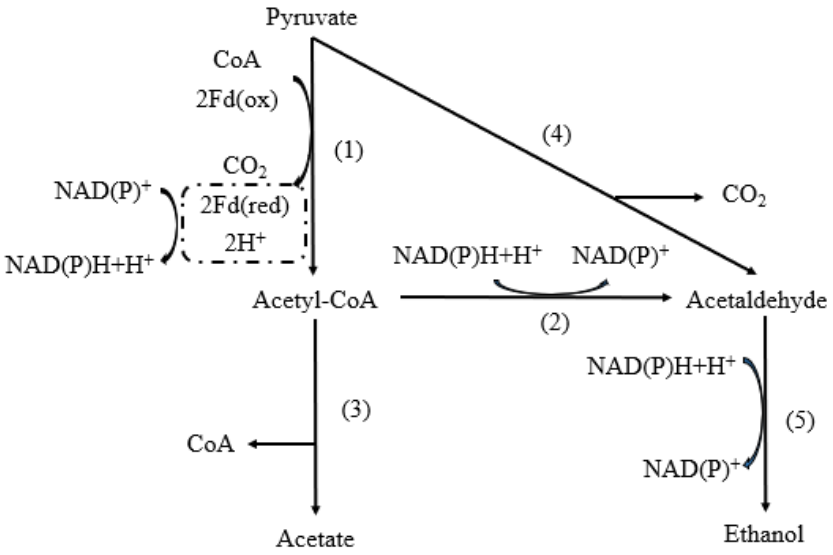

Figure 2.4: Fermentation of carbohydrates with ethanol production. The scheme displayed is from the stage of pyruvate to end products, the enzyme involved are (1) pyruvate: ferredoxin oxidoreductase, (2) acetaldehyde dehydrogenase, (3) acetate thiokinase, (4) pyruvate decarboxylase, (5) alcohol dehydrogenase.

Generally, the ethanol production pathway is the metabolism for the anaerobic protozoa without hydrogenosomes. However, in the research of Čerkasovová et al. (1984), they forced *T. foetus* to lose the function of hydrogenosome. The fermentation becomes the same as the way of the anaerobic protozoa without hydrogenosomes, which mainly generate ethanol, acetate and carbon dioxide. Besides, it is noticeable that the fermentation involving hydrogen production is depressed by a high hydrogen partial pressure (Coleman, 1986; Fenchel & Finlay, 1995; Fenchel & Finlay, 1992; Worm et al., 2010). Therefore, it can be possible that under high hydrogen partial pressure, the hydrogenosome-containing anaerobic protozoa change their metabolic pathways from hydrogen generation to ethanol formation in order to sustain growth.

3 MATERIALS & METHODS

3.1 PROTOZOA THEORETICAL RESEARCH DESCRIPTION

3.1.1 OBJECTIVES

In the literature about particle removal in AGS, protozoa are often mentioned (De Kreuk et al., 2010; Pronk, De Kreuk, et al., 2015; Schwarzenbeck et al., 2004). In these studies, the protozoa contributed to the removal of particulate organics in wastewater and improved the effluent quality. However, little attention is specifically paid to the performance of protozoa on capturing and consuming domestic wastewater particles in AGS during anaerobic period. Particle removal by protozoa in AGS in anaerobic period can be one of the particle removal mechanisms in domestic wastewater. Since the wastewater particles can hardly enter the granules (De Kreuk et al., 2010), only the protozoa living on granule surfaces can contribute to the particle capture and removal in anaerobic period.

Therefore, the objective was to investigate protozoa contribution on particle removal in anaerobic phase. The protozoa research was analyzed through theory. The theoretical analysis result shows it was not sufficient to quantify the contribution of protozoa on particle removal. Thus, the experiments can be performed which is discussed in Paragraph 3.1.2 and 3.1.3.

3.1.2 HYDROGEN PRODUCTION PATHWAY

As mentioned in Paragraph 2.5.3.1, the anaerobic protozoa can consume particles through hydrogen production pathway. Besides, high hydrogen partial pressure depresses the growth of protozoa, which can be mediated by methanogens. But methanogens are possibly hard to survive on the aerobic granules' surfaces.

In the full-scale AGS plant, the influent is fed to the AGS reactor during feeding or anaerobic period. It can be possible that the hydrogen partial pressure is decreased by the influent flow. The protozoa cannot produce hydrogen if the hydrogen partial pressure is beyond their limitation. The limitation is determined by the relation between actual Gibbs free energy and the hydrogen partial pressure. Therefore, this theoretical research focused on investigating their hydrogen partial pressure limitation and the role of the influent flow on mitigating the hydrogen partial pressure. Also, the contribution

of protozoa on particle removal within bearable hydrogen partial pressure was studied. The details are discussed in Paragraph 4.1.

Assumption and conditions

The domestic wastewater influent used for research was taken from Harnaschpolder in Delft. The total COD (TCOD) was 601 mg/L and the particulate COD (PCOD) between 0.45 μm and 100 μm was 243 mg/L. Since the composition of organic matter in the domestic wastewater influent was quite complicated, it was more convenient to assume one easily biodegradable substrate. For simplifying calculation, glucose was assumed to be the sole substrate in the domestic wastewater influent. The applied temperature (10 ℃, 15 ℃ and 20 ℃) was in the range of the yearly wastewater temperature range in the full-scale AGS plant (Pronk, De Kreuk, et al., 2015). Since it was unsure whether there was methanogen in AGS, this contribution estimation was without the participation of methanogens.

The metabolic reactions for hydrogen production pathway are shown in Table 3.1.

Table 3.1: Metabolic reactions (Flamholz et al., 2012; Kengen et al., 2009; Muller, 1988)

Reactions
$C_6H_{12}O_6+4H_2O \rightarrow 2CH_3COO^- + 2HCO_3^- + 4H^+ + 4H_2$
$C_6H_{12}O_6 + 2NAD^+ \rightarrow 2CH_3COCOO^-(\text{Pyruvate}) + 2NADH + 4H^+$
$CH_3COCOO^- + CoA + 2Fd(ox)+H_2O \rightarrow Acetyl-CoA + HCO_3^- + 2Fd(red) + 2H^+$
$2Fd_{red} + 2H^+ \rightarrow 2Fd_{ox} + H_2$
$Acetyl-CoA + H_2O \rightarrow CH_3COO^- + CoA + H^+$
$C_6H_{12}O_6+6O_2 \rightarrow 6CO_2 + 6H_2O$

The standard Gibbs free energy and enthalpy of formation for each component can be found in Appendix A Table A. 1. The reactor had a diameter of 6.25 cm. The applied up-flow velocity was 1 m/h and the duration for anaerobic period was 1 h.

3.1.3 ETHANOL PRODUCTION PATHWAY

As mentioned in Paragraph 2.5.3.2, ethanol production pathway is one of anaerobic protozoans' metabolisms. However, by searching protozoa ethanol production on Scopus, there were only 32 relevant literature since 2000, compared to 199 relevant literature about protozoa hydrogen production. Among these 32 literatures, some of them were only relevant with 'ethanol production' instead of all the key words. Only 8 literature were into ethanol-production protozoa. However, there were 6 literatures describing the metabolism of Sporozoa. The sporozoa are unlikely to present in AGS system as stated in Paragraph 2.5.2. Although the left two literature were about flagellates and the flagellates can be present in the AGS system, one of the flagellate

lives and infects tomato crops which is irrelevant with water treatment (Ienne et al., 2014). Since few protozoa with ethanol production metabolism were studied, it was hard to carry on theoretical research in this field. It is most likely that the ethanol production is not the common metabolic pathway for anaerobic protozoa.

Hence, only the hydrogen production pathway can be further studied through theory. The contribution estimation on particle removal by protozoa only includes hydrogen production pathway presented in Paragraph 4.1.

3.2 EXPERIMENT DESCRIPTION

3.2.1 INFLUENT CHARACTERIZATION

There were four domestic wastewater influents collected from Delft and Utrecht wastewater treatment plants. Three samples were from Delft and the remaining one was from Utrecht. The sample date, location and weather condition for these samples are shown in Table 3.2.

Table 3.2: Sample information

WW Sample	Sample date	Sample location	Weather condition
Delft 1st	2:00 PM, 29th November (Friday)	After screening	DWF*
Delft 2nd	10:00 AM, 31st January (Friday)	After screening	DWF
Delft 3rd	10:00 AM, 26th February (Wednesday)	After screening	WWF*
Utrecht	2:25 PM, 16th January (Thursday)	Before the fine screening	DWF

*DWF = Dry weather flow; WWF = Wet weather flow

To characterize the influent, the chemical oxygen demand (COD), volatile suspended solids (VSS), total suspended solids (TSS), and particle size distribution (PSD) were measured.

COD concentration in the domestic wastewater influent was measured spectrophotometrically with standard test kits (Dr. Lange type LCK 314 & 514; manufacturer: Hach Lange, Düsseldorf, Germany). COD fractionation for the domestic wastewater influent were analyzed. The procedure was that firstly different size sieves and filter paper were used to filter the wastewater in a sequential way, which included a 100 μm and a 45 μm woven wire mesh sieve, as well as 10 μm filter paper (Cyclopore polycarbonate membranes, Code: 7060-4715, manufacturer:

Whatman, UK) and 0.45 μm filter paper (Cellulose acetate membranes, Code: 7000-0004, manufacturer: Whatman, UK). Then, COD concentration was measured and analyzed for each size fraction. TSS and VSS were analyzed according to Standard Methods (APHA, 2017). TSS and VSS fractionation were also analyzed by using sieves and filter paper.

To measure the particle size distribution (PSD) in domestic wastewater, the particle size analyzer (Microtrac Bluewave, Germany) was used. The PSD analyzer can measure the particle in the size range of 0.02 to 2000 μm. There were three lasers inside in different positions, which were used to measure the size of particles. The PSD analyzer did triplicate measurement for each sample. Since the three lasers were in different positions, the particles were measured from multiangle. The output includes the PSD from each time measurement and the average among three measurements. For irregular shape particles, the average size became their particle sizes. Besides, the ultrasonic device inside made the particles disperse in solution, preventing the particles from merging together. Since it already contained demineralized water in the influent line, the wastewater influent was diluted automatically once it drops in. Thus, there were few shielding effects and there was no need to do extra dilution for the influent.

3.2.2 AEROBIC GRANULE SIZE MEASUREMENT

The aerobic granular sludge (AGS) used in this study was sampled from Utrecht WWTP in Jan 16th.

To characterize AGS, the size fractionation was analyzed by firstly sieving and then total solids (TS) was measured for each fraction. The sieving process was by use of different size sieves, including 2.5 mm, 2 mm, 1.4 mm, 1 mm, 0.5 mm and 0.2 mm. The first four were stainless steel mesh sieves and the last two were woven wire mesh sieves. The lower limit was 0.2 mm since the minimum size of aerobic granules is this size (De Kreuk et al., 2007). The concentration of AGS for measuring TS was 100 mL/L. The procedure of TS measurement was the same as the method described in the literature (Beun et al., 2002).

3.2.3 PLUG-FLOW EXPERIMENTAL SET-UP

The configuration of the experimental set-up is shown in Figure 3.1. The feed tank was used to feed the domestic wastewater or tap water to the reactor with the influent pump (Watson-Marlow Pumps 120U/114DV, UK). The tap water tank was used to apply tap water while fluidization with the use of the fluidization pump (Watson-Marlow Pumps 323E/313D/313X, UK). Both the influent pump and the fluidization pump were calibrated, and the method was described in Appendix B.1. The function of the valve 1 and valve 4 were used to purge air from the pipelines. The valve 3

was only open while fluidization. To investigate the contribution of filtering effect, the minimum fluidization velocity should be applied. The method for calculating the minimum fluidization velocity is discussed in Appendix B.2.

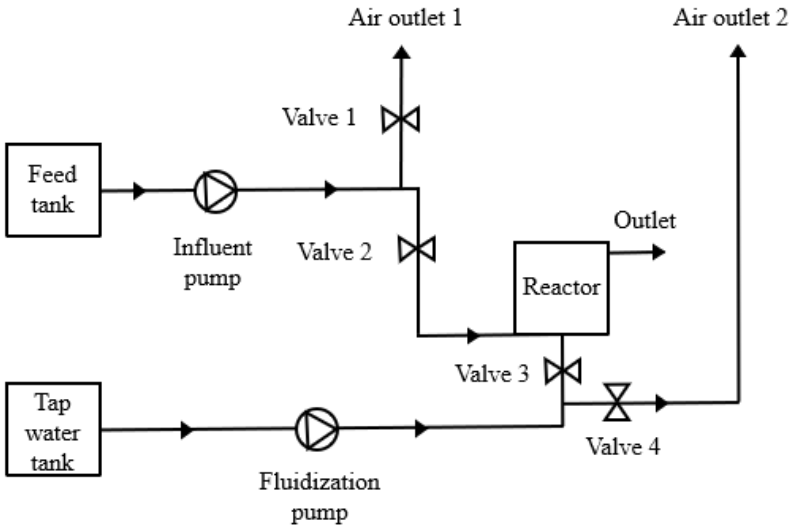

Figure 3.1: Experimental set-up

3.2.4 PLUG-FLOW EXPERIMENTS

Experiments were performed in one column operated under anaerobic condition. The reactor had a working volume of 1 L with the diameter of 6.25 cm. The effluent extracted at the height of 34 cm under 20 ℃. The granules were initially settled with tap water in the reactor with the granule layer height of 30 cm.

In the full-scale Nereda, the typical up-flow velocity in DWF is 1 to 1.5 m/h and in WWF is 3 to 5 m/h. Since DWF is more common than WWF in Netherlands and the particle concentration in DWF is higher than WWF, the DWF up-flow velocity was chosen for plug-flow experiments.

According to Pronk, De Kreuk, et al. (2015), the duration of the anaerobic period was 1 h during DWF. To investigate if the particle capture efficiency would change with time, the duration in plug-flow experiments was set to be 2 h.

To determine the required experiment duration, the tracer experiment was planned to be carried out. Due to COVID-19, this experiment cannot be done, but the method for this experiment is presented in Paragraph 3.2.4.1.

3.2.4.1 EXPERIMENT WITH SALT TRACER

The AGS was immersed in tap water before applying influent into reactor. To make sure the effluent from the reactor was undiluted by the initial tap water in the pores, all the tap water in the granular bed should be displaced by the influent. According

to the literature, at least 6 times pore volumes were needed under the up-flow velocity of 4.4 m/h which took about 13 min and at least 4 times pore volumes were necessary under the up-flow velocity of 0.4 m/h which took about 90 min (Weissbrodt et al., 2017).

The number of pore volumes of influent needed to replace the original solution in the pores was possibly dependent on the up-flow velocity once the bed volume was fixed. Additionally, it was also likely to be influenced by the different set-up characteristics (e.g. reactor internal diameter). The different reactor internal diameters can affect the way influent feeding into the reactor. The reactor internal diameter, the granular bed height and the up-flow velocity in the literature (Weissbrodt et al., 2017) were different from ours, which are shown in Table 3.3.

Table 3.3: Set-up comparison (Weissbrodt et al., 2017)

Property	Set-up in the literature	Experimental Set-up
Reactor internal diameter, m	0.059	0.0625
Bed height, m	0.33	0.22
Up-flow velocity, m/h	4.4; 0.4	0.5; 1; 2

Based on the literature (Weissbrodt et al., 2017), the inert tracer of NaBr can be used as influent and fed to the reactor by initially step-changing influent concentration from 0 to 5 g/L. NaBr concentration can be measured by an EC sensor. Compared to a Dirac tracer pulse, the step-change inlet concentration feeding regime avoids the toxicity and inhibition to the biomass growing in AGS (Weissbrodt et al., 2017). The conductivity sensor can be installed near the outlet of the reactor. The time used for effluent to reach same conductivity as the influent conductivity is the minimum duration for later column experiments. Since the influence of up-flow velocity was planned to be investigated, the tracer experiment should be applied with the up-flow velocity of 0.5 m/h, 1 m/h and 2 m/h.

3.2.4.2 EXPERIMENTS WITH TAP WATER AND WASTEWATER

Since the AGS collected from the Utrecht WWTP could already have adsorbed substrate, it can be possible that the granules release substrate during the experiments. This release process is called COD liberation. To investigate COD liberation by AGS, a column experiment was firstly conducted with tap water with an up-flow velocity of 1 m/h and a duration of 2 h. After that, the column was equilibrated with no COD liberation. Then, the plug-flow experiment was applied with domestic wastewater under same feeding conditions.

To prevent the set-up from clogging, the domestic wastewater influent used in plug-flow experiments was firstly filtered with a 100 μm sieve. The VSS, TSS and PSD were measured for the filtered influent.

For the plug-flow experiment with tap water or wastewater, effluent samples were collected at 30 min, 60 min, 90 min and 120 min. Thus, there were four effluent samples for each experiment with the duration of 2 h. COD and turbidity were measured for effluent samples. COD fractionation was also analyzed for the effluent. The methods for COD and COD fractionation were the same as that mentioned in Paragraph 3.2.1. The turbidity was measured by using a turbidimeter (Hach 2100N, Germany).

3.2.4.3 EXPERIMENT WITH VARIOUS UP-FLOW VELOCITIES

To investigate the influence of up-flow velocity on particle capture efficiency, the column experiment was designed to be carried out under different up-flow velocities. They include 0.5 m/h, 1 m/h and 2 m/h. The domestic wastewater was planned to be used as influent for these column experiments. The duration of each column experiment under each up-flow velocity is determined by the results from the tracer experiments as mentioned in Paragraph 3.2.4.1. The effluent coming out from the reactor should be collected. Both the COD concentration and turbidity should be measured for both influent and effluent. Then, the particle capture efficiency under different up-flow velocities can be analyzed.

3.2.4.4 EXPERIMENT WITH FLUORESCENT MICROBEADS

Due to the variability of wastewater, the fluorescent microbeads (FMBs) were planned to be used after the plug-flow experiment with domestic wastewater. The experiment aimed to observe the distribution of FMBs on the granule surface and investigate the contribution of different mechanisms. The chosen FMBs is described in Appendix B.3. The FMBs solution can be made by the particle concentration for each size range, which is displayed in Appendix B Table B. 1. The up-flow velocity is 1 m/h and the duration is determined by the tracer experiment.

The effluent coming out from the reactor at the end of duration should be collected. To investigate the contribution of the filtering effect on particle removal, fluidization should be applied to release any particles that might be stuck in the granule bed. Since the granular bed can be quickly loose and mixed, the fluidization duration should not be too long. The actual time required for fluidization should be determined by experiments. Since the effluent is diluted by the tap water during fluidization, the effluent concentration needs to be corrected for the dilution. The calculation method is described in Appendix B.4.

For measurement, the particle counter can be used for counting the number of FMBs in the influent and the effluent for each size range. Then, the total capture efficiency is the difference between influent and effluent particle number divided by influent particle number. The effluent concentration should be corrected for the dilution factor. The capture efficiency after fluidization includes the contribution of both adsorption mechanism and protozoa mechanism. The contribution of the filtering effect is the difference between the total capture efficiency and the capture efficiency after fluidization. Besides, the microscope is also useful on observing the particle distribution around the granules.

To investigate the contribution of protozoa, since low temperature can depress the activity of protozoa (Müller & Geller, 1993; Rose et al., 2007), the FMBs influent temperature is firstly cooled to 4 °C. Then, the influent is applied to the reactor with 1 m/h up-flow velocity and the duration determined by the tracer experiment. The effluent from the reactor should be collected and measured by both the particle counter and the microscope. The capture efficiency difference between the plug-flow experiment under room temperature and 4 °C is the contribution of protozoa.

Due to the outbreak of COVID-19, the experiment mentioned in Paragraph 3.2.4.1, 3.2.4.3 and 3.2.4.4 cannot be carried out.

3.3 MODEL DESCRIPTION

3.3.1 MODEL OBJECTIVE

In anaerobic feeding period, AGS beds are possibly like granular filtration beds (Paragraph 2.1). This is further discussed in Paragraph 5.4. Since the objective for building up the model was to study the performance of filtration in the AGS bed on particle capture. Therefore, the model only included transport mechanism. The model method in Stevenson (1997) was applied. The model was verified, and then the plug-flow experiment with wastewater was simulated. The results are stated in Paragraph 4.3.

3.3.2 MODEL STRUCTURE

In the mathematical model, the filtration bed was divided into 50 layers and each layer had 25 cells. Each layer contained five different sizes of grains and five different porosities. The grains in the model were assumed to be inorganic solids without pores inside. The influent particles in Stevenson (1997) model were classified into five size fractions. The particles in domestic wastewater were grouped into three size fractions. For each time step, the effluent concentration of each particle size fraction in each cell for every layer was recorded. Also, the

porosity that deposited particle took up was recorded. The definition of the time step is introduced in Paragraph 3.3.9.

3.3.3 PARTICLE TRANSPORT MECHANISMS

According to Yao et al. (1971) and Ives (1982), interception, settlement and diffusion are the dominant particle transport mechanisms in filtration processes. Therefore, the model focused on these three mechanisms' influence on particle capture.

3.3.3.1 INTERCEPTION

The mechanism of interception is controlled by the flow. As shown in Figure 3.2, when the streamline carries a particle close to the grain from the polar direction with the distance less than particle radius, the particle can be captured.

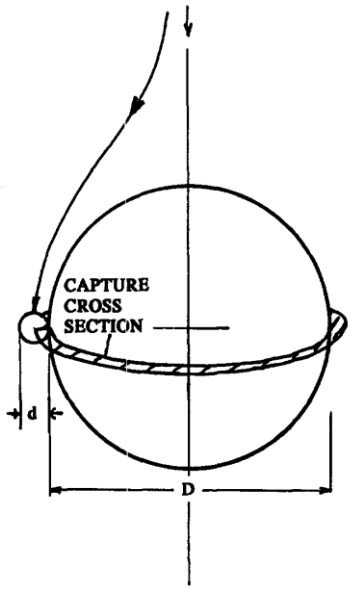

Figure 3.2: Concept of an equatorial capture cross section for interception (Stevenson, 1997)

The capture cross section area (A_c) forms when all streamlines which lead to capture around the grain are considered. The capture cross section area is the ring area around the grain with the width of the radius of the arriving particle. Stevenson used Equation (1) for A_c calculation, which is inaccurate for big particles. In thesis model, the capture cross section area for a clean grain was obtained by calculating the area difference. The ratio (C/C_0) of effluent concentration over influent concentration for interception was acquired by Equation (2). The equation derivation is shown in Appendix C.1.

$$A_c = \pi D \cdot d/2 \qquad (1)$$

$$\frac{C}{C_0} = \exp\left(-\frac{K_F \cdot K_M \cdot d^2 \cdot e \cdot \rho \cdot g \cdot \Delta H}{8 \cdot D \cdot \mu \cdot v_{cm}}\right) \quad (2)$$

K_F is a calculated factor for correcting grain surface roughness or capture cross section area after particle deposition. The value of this factor is discussed in Paragraph 4.3.1.2. K_M is the other calculated geometrical correction factor for the reduction of capture cross section area in high shear stress condition. Since the calibration of K_M has little effect, K_M was assumed to be 1.

3.3.3.2 SETTLEMENT

Different from interception, the mechanism of settlement works without the flow effect. The effective area for particle settlement depends on the projected area of grains. The projected area is followed the influent feeding direction. The projected area for a bed unit area (A_p) was calculated by Equation (3), which is influenced by the angle of repose (α). This angle was assumed to be 45° because it was hard to estimate this angle for the combination of various size grains without measurement. The ratio (C/C_0) for settlement was obtained by Equation (4). The equation derivation is presented in Appendix C.2.

$$A_p = 1.5 sin^2\alpha \cdot \frac{h}{D} \cdot (1 - e_0) \quad (3)$$

$$\frac{C}{C_0} = \exp\left(-sin^2\alpha \cdot (1 - e_0) \cdot (\rho_s - \rho_L) \cdot \frac{g d^2 h}{12 D v_{cm} \mu}\right) \quad (4)$$

3.3.3.3 DIFFUSION

Diffusion is the dominant mechanism for the deposition of small particles with diameter below 1 μm. The ratio (C/C_0) for diffusion was calculated by Equation (5). The equation derivation process is stated in Appendix C.3.

$$\frac{C}{C_0} = \exp\left(-\frac{6(1 - e_0) h K_L}{v_{cm} D}\right) \quad (5)$$

The total C/C_0 was obtained by the product of these three mechanisms' ratio (C/C_0).

3.3.4 BED HYDRAULICS

The headloss for each cell was the same as the headloss for the corresponding layer. The layer headloss (ΔH) was calculated by Equation (6) to (8). The application range of Equation (6) and (7) includes both laminar and transitional flow (Carman, 1937). The porosity (e) used in Equation (7) was the layer average porosity. The Reynolds number (Re) was calculated by Appendix C Equation (C 14). The velocity applied in Equation (C 14) and (7) were filtration velocity (v) instead of the cell superficial

velocity (v_{cm}). The constant ($\frac{R'}{\rho v^2}$) was obtained from Equation (6). The porosity was changed by particle deposition in each time step, leading to the change of headloss.

$$\frac{R'}{\rho v^2} = 5Re^{-1} + 0.4Re^{-0.1} \quad (6)$$

$$\frac{\Delta p}{h} = \left(\frac{R'}{\rho v^2}\right) \cdot \frac{S(1-e_0)}{e^3} \cdot \rho v^2 \quad (7)$$

$$\Delta H = \frac{\Delta p}{\rho g} \quad (8)$$

3.3.5 VELOCITY DISTRIBUTION CALCULATION

The flow in the model was laminar flow no matter with the filtration velocity of 1 m/h in experiment simulation or 7.5 m/h in Stevenson model verification. Thus, for simplifying the cell superficial velocity calculation, the Kozeny Equation (9) (Kozeny, 1927) was applied. The uncalibrated cell superficial velocity (v_c) can be obtained by Equation (9), but the porosity (e) applied here was the porosity for this cell.

$$\frac{\Delta p}{h} = 5 \cdot \frac{(1-e_0)^2}{e^3} \cdot S^2 v_c \mu \quad (9)$$

The calculated average cell superficial velocity per layer was not equal to the filtration velocity. But in reality, the layer superficial velocity should be the same as the filtration velocity. Thus, the cell superficial velocity (v_{cm}) was calibrated by Equation (10).

$$v_{cm} = \frac{v_c}{v} \cdot v_{c\_avg} \quad (10)$$

3.3.6 SURFACE SHEAR STRESS

The surface shear stress was determined by Equation (11) for each cell based on Coulson et al. (1996). Particles cannot deposit in the cell when the surface shear stress exceeded a given limit. The already deposited particles were released when the surface shear stress was higher than the limit by a defined factor. In this case, the wormhole was formed. This was happened in the situation when the filtration bed got clogging. In this case, there was a highway to penetrate influent into next working layers, which was made up of wormholes in each layer. The wormhole phenomenon was discussed in Paragraph 4.3.1.1.

$$R' = \frac{\Delta H}{h} \cdot \frac{\rho g e D}{6(1-e_0)} \quad (11)$$

3.3.7 UPDATED POROSITY

The porosity was updated for each cell for every time step. The volume of deposited particles per cell (V_{dp}) was calculated by Equation (12). Then, the ratio (e_{dep}) of deposited particle volume and cell volume was obtained by Equation (13), which was the porosity taken up by deposited particles at this time step. The updated porosity was determined by using previous porosity minus deposition porosity. The total deposition porosity (DEP) was the summation of e_{dep} for each time step.

$$V_{dp} = (C_0 - C) \cdot v_{cm} \cdot dT \cdot A_{cell} \tag{12}$$

$$e_{dep} = \frac{V_{dp}}{V_{cell}} = \frac{(C_0 - C) \cdot v_{cm} \cdot dT \cdot A_{cell}}{h \cdot A_{cell}} = \frac{(C_0 - C) \cdot v_{cm} \cdot dT}{h} \tag{13}$$

3.3.8 EFFLUENT AND INFLUENT CONCENTRATION FOR EACH LAYER

The effluent particle concentration for each fraction was calculated for each cell. The method to obtain the ratio (C/C_0) was described in Paragraph 3.3.3. The effluent particle concentration was calculated by using C/C_0 to multiply the initial particle concentration (C_0). For each particle size fraction, the summation of effluent concentration of 25 cells was calculated and the average concentration was produced. The average concentration for each particle size fraction was not only the effluent particle concentration of this layer, but also the influent particle concentration for the next layer.

3.3.9 TIME STEP AND MODEL DURATION

The time step set in Stevenson (1997) was described briefly. So the exact time step was hard to know. The possible time step used in Stevenson (1997) was 15 min according to the output table (Appendix C Table C. 1). In this study, to simplify the model, the time step related to the layer number. The time needed for passing each layer was defined as the time step, which was determined by layer height divided by filtration velocity. When verifying the model in this study, the time step applied was 8.64 s. The time step was 24.48 s while simulating the experiment. The model duration was 1 h, which was the typical value for anaerobic feeding period in AGS system.

3.3.10 INITIAL CONDITIONS AND MODEL FLOW CHART

The constant parameters applied in the model is shown in Table 3.4. The initial porosity was the same as the clean bed porosity. The influent particle concentration in model verification was evenly distributed to five fractions. So each particle fraction had the same influent concentration. The influent particle concentration for each fraction in experiment simulation was further divided into organic group and

inorganic group. These concentration values were based on the results from PSD, VSS and TSS measurement (Figure 4.3 and Table 4.3). The organic and inorganic particle density values were according to Haan et al. (1994). The particle density applied in verification was the average density of organic particle density and inorganic particle density.

Table 3.4: Parameter properties

Symbol	Parameter	Unit	Values for verification	Values for experiment simulation
C_0	Influent total particle concentration	m^3/m^3	2×10^{-3}	8×10^{-5}
d	Particle diameter	µm	[1, 3, 5, 7.5, 10]	[5, 27, 72]
D	Grain diameter	mm	[0.615, 0.7544, 0.82, 0.984, 1.23]	[0.7, 1.2, 1.7, 2.2, 2.7]
dT	Time step	s	8.64	24.48
e0	Clean bed porosity	-	[0.37, 0.40, 0.43, 0.46, 0.49]	[0.40, 0.43, 0.46, 0.49, 0.52]
h	Layer height	m	0.018	0.0068
H	Bed height	m	0.9	0.34
K_B	Boltzmann constant	J/K	1.38×10^{23}	1.38×10^{23}
K_m	Correction factor for rough	-	1	1
T	Temperature	K	293.15	293.15
v	Filtration velocity	m/h	7.5	1
α	Angle of repose	°	45	45
µ	Viscosity	Pa·s	1.01×10^{-3}	1.01×10^{-3}
ρ_{inorg}	Inorganic particle density	kg/m^3	-	2600
ρ_L	Fluid density	kg/m^3	1000	1000
ρ_{org}	Organic particle density	kg/m^3	-	1300
ρ_p	Particle density	kg/m^3	1950	-

Based on the model description, the model flow chart was made for one cell (Figure 3.3). The model began the calculation for next layer once the index of cells reached

25. The time (t) was moved forward with a time step (dT) once the index of layers reached 50. Otherwise, the calculation went on in this layer or at this time. The mass balance was reached in the model.

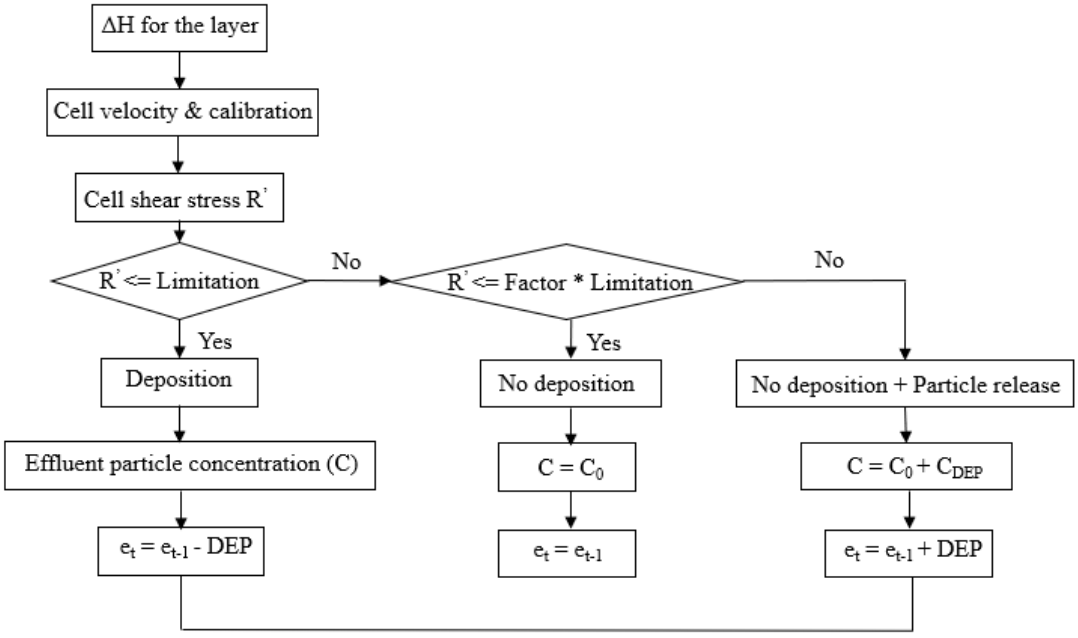

Figure 3.3: Model flow chart for one cell. DEP: porosity taken up by deposited particles

4 RESULTS

4.1 PROTOZOA RESULTS

As mentioned in Paragraph 3.1, only the hydrogen production pathway could be further studied through theory. Therefore, the contribution estimation on particle removal by protozoa only includes hydrogen production pathway.

The standard Gibbs free energy (ΔG^0) and enthalpy (ΔH^0) values for each metabolic reaction can be found in Appendix A Table A. 2. The calculation was based on the data displayed in Appendix A Table A. 1. Note that the hydrogen produced was in aqueous form.

$$\Delta G^{01} = \Delta G^0 + \mathrm{RTln}((1 \times 10^{-7})^{\eta}) \qquad (14)$$

The Gibbs free energy ΔG^{01} at standard conditions (1 M concentration of the reactants, 25 °C, pH 7) was calculated via Equation (14) (Heijnen & Kleerebezem, 2009). The results are displayed in Table 4.1. Since the Gibbs free energy ΔG^{01} for the overall Reaction (1) was less than zero, it seems like the reaction was feasible under standard conditions. However, when focusing on each step of reactions, the Gibbs free energy of the hydrogen generation Reaction (4) was larger than zero which means it was thermodynamically unfeasible. Therefore, no hydrogen can be produced and Reaction (1) or the hydrogen production pathway cannot carry on under standard conditions. Under actual conditions, the lower the hydrogen partial pressure, the lower the actual Gibbs free energy.

Table 4.1: ΔG^{01} for hydrogen production pathway

No.	Reaction	ΔG^{01}, kJ/reaction (298 K)
(1)	$C_6H_{12}O_6 + 4H_2O \rightarrow 2CH_3COO^- + 2HCO_3^- + 4H^+ + 4H_2$	-136.84
(2)	$C_6H_{12}O_6 + 2NAD^+ \rightarrow 2CH_3COCOO^-(\mathrm{Pyruvate}) + 2NADH + 4H^+$	-143.07
(3)	$CH_3COCOO^- + CoA + 2Fd(ox) + H_2O \rightarrow Acetyl - CoA + HCO_3^- + 2Fd(red) + 2H^+$	-21.73
(4)	$2Fd_{red} + 2H^+ \rightarrow 2Fd_{ox} + H_2$	+21.33
(5)	$Acetyl - CoA + H_2O \rightarrow CH_3COO^- + CoA + H^+$	-31.36

Therefore, the relationship between the actual Gibbs free energy ΔG^1 and the hydrogen partial pressure for Reaction (4) should be investigated.

Since the actual temperature (10 ℃, 15 ℃, 20 ℃) was not 25 ℃, temperature calibration was applied for ΔG^0 before calculating the actual Gibbs free energy ΔG^1. The Gibbs-Helmholtz Equation (15) was used for temperature calibration of Gibbs free energy where T_S was the standard temperature (25 ℃) (Heijnen & Kleerebezem, 2009). ΔH_f^0 of ferredoxin could not be found in the literature. ΔH_f^0 for each compound shown in Appendix A Table A. 1 accounted for 4% calibration in average for ΔG_f^0 in the temperature range of 10 - 20 ℃. Therefore, 4% was assumed to be the contribution of ΔH_f^0 for the temperature calibration of ferredoxin.

$$\Delta G_R^{0,T} = \Delta G_R^0 \cdot \frac{T}{T_S} + \Delta H_R^0 \cdot \frac{T_S - T}{T_S} \qquad (15)$$

The Figure 4.1 displays the relation between temperature and the Gibbs free energy (ΔG^0) under 10 ℃, 15 ℃ and 20 ℃ for Reaction (4). These values were calculated by Equation (15), which can be found in Appendix A Table A. 3. It is obvious that the effect of temperature on the Gibbs free energy (ΔG^0) was not significant. Therefore, only 15 ℃ was applied for later calculations.

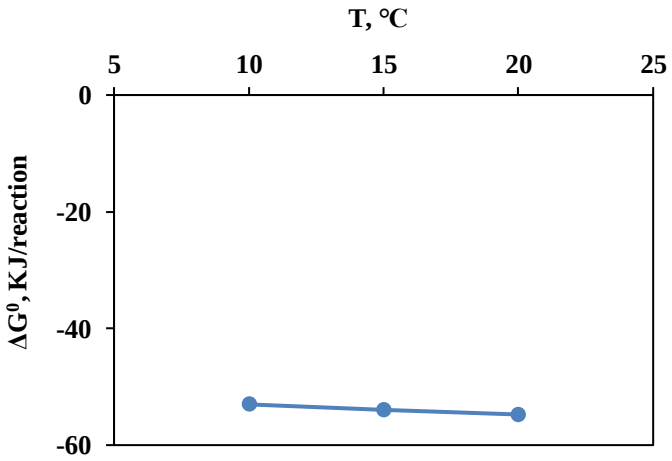

Figure 4.1: ΔG^0 under different temperature for Reaction (4)

After that, the formula for actual Gibbs free energy change (ΔG^1) was calculated via the Equation (16) and displayed in Appendix A Table A. 4 (Heijnen & Kleerebezem, 2009). Note that the concentration of each components except H_2 and H^+ was assumed to be 1 M under pH 7.

$$\Delta G^1 = \Delta G_0 + RT\ln\left(\frac{[A]^a[B]^b}{[C]^c[D]^d}\right) \qquad (16)$$

ΔG^1 for Reaction (4) under 15 ℃ and hydrogen partial pressure between 1 and 10^{-10} atm was calculated and shown in Figure 4.2. The exact values can be found in Appendix A Table A. 5.

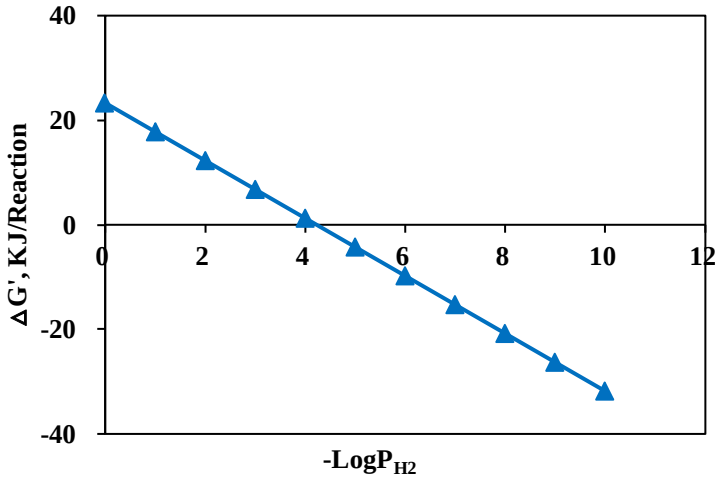

Figure 4.2: Effect of the hydrogen partial pressure on the actual Gibbs free energy change

Based on Figure 4.2, the maximum hydrogen partial pressure was the intersection with x-axis, which was $10^{-4.23}$ atm.

The flow rate was 3.07 L/h and the Henry's constant in different temperature was calibrated via Equation (17) (Smith & Harvey, 2007). ΔH_{sol} is the enthalpy of dissolution and R is the molar gas constant. The Henry's constant is $7.8 \times 10^{-4} \frac{mol}{L \cdot atm}$ under 25 ℃ and ΔH_{sol} for hydrogen is -4.2 kJ/mol (Alberty, 2005; Sander, 2015)

$$\frac{H(T_1)}{H(T_0)} = \exp\left(\left(\frac{\Delta H_{sol}}{R} \times \left(\frac{1}{T_1} - \frac{1}{T_0}\right)\right)\right) \quad (17)$$

Then the amount of hydrogen removed by flow was calculated by Equation (18). As shown in Reaction (1), 1 mol glucose can generate 4 mol hydrogen, so the glucose consumption of protozoa was calculated by using the H_2 removal divided by 4.

$$C_6H_{12}O_6 + 4H_2O \rightarrow 2CH_3COO^- + 2HCO_3^- + 4H^+ + 4H_2 \quad (1)$$

$$H_2 \text{ removal} = Duration \times P_{H2} \times H(T1) \times Q \quad (18)$$

Since 6 mol oxygen was needed to consume 1 mol glucose as shown in Reaction (6) and the influent volume in 1 h was 3.07 L, the COD consumption can be calculated. Lastly, the COD capture efficiency was calculated via Equation (19). These results mentioned above are shown in Table 4.2.

$$C_6H_{12}O_6 + 6O_2 \rightarrow 6CO_2 + 6H_2O \quad (6)$$

$$COD\ capture\ \% = \frac{COD\ consumption}{Particulate\ COD(45 - 100\ \mu m)} \quad (19)$$

Table 4.2: Relevant parameter under 15 ℃

Parameter	Value
H, $\frac{mol}{L \cdot atm}$	7.4×10^{-4}
H_2 removal, mmol	1.3×10^{-4}
Glucose consumption, mmol	3.4×10^{-5}
COD consumption, mg/L	2.1×10^{-3}
COD capture efficiency, %	8.6×10^{-4}

The COD capture efficiency was near zero. Therefore, it is impossible for the anaerobic protozoa to contribute significantly on particle removal through the hydrogen production pathway without methanogens.

Overall, the protozoa with ethanol production pathway was hard to be studied via theoretical way. For the protozoa with hydrogen production pathway, no matter there is the presence of methanogens or not, this kind of protozoa have possibilities to contribute to particle capture and removal. Thus, experiments can be performed for investigating the exact contribution of protozoa on particle removal in anaerobic period. The relevant experiment plans are described in Paragraph 5.1.

4.2 EXPERIMENT RESULTS

4.2.1 INFLUENT CHARACTERIZATION

The influent parameters (COD, TSS, VSS, TN and TP) were measured and displayed in Table 4.3.

Table 4.3: Influent parameters

Parameters	Delft 1st	Delft 2nd	Delft 3rd	Utrecht
TCOD*, mg/L	373	601	138	1000
COD (0.45-10 µm), mg/L	134	166	-	61
COD (10-45 µm), mg/L	35	51	-	455
COD (45-100 µm), mg/L	34	26	-	543
TSS (< 100 µm), mg/L	121	166	-	1137
VSS (< 100 µm), mg/L	97	138	-	382
VSS/TSS (< 100 µm)	0.8	0.83	-	0.34
TN*, mg/L	-	79	-	78
TP*, mg/L	-	24	-	27

*TCOD = total COD; TN = total nitrogen; TP = total phosphorus.

4.2.1.1 COD, TSS AND VSS

The average COD of domestic wastewater in Netherlands was roughly around 300-450 mg/L (Bernardes & Klapwijk, 1996; De Kreuk & van Loosdrecht, 2006; Pons et al., 2004). As shown in Table 4.3, since wastewater composition cannot be always the same, TCOD values were not exactly constant. TCOD for Delft 1st was in the range between 300-450 mg/L. For Delft 2nd WW, it was a bit higher than 450 mg/L, which could have been due to the morning peak. The Delft 3rd had the lowest TCOD likely because of the rain dilution. The high TCOD from Utrecht WW was due to a high discharge of cleaning wastewater from on-site the WWTP. This led to extra pollutants or COD. Thus, Utrecht WW was not suitable for experiments. Compared to Delft 1st and 2nd WW, under the same up-flow velocity, the low COD concentration of Delft 3rd WW was harder to lead to obvious COD capture efficiency.

COD fractionation results for Delft 1st and 2nd WW (Table 4.3 and Figure 4.4) show that particles in the range of 0.45-10 µm took up around 70 % COD in the range of 0.45-100 µm, which was much higher than COD values in the other two size ranges.

Since the ratio of VSS/TSS was mostly in the range of 70%-85% (Lew et al., 2003; Neralla et al., 2000; Vlyssides et al., 2002), the ratios for Delft WW shown in Table 4.3 were all in this range.

Therefore, the first two Delft influents were more suitable for experiments than the others. The Delft 2nd WW was used for plug-flow experiments.

4.2.1.2 PSD

Figure 4.3 shows the PSD for the two Delft influents and their average distribution. There were some particles larger than 100 µm, even though the influent was sieved over a 100 µm sieve. This can be due to the inaccuracy of the 100 µm sieve and the irregular shape of the particles.

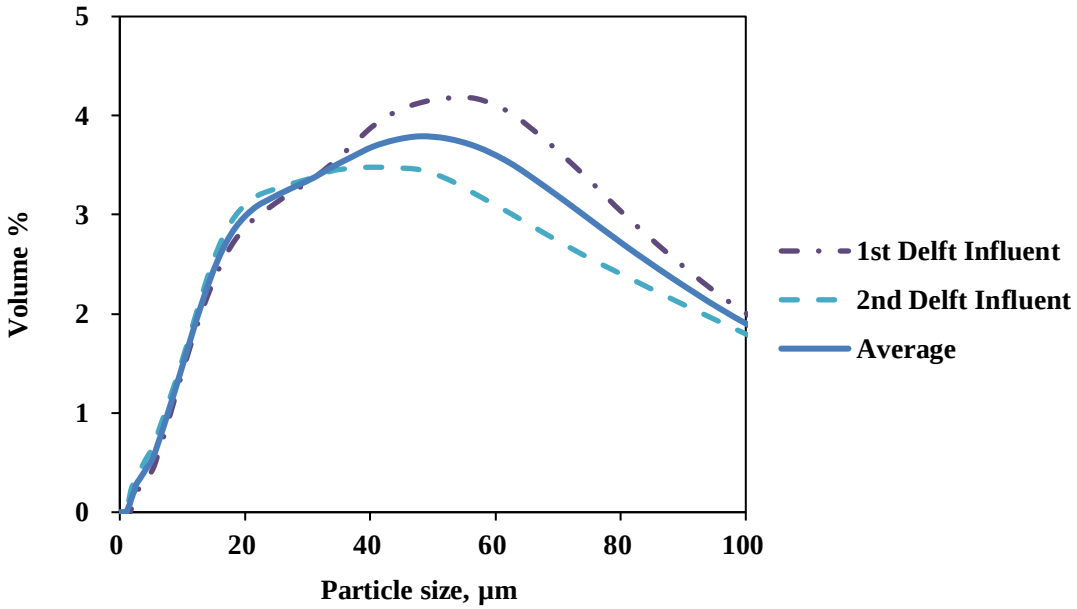

Figure 4.3: Delft influent PSD less than 100 µm

To compare the PSD with the COD fractionation of the influent, the PSD was divided into three parts. The particle volume percentage (V%) for each fraction was accumulated. As shown in Figure 4.4, the COD % in the size range of 0.45 to 10 µm was quite high, while the V% in this fraction was quite low. Since higher the organic matter content, higher the COD concentration. More particles in this small size range can be organic and the organic content can be expressed by VSS.

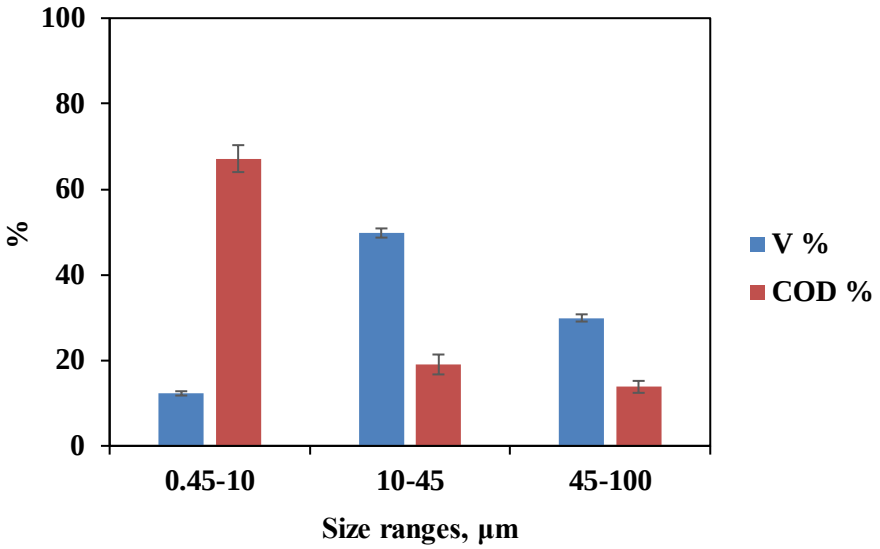

Figure 4.4: Average V% and COD% in different size ranges. V% for each size range was calculated by accumulation according to influent PSD (Figure 4.3). COD% for each size range was calculated through using COD per size range divided by COD in the size range of 0.45 µm to 100 µm and the result times 100.

To investigate if the organic content can lead to such a big difference between V% and COD% in the size range of 0.45 to 10 µm, VSS/TSS for each fraction was measured and analyzed. The result is shown in Figure 4.5.

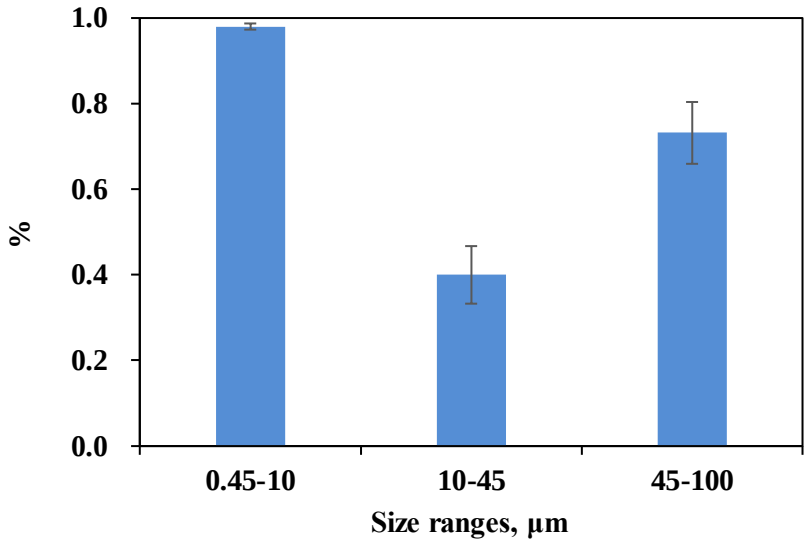

Figure 4.5: VSS/TSS in different size ranges. The result was measured and calculated from the 2nd Delft influent.

As displayed in Figure 4.5, VSS/TSS % between 0.45 µm and 10 µm almost reached 0.98 which was much higher than the values in the other size ranges. This means the organic matter in this small size range was much higher than that in the other size ranges, resulting in the high COD content. Since particles in different size

ranges had different characteristics according to Figure 4.4, and different size particles can behave differently, the particle in this small size range cannot be combined with others. Hence, the PSD figure was divided into three parts, which were 0.45-10 µm, 10-45 µm and 45-100 µm shown in Table 4.4.

Table 4.4: Volume of particles in each size range of Delft Influent (less than 100 µm)

Size range in PSD, µm	0.45-10	10-45	45-100	Total (0.45-100)
V_o% (Delft Influent PSD)	12	50	30	92
V_n% (Delft Influent < 100 µm)	13.3	54.1	32.5	100
V_a% (Assumption)	15	55	30	100
C_{org}^*, mL/L	0.015	0.022	0.022	0.059
C_{inorg}^*, mL/L	0	0.017	0.004	0.021

*C_{org} = organic particle volumetric concentration; C_{inorg} = inorganic particle volumetric concentration

Since some particles were lager than 100 µm, the total V% between 0.45 µm and 100 µm was less than 100 %. V_o% for each size range was normalized via using each V_o % divided by the total V_o % between 0.45 µm and 100 µm, which was 91.96 % in this case. The normalized result was expressed as V_n % in the third column in Table 4.4. To roughly simulate the domestic wastewater and based on V_n %, the volume of particles in the size range of 0.45-10 µm, 10-45 µm and 45-100 µm took up 15%, 55% and 30% of the total particle volume respectively (Table 4.4). The average TSS of the first two Delft influents was calculated by using the TSS data in Table 4.3. The average TSS can be used to calculate the total particle volume in this range. However, since the PSD figure shows some particles were larger than 100 µm and the 100 µm sieve was used for measuring PSD, VSS and TSS, the measured TSS must contain particles larger than 100 µm. To calculate the total volume concentration of particles in this size range, the volume of particles larger than 100 µm should be get rid of. Both averaged TSS and total V_o% between 0.45 µm and 100 µm were used for calculation. The density of organic matters is 1.3 g/mL and the density of inorganic compounds is 2.6 g/mL (Haan et al., 1994). Thus, the average density for particles in the domestic wastewater was assumed to be 1.95 g/mL. The total particle volume concentration was calculated by Equation (20).

$$\text{Total particle volumetric concentration (mL/L)} = \frac{\text{TSS(mg/L)}}{1000\text{(mg/g)} \times \rho\_\text{praticle(g/mL)}} \times \text{Total } V_0\% \quad (20)$$

The thesis focused on the performance of AGS on treating particulate COD, which was in organic form. But since the existence of inorganic particles can have an

impact on the capture process of organic particles, both kinds of particles were important. The organic and inorganic particle volumetric concentration for each size range was calculated via Equation (21) and (22). The result is displayed in the last two columns of Table 4.4. The VSS/TSS for different size ranges shown in Figure 4.5 was used for calculating the corresponded size ranges of the organic and inorganic particle volumetric concentration.

$$\text{Organic particle volumetric concentration (mL/L)} = \text{Total particle volume} \times V_a\% \times \frac{\rho\_particle(g/mL)}{\rho\_org(g/mL)} \times \frac{VSS(mg/L)}{TSS(mg/L)} \quad (21)$$

$$\text{Inorganic particle volumetric concentration (mL/L)} = \text{Total particle volume} \times V_a\% \times \frac{\rho\_particle(g/mL)}{\rho\_inorg(g/mL)} \times \frac{VSS(mg/L)}{TSS(mg/L)} \quad (22)$$

4.2.2 AEROBIC GRANULE SIZE MEASUREMENT

The Figure 4.6 shows the result of AGS size fractionation. It is obvious that the granules with the size range of 1.4 to 2 mm took up the most part. The TS weight percentage summation of the first three size ranges was less than 50% and it was higher than 50 % after adding the weight % of the fourth size range (1.4–2 mm). Hence, the average granule size was 1.7 mm, which was the average value in the range 1.4-2 mm.

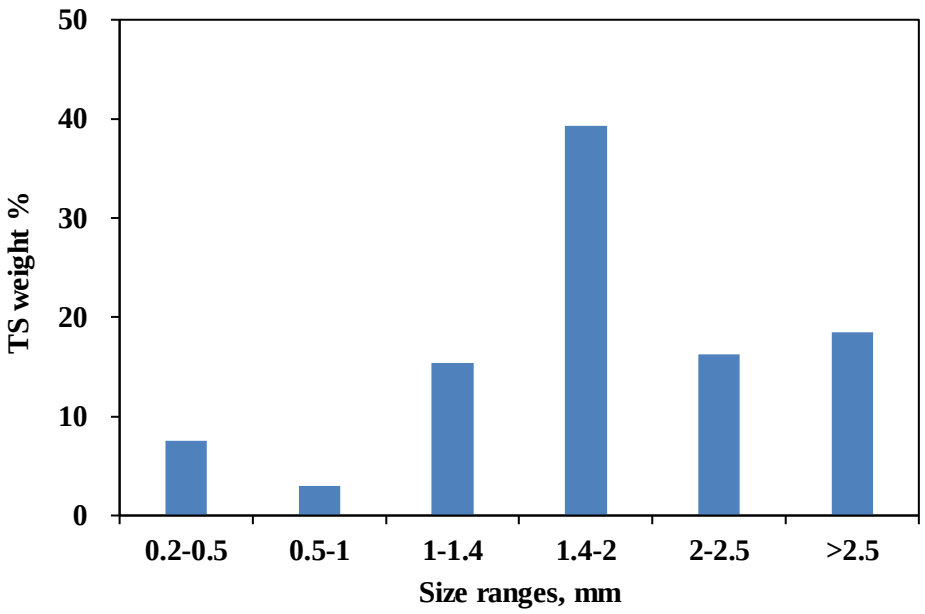

Figure 4.6: AGS size fractionation

4.2.3 PLUG-FLOW EXPERIMENT

4.2.3.1 TAP WATER INFLUENT

To study the COD liberation from AGS, the tap water experiment has been carried out duplicate. The results are the average value of these two experiments, which are displayed in Figure 4.7 and Figure 4.8.

Figure 4.7 shows that the effluent turbidity declined with the time. The granules were in the tap water in one glassware for couple days before doing the experiment, it gave granules a long time to liberate the COD. It also made the tap water in the glassware more turbid than its initial state.

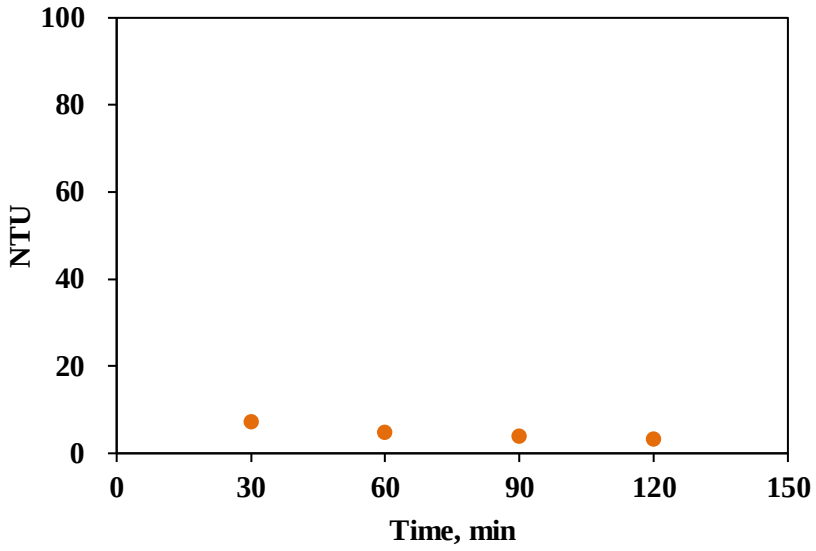

Figure 4.7: Effluent turbidity (tap water experiment)

As mentioned in Paragraph 3.2, since the tracer experiment cannot be done, the number of pore volumes needed at 1 m/h cannot be determined. Based on literature values at 0.4 and 4.4 m/h (Weissbrodt et al., 2017) mentioned in Paragraph 3.2.4.1, approximately 4.6 pore volumes were needed under the up-flow velocity of 1 m/h. The duration needed for reaching 4.6 pore volumes was 43 min, based on the calculation with the bed height of 0.34 m and the porosity of 0.46. At 30 min, the volume of influent only reached 3.2 pore volumes under 1 m/h.

Hence, the effluent at 30 min was not pure tap water. It contained some water in which the aerobic granules were stored, taking up at least 5 %. This led to the relatively high turbidity. As time went, less original tap water was in the pores of granule bed, resulting in the decreasing turbidity. Besides, the low turbidity along the duration of 2 h also shows that the COD liberation rate was too low.

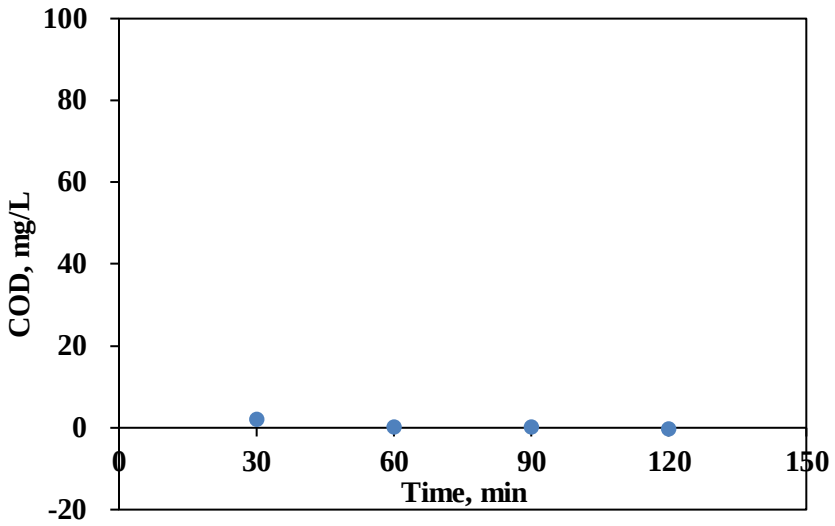

Figure 4.8: Effluent COD (tap water experiment)

Figure 4.8 shows the effluent COD changing with time within 2 h. Due to the COD measurement limitation of 15 mg/L, it is obvious that all the COD were lower than the limitation. This means the granules release little COD that was hardly to be detected even in the beginning of the experiment in which the turbidity was highest.

Therefore, the COD liberation from the granules can be negligible based on the results.

4.2.3.2 DOMESTIC WASTEWATER INFLUENT

To investigate the performance of AGS on capturing particles, the plug-flow experiment was conducted with the domestic wastewater. Figure 4.9 shows the turbidity of effluent was constant within 2 h. The effluent was collected and measured at each half an hour. It is unknown how the turbidity changed within each 30 min especially during the first 30 min. Since there were few COD liberation and this experiment was carried out right after the tap water experiment, the effluent in the beginning contained both the tap water from the AGS bed pores and the wastewater influent. The turbidity of the effluent in the first 30 min can be an increasing trend from roughly 0 NTU (tap water) to around 40 NTU (first effluent measurement at 30 min.). The tap water in the pores was flushed out by the wastewater influent generally, resulting in a rising percentage of wastewater in the effluent as time passed by. As mentioned in last paragraph, at least 5 % of effluent contained tap water at 30 min. Thus, more than 90 % effluent was from wastewater influent. It can take 43 min to reach 100 %. As shown in Figure 4.9, the effluent turbidity at 60 min, 90 min and 120 min was quite similar to that at 30 min. Therefore, although there were some dilution effects in effluent at 30 min, it did not lead to a big difference in turbidity. The turbidity from 30 min to 120 min can be

stable with time. Besides, the turbidity decreased dramatically by 50 % compared to influent turbidity.

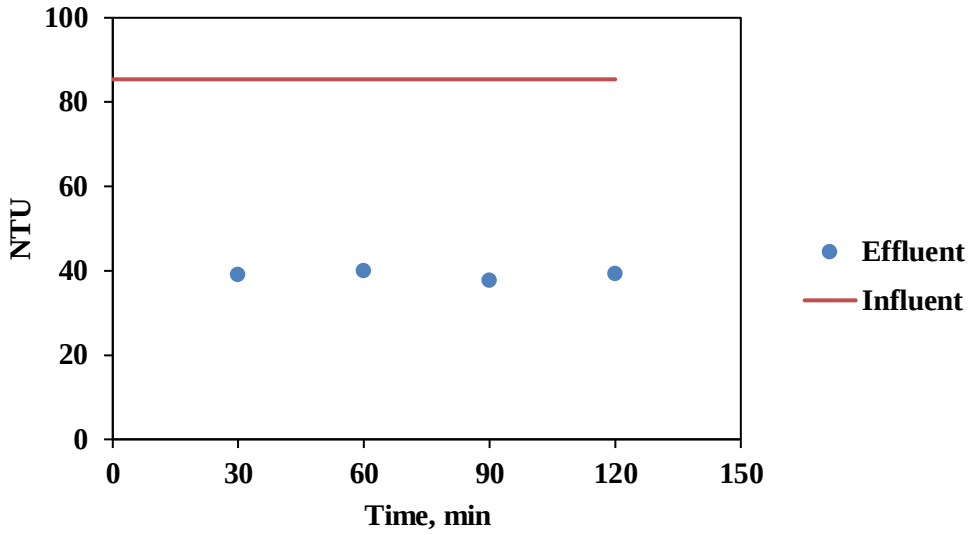

Figure 4.9: Effluent turbidity (wastewater experiment)

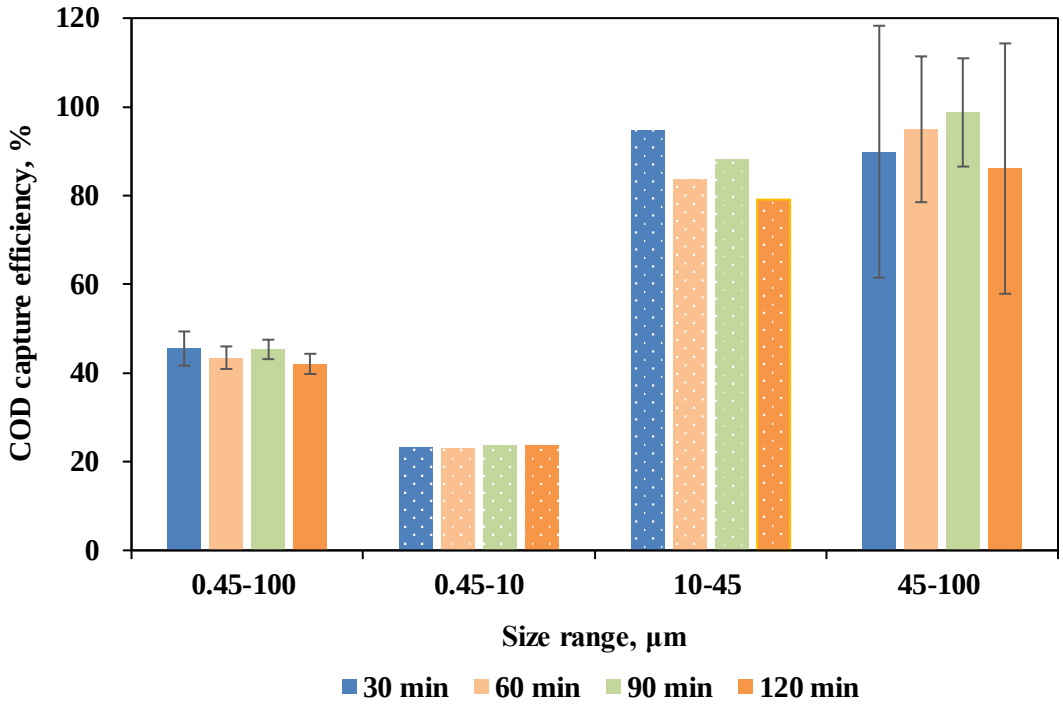

Figure 4.10: PCOD capture efficiency

Figure 4.10 shows the COD capture efficiency at 30 min, 60 min, 90 min, and 120 min. Since the effluent was collected at each 30 min, the effluent in the first 30 min can be diluted by the tap water from the AGS pores. This can result in the low COD concentration of effluent and high COD capture efficiency in the first 30 min. Since the capture efficiency for the last three time point was the same as that at 30 min,

the capture efficiency can be stable from 30 min to 120 min in each size range. The effluent COD for the particle less than 10 µm was measured once, so there is no error bar in the dashed parts in Figure 4.10. The COD for the particle less than 10 µm was measured triplicately in total, but the time to measure the second and third samples was not the same as the first sample. The last two samples stayed in room temperature overnight before measurement, possibly leading to the degradation process of COD content by bacteria. Therefore, the COD of these two samples decreased, which cannot be used for comparison.

Thus, the effluent turbidity and COD can be constant from 30 min to 120 min in the wastewater plug-flow experiment. The average capture efficiency for all the particles less than 100 µm was 43 % and the capture efficiency in different size ranges was quite different. The highest capture efficiency was in the size range of 45 µm to 100 µm. The capture efficiency in the size ranges of 0.45-10 µm was much lower than that in the other two size ranges. As displayed in Figure 4.11, there were almost no PCOD in the size range of 10 µm to 100 µm, but there were still a lot PCOD in the size range of 0.45 µm to 10 µm.

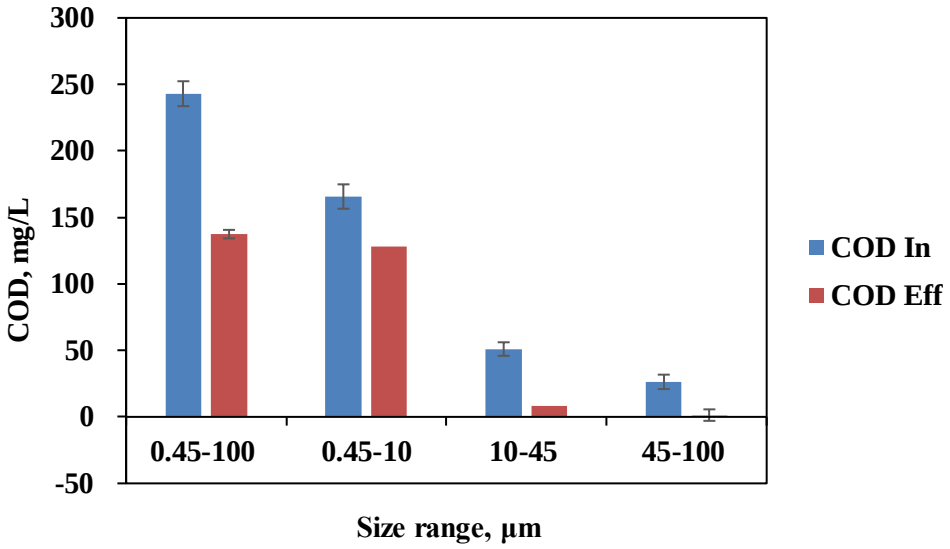

Figure 4.11: Comparison between influent and effluent COD at 60 min

4.3 MODEL RESULTS

4.3.1 MODEL VERIFICATION

The wormhole and the capture cross section area were paid attention when verifying the model with Stevenson model. This was because these two aspects can influence the model result to some extent.

4.3.1.1 WORMHOLE

The wormhole formation happens in filtration beds when they are clogged (Emelko et al., 2005). With deposition going on, the porosity in the filtration bed decreases and the headloss increases. For one clogged layer, there are some cells that have relatively higher porosity than others, leading to higher shear stress according to Equation (11). The high shear stress scours the grains, resulting in the detachment process. Then, the porosity becomes even higher. The shear stress further increases until the cell is completely clean. This is the process of wormhole formation. Besides, since all the cell headloss within one layer is equal, the more open the pore is, the higher cell velocity it is according to Equation (7). Thus, the influent flow can still pass the clogged filtration bed through the wormholes in each layer. The wormhole formation can be an important phenomenon in filtration field since it can show whether the performance of filtration bed is getting worse.

4.3.1.1.1 FILTRATION MODEL

In Stevenson model, the wormhole formed in the first layer after 1.5 h with 7.5 m/h filtration velocity (Stevenson, 1997). The wormhole acts as part of highway in the whole filtration bed. The porosity of that wormhole was the same as the clean bed porosity and the velocity was the highest among these 25 cells.

4.3.1.1.2 AGS SYSTEM

As mentioned in Paragraph 3.3.10 (Table 3.4), the particle concentration in domestic wastewater was 100 times lower than that in Stevenson model. Therefore, there can be possibly no wormholes in AGS system. For investigating this, it was assumed that all the particles in domestic wastewater were captured in the first layer of AGS bed with 3 h feeding duration and 1 m/h up-flow velocity. The result shows the average porosity decreased from 0.46 to 0.42 with less than 9 % decrease. Additionally, by applying this assumption in the model, the result shows the average porosity was changed to 0.45 and there was no wormhole formation in the AGS bed. Thus, it is very likely that there was no wormhole formation in AGS system due to low particle concentration and low up-flow velocity. Therefore, only particle deposition was considered in the model. The particle detachment process, which was related to the shear stress comparison, was not considered.

4.3.1.2 CAPTURE CROSS SECTION AREA

The capture cross section area can improve the interception efficiency by increasing the roughness of grain surfaces, which has been mentioned in Paragraph 3.3.3.1. Since the way to obtain the correction factor (K_F) for the capture cross section area was only described briefly in Stevenson (1997), two ways were tried to estimate the area. The results from these two estimation methods were compared with the model

result from Stevenson (1997), and the result of the situation without capture cross section area calibration.

The model result with 7.5 m/h filtration velocity from Stevenson (1997) is displayed in Table 4.5. The data was collected at 0.25 h and 1 h filtration period. Table 4.5 shows that from 0.25 h to 1 h, the porosity taken up by deposited particles (DEP) increased exponentially. This exponential increase can be due to the increase of capture cross section areas.

Table 4.5: Average DEP in the first layer matrix

Method	DEP	
	0.25 h	1 h
Stevenson (1997)	0.01	0.19
K_F & d_2/d_1	0.02	0.07
Geometry	0.03	0.14
Without A_c calibration	0.01	0.04

4.3.1.2.1 ESTIMATED FROM STEVENSON

Since the larger the capture cross section area, the higher the interception efficiency (Equation (2)). The lager particles can create more capture cross section area after arriving on grain surface than smaller particles. Besides, the large particles have benefits of capturing small particles (Mackie, 1989). Based on Stevenson (1997), there were three data groups, which were the relation between K_F and the ratio d_2/d_1 as shown in Table 4.6. The lower the ratio, the higher the K_F and then the capture efficiency.

Table 4.6: Data groups of d_2/d_1 and K_F

d_2/d_1 *	K_F
0.1	4.4
1	1.57
10	1.06

*d_1: diameter of the resident particle; d_2: diameter of the arriving particle

A trendline was obtained based on Table 4.6 and utilized to estimate K_F. It should be paid attention that there was not only one particle deposit on grains' surfaces. Also, it was hard to know the exact deposition position of arriving particles. Thus, the diameter of the resident particle d_2 was assumed to be the weighted average diameter of all resident particles. The weight for each particle fraction was the porosity taken up by corresponded particle size fraction. The model result is

displayed in Table 4.5, which shows that the deposition increased linearly with time. The capture cross section area was not playing an important role on capturing particles compared to the result from Stevenson (1997) (Table 4.5).

4.3.1.2.2 ESTIMATED FROM PARTICLE GEOMETRY

As displayed in Figure 4.12, the capture cross section area for a clean grain is the circle area difference between the green circle and the red dashed circle, which is highlighted by yellow.

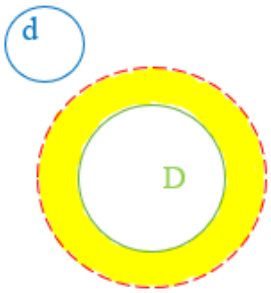

Figure 4.12: Capture cross section area for a clean grain. D was the diameter of the grain. d was the diameter of the arriving particle. The radius of the red dashed circle was the summation of the radius of the green circle and the blue circle.

As shown in Figure 4.13, after one particle deposited on the grain surface, the capture cross section area increased, which is the yellow area highlighted in the figure. The Law of Cosines and the sector area calculation method were applied for calculation. The detailed calculation procedure is presented in Appendix C.4.

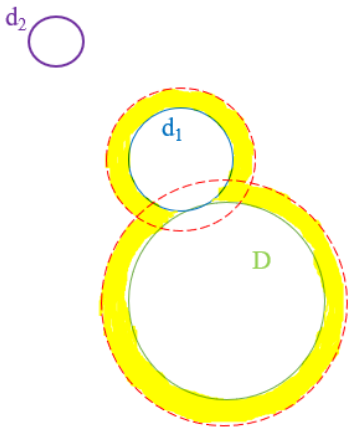

Figure 4.13: Capture cross section area after deposition of one particle. d_1 was the diameter of the resident particle. d_2 was the diameter of the arriving particle. The red circles

had the radius of green or blue circle plus the radius of purple circle. The yellow area was the capture cross section area for d_2.

The model result for this estimation method is shown in Table 4.5 and Figure 4.14. The table result shows relatively exponential increase compared to the result of the other method (Table 4.5). But the exponential trend was less strong than the Stevenson result (Table 4.5). The possible reasons for it and the comparison between these two methods are discussed in Paragraph 5.5. Figure 4.14 shows an initial decrease trend in the first several minutes, which can be due to the effect of capture cross section area.

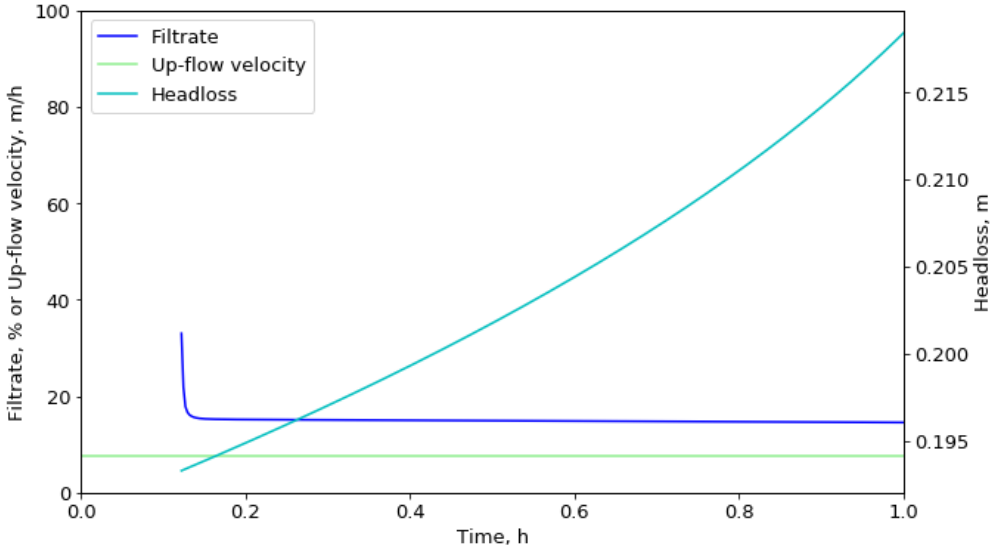

Figure 4.14: Calculated filtrate (C/C_0) profile with the duration of 1 h from model verification with the complex method for A_c estimation.

4.3.1.2.3 FIXED CAPTURE CROSS SECTION AREA

To investigate the role of capture cross section area on particle capture, the capture cross section area was fixed as initial state. This means K_F was equal to 1 and the area was the ring area around the clean grain. The results are displayed in Table 4.5 and Figure 4.15.

Table 4.5 shows that there was a linear increase with time in DEP when the capture cross section area was not calibrated. The constant particle capture efficiency was observed in Figure 4.15. Compared to the result from geometrical estimation of the capture cross section area, they had big differences. It was likely due to the participation of the changes in capture cross section area. The increasing capture cross section possibly contribute to the improvement of particle capture in granular filtration beds.

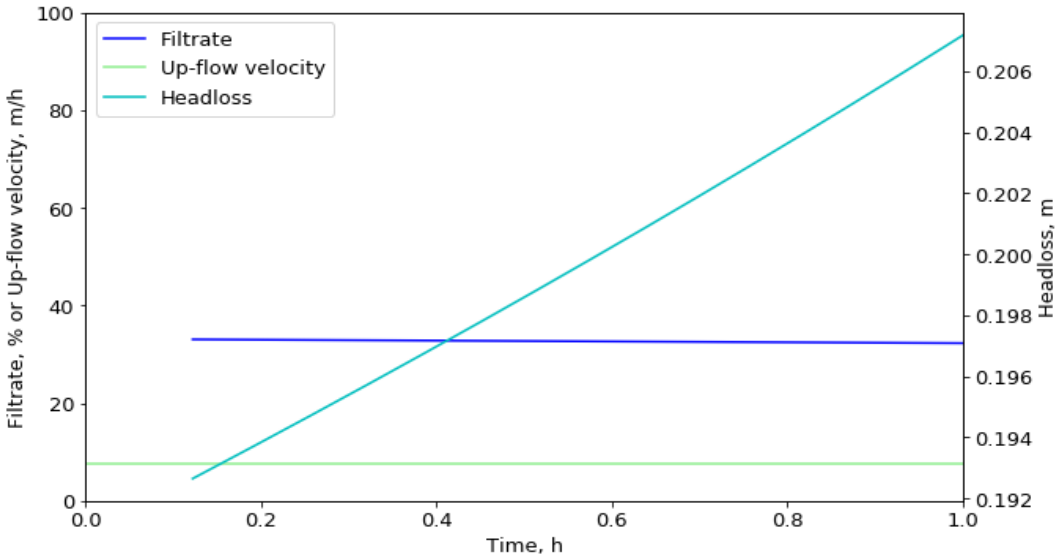

Figure 4.15: Filtrate (C/C_0), headloss and up-flow velocity profile with the duration of 1 h from model verification without A_c calibration.

4.3.1.3 FILTRATION EFFICIENCY COMPARISON

As compared to the figure from Stevenson (1997) model (Figure 4.16), the two curve trends within 1 h were the same. Initially, the filtration efficiency in the thesis model was similar to that in the Stevenson (1997) model. After that, the filtration efficiency in thesis model was a bit lower than that in the Stevenson (1997) model. In addition, the time cost for experiencing the ripening stage in Stevenson (1997) model was about four times longer than that in thesis model. The other possible reasons for these two differences are discussed in Paragraph 5.5.

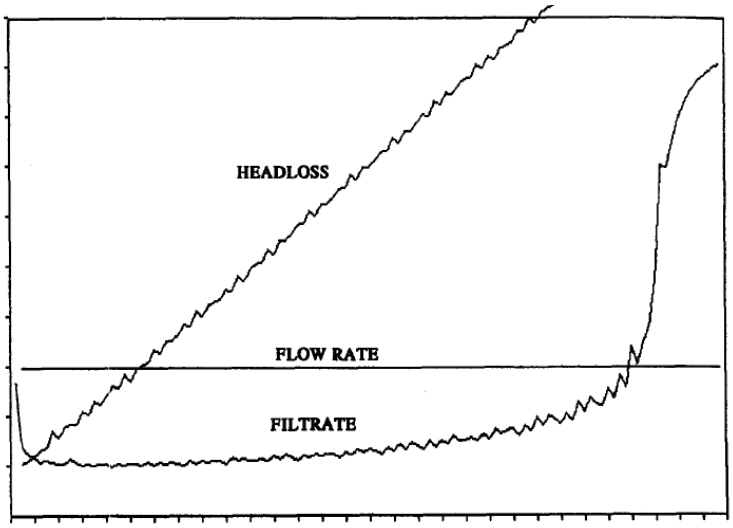

Figure 4.16: Filtrate (C/C_0), headloss and up-flow velocity profile (Stevenson, 1997) with 30 h duration. The unit for y-axis was m (meters) for headloss, m/h for flow rate and %

for filtrate. The unit for x-axis was h (hours) with 1 h interval. The maximum value in y-axis was 2 m for headloss, 100 % for filtrate and 2.5 m/h for flow rate.

4.3.2 EXPERIMENT SIMULATION

The experiment was simulated by the thesis model and the applied initial conditions are shown in Table 3.4. The simulation results are displayed in Table 4.7, which shows that almost all particles less than 100 µm can be captured by the bed except 5 µm organic particles. The total organic capture efficiency (94 %) in the model contained the contribution of transport mechanism, which was much higher than the result (43 %) from the wastewater plug-flow experiment (Figure 4.10). This is discussed in Paragraph 5.5.

Table 4.7: Capture coefficient ($(C_0-C)/C_0$ %) for different particle size fractions

Particle property	5 µm (0.45-10 µm)	27 µm (10-45 µm)	72µm (45-100 µm)	Total (organic or inorganic)
Organic	76	100	100	94
Inorganic	100	100	100	100

To investigate the main transport mechanism in different particle size fraction, each mechanism was tried while the remaining two mechanisms were shut off. The result is shown in Table 4.8. The result from settlement was classified into organic part and inorganic part. This was because that settlement efficiency calculation related to the particle property (density). There was a big difference in density between organic particles and inorganic particles (Table 3.4).

It is obvious in Table 4.8 that the capture efficiency of interception increased with increasing particle size. The capture efficiency of diffusion worked in an adverse way, which decreased with increasing particle size. Therefore, for the particles in the range of 10-45 µm and 45-100 µm, the main capture mechanisms were possibly settlement and interception. For the 0.45-10 µm particles, the main capture mechanism was likely settlement. When changed the average particle size of 5 µm for 0.45-10 µm size range to 0.45 µm, the main capture mechanism was possibly diffusion. As shown in Table 4.8, the settlement mechanism reached the highest total capture efficiency compared to the other two mechanisms.

Table 4.8: Capture coefficient ($(C_0-C)/C_0$ %) for different particle size fractions in the sole function of each mechanism.

Mechanism		5 µm (0.45-10 µm)	27 µm (10-45 µm)	72 µm (45-100 µm)	Total
Settlement	Organic	74	100	100	95
	Inorganic	100	100	100	
Interception		7	83	100	74
Diffusion		2	1	0.3	1

5 DISCUSSIONS

5.1 LITTLE CONTRIBUTION OF PROTOZOA

It is quite likely that the protozoa can contribute little on wastewater particle capture and removal in anaerobic period.

Firstly, anaerobic protozoa can be hard to survive in several aeration periods in AGS system due to their oxygen sensitivity.

Secondly, the produced hydrogen through hydrogen production pathway cannot be efficiently removed by influent flow. The assumption that glucose was the only substrate in domestic wastewater indeed disobeyed the real situation since the composition in wastewater is more complicated. In the wastewater, more energy is needed for protozoa to convert different kinds of complex substrate to hydrogen. Thus, it is harder than only consuming glucose, and even less contribution of protozoa can be made on particle removal. The protozoa activities will be depressed by the high hydrogen partial pressure. Besides, few detections of methanogens on AGS and short anaerobic SRT led to low possibility of hydrogen removal by methanogens. Additionally, the position of methanogen should be near the anaerobic protozoa for consuming hydrogen immediately. This means the methanogens should be on granule surfaces. But it is hard for strictly anaerobic methanogens to live on granule surfaces. Experiments can be carried out if the presence of methanogens needs be checked. There are two methods that can be applied to detect the existence of methanogens. The first method is to apply metagenomics to analyze the presence of methanogens. The second method is similar to the method of Pronk, Abbas, Kleerebezem, et al. (2015), which is mentioned in the previous paragraph. One small volume glassware can be prepared, and the aerobic granules can be put into the bottle. The nitrogen gas can be used for flushing the glassware for creating an anaerobic condition. The methanol can be injected into the glassware. Then, the glassware can be put on the shaker for shaking couple hours under room temperature (20 ℃). Gas samples can be collected from the headspace of the glassware. The existence of methane can be analyzed by the use of the gas chromatograph (GC).

Lastly, ethanol production pathway is likely to rarely happen in anaerobic protozoa due to much less studies on ethanol production pathway compared to hydrogen production pathway. If the existence of ethanol-production protozoa in AGS is necessary to be verified, the experiments can be applied. If the experiment can prove the production of ethanol, the ethanol-production protozoa can exist in AGS.

Besides, it is also possible that this kind of protozoa can degrade complex particulate organic matter into easily biodegradable substrate, which is ethanol. Then, the produced ethanol can be food to feed microorganisms in AGS during aerobic period. Thus, compared to degrade all complex organic matter in aerobic period, the ethanol production process during anaerobic period can increase degradation rate in aerobic period. Therefore, the contribution of ethanol-production protozoa can show potential abilities to increase particle removal efficiency among the whole Nereda process.

To investigate the production of ethanol via experiment, the easily biodegradable glucose solution can be prepared. The aerobic granules and the glucose solution can be put in a small volume glassware. Then, the nitrogen gas can be applied into the glassware to make it anaerobic. The glucose solution can be injected into the glassware and the glassware can be put on the shaker for several hours under room temperature (20 ℃). Then, the solution can be sampled. To detect the existence of ethanol in the samples, GC can be utilized.

5.2 CONSTANT PARTICLE CAPTURE IN AGS

As shown in the wastewater plug-flow experiment result (Figure 4.10), the particle capture was constant with time. Since the AGS bed can be like the granular filtration bed, the constant particle capture was possibly due to the low influent particle concentration. As stated in Paragraph 4.3.1.1.2, the low particle concentration is likely to result in no wormhole formation in AGS systems. The change in bed porosity with 1 h feeding duration was very small, because there was only a 9 % decrease in porosity even under an extreme assumption (Paragraph 4.3.1.1.2). Besides, if all influent particles are captured by the first layer with 1 h duration, the capture cross section area only increased by 0.1 %. The calculation was simplified by not considering the overlapping area. The overlapping area includes the intersection area between deposited neighboring particles, and between deposited particles and granules. Therefore, the actual capture cross section area increased by even less than 0.1 %. Additionally, in rapid sand filtration, the filtration velocity is 5 to 25 m/h (Au, 2005), which is much higher than the up-flow velocity of 1 m/h in plug-flow experiment. Since the rapid sand filtration is mostly utilized for surface water and groundwater treatment (TUDelft), the influent particle concentration is lower than that in wastewater. In this case, the runtime of rapid sand filtration is few days (TUDelft). The filtration velocity in Stevenson (1997) was 7.5 m/h which is in the range of 5 to 25 m/h, and the particle concentration was higher than that of wastewater used in the plug-flow experiment. The breakthrough happened in Stevenson (1997) when the duration reached nearly 30 h. Since the up-flow velocity

and the particle concentration in wastewater plug-flow experiment are lower than that in Stevenson (1997), the influence of deposited particles on granules' surface roughness can be not as significant as that in Stevenson (1997). Thus, the capture cross section area is unlikely to greatly affect the capture efficiency. The AGS bed was possibly in the initial period of the ripening stage, in which there was not so much particle deposited on granules. The ripening stage is the first stage in filtration process (Figure 2.1), which is caused by the effect of deposited particles (Ginn Jr et al., 1992; Keir et al., 2009). Therefore, it is likely that most of surface areas in AGS bed were available for particle capture.

According to Vigneswaran et al. (1990) who conducted a granular filtration experiment, the removal efficiency in their experiment for all sizes particle was improved when the duration was 5 h as compared to the removal efficiency with 1 h and 2 h duration (Table 5.1). But after 5 h, the performance of particle removal started to worsen due to particle detachment. Therefore, there was an improving performance in the first several hours in the filtration bed, which is likely to experience the ripening stage and effective filtration stage. The particle concentration is similar to that in wastewater plug-flow experiment, and the filtration velocity (5 m/h) is much higher than 1 m/h in plug-flow experiment. Hence, most likely that the high filtration velocity and long duration led to porosity decrease, and then causes capture efficiency improvement. It is possible to improve the capture efficiency in AGS bed by prolonging anaerobic feeding duration for more than two hours. Longer anaerobic period gives more time for the fermentation of adsorbed substrate and have positive impact on the stability of AGS (Corsino et al., 2017; De Kreuk et al., 2010). However, the extended anaerobic period (more than 90 min) negatively influences the phosphorus removal process (Wang et al., 2011; Wang et al., 2013). And the nitrogen removal is affected by the ratio of anaerobic and aerobic duration (Huang et al., 2019). Therefore, the duration adjustment can be limited by the performance of phosphorus removal and nitrogen removal. So the capture efficiency can be hardly affected.

Table 5.1: Removal efficiency for each size particle with different duration (Vigneswaran et al., 1990)

Duration, h	Particle size, μm		
	22	50	85
1	20 %	35 %	60 %
2	35 %	40 %	65 %
5	55 %	70 %	70 %

5.3 IMPORTANCE OF SMALL PARTICLES

For the influent particles smaller than 100 μm, the small particles in the size range of 0.45 to 10 μm should be paid more attention in later AGS research than the other two size ranges particles.

Figure 4.10 describes the capture efficiency for the particle in the range of 45-100 μm and 10-45 μm was much higher than the 0.45-10 μm particles. In addition, as shown in Figure 4.11, influent and effluent COD concentration in both 10-45 μm and 45-100 μm particles was much lower than that in 0.45-10 μm particles. Thus, high amount of COD in 0.45-10 μm was not captured in the sludge bed at the end of anaerobic period.

As presented in Paragraph 2.1, the AGS bed is likely to act as the granular filtration bed in the anaerobic period. In a filtration bed, the larger particles are easier to be retained in the filter bed than smaller particles (Tiehm et al., 1999). Even for small particles with the size range of 1 to 10 μm, the bigger the particles, the higher the removal efficiency (Kim et al., 2018). Differently sized particles are dominated by different transport mechanisms. The particles with the size less than 1 μm are mainly captured by diffusion. For the particles with big sizes, they are mainly captured through settlement. The capture process of relatively big particles can also be controlled by interception (Kaminski et al., 1997). In the plug-flow experiment with wastewater (Figure 4.10), the particle capture efficiency shows a rising trend with increasing particle size, which was the same as the experiment result from Vigneswaran et al. (1990). In Figure 4.10, the 45 to 100 μm particles' capture efficiency was a bit higher than that of 10 to 45 μm particles and much higher than that of 0.45 to 10 μm particles. Thus, based on the aforementioned literature, the plug-flow experiment result in Figure 4.10, and the experimental simulation result in Table 4.8, the main contributed transport mechanisms for 1-100 μm particles are likely settlement and interception due to their relatively big size. For the size range of 0.45-1 μm, diffusion can be main transport mechanism.

However, as shown in Table 5.2, the settlement velocity of organic particles is less than the up-flow velocity of 1 m/h until the particle size is 40 μm. The settlement velocity increases with particle size based on the Stokes' equation. Therefore, the organic particles with the size between 40 to 100 μm was most likely stay in the reactor, resulting in a bit higher COD capture efficiency in 45-100 μm particles than 10-45 μm particles. The low settlement velocity for particles in the size range of 0.45-10 μm can possibly lead to low COD capture efficiency. The settlement velocity of inorganic particles reaches 1 m/h when the particle size is 18 μm. Hence, the majority particles in the effluent were possibly 0.45-10 μm particles and 10-45 μm organic particles. This speculation stated above can be verified by carrying out

the up-flow wastewater experiment without granules. Besides, as mentioned in the Paragraph 2.2, inertia is one of transport mechanisms, which increases with mass. So the big size particles have stronger inertia than small particles. When the streamline of influent is going to encounter the granules, the streamline starts to bend in order to pass the granule. At this moment, the particles with enough big inertia keep the trajectory of previous streamline, possibly resulting in the collision between particles and granule surfaces. The inertia can possibly explain the phenomenon that the particle capture efficiency increased with increasing particle size.

Table 5.2: Settlement velocity (m/h) for different property and size particles

Particle property	Particle size, μm			
	1	18	40	100
Organic	5.8×10^{-4}	0.2	1	5.8
Inorganic	3.1×10^{-3}	1	5	31

The phenomenon of low treatment efficiency of 0.45 to 10 μm particles was also observed in biofilm systems. Bouwer (1987) theoretically studied the influence of particle size on the treatment efficiency of carrier biofilm. He summarized that for particles larger than 10 μm, they were mainly removed by settlement. For particle less than 1 μm, the removal process was controlled by diffusion. The particles in the range of 1 to 10 μm were hardest to be removed in biofilm system, which was also concluded in the research of García-Mesa et al. (2010). Since carrier biofilm can be like aerobic granules, both of which contain EPS on the surface as the main component (Zhu et al., 2012). The porosity in biofilm can be different from that in AGS. According to Eisenmann et al. (2001), Van Benthum et al. (1995) and Tijhuis et al. (1994), the presence of pores, including cracks, fissures or crevices, gave rise to the absorption of around 1 μm particles. However, the particulate substrate (> 0.45 μm) is unable to be incorporated in aerobic granules (De Kreuk et al., 2010). In the domestic wastewater used in the plug-flow experiment, the COD between 0.45 to 1 μm and 1 to 10 μm took up 7 % and 93 % COD in the range of 0.45 to 10 μm, respectively. Therefore, most particles (0.45 to 10 μm) which were not captured in the bed are in the size range of 1 to 10 μm. Thus, the particles in the range of 1 to 10 μm can be more difficult to be captured by AGS than other size ranges of particles. Due to dense structure of aerobic granules, 1 to 10 μm particles are possibly harder to be captured in AGS systems within anaerobic period than that in biofilm systems.

The small size range of particles (1 to 10 μm) possibly needs more focus in the research of the interaction with granule surfaces, and the investigation of applicable

methods to increase the capture efficiency than other size ranges. The importance of small size particles is due to the low capture efficiency in anaerobic period. Besides, the COD content in small size particles (1 to 10 µm) took up 28 % of total COD as displayed in Figure 5.1. The low capture efficiency of small particles in anaerobic phase can possibly lead to high COD content left in the effluent, negatively influencing wastewater treatment efficiency.

Nevertheless, wastewater particles larger than 100 µm was not considered in this study, but in real wastewater, there are particles larger than 100 µm. Figure 5.1 displays the influent COD % for particles in five size ranges. It is obvious that COD % in 0.45-10 µm and >100 µm was much higher than that in 10-100 µm particles, and similar to the COD % in soluable content (< 0.45 µm). There was no big difference in COD % between particles in the size range of 0.45-10 µm and larger than 100 µm.

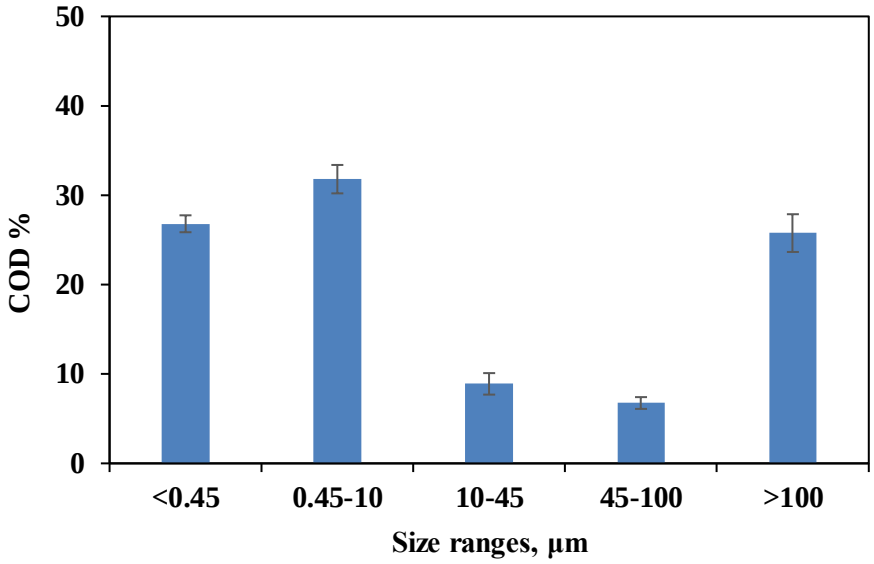

Figure 5.1: Influent COD % for particles in four size ranges. COD % = COD for each size range / TCOD

The relatively low removal efficiency of big wastewater particles was observed in the AGS research of Schwarzenbeck et al. (2004). The malting wastewater with high particle concentration was used for feeding the AGS bed. The reactor was working for the whole cycle with total duration of 8 h with 6 min filling period and 2 h anaerobic no mix condition. The particle removal efficiency for each size range is shown in Table 5.3. Different particle fractionation methods were applied for wastewater fractionation. Settlement with 1 h duration was applied for classifying particles with the size roughly larger than 25 to 50 µm. The particles larger than 1 µm was separated through centrifugation. For wastewater content less than 0.2 µm, filtration was applied. Schwarzenbeck et al. (2004) regarded wastewater substrate less than 0.2 µm as soluble content. Most particles were larger than 25-50 µm, taking up 91 % of total COD. In the domestic wastewater used for the plug-flow experiment,

PCOD took up 67 % of total COD, which is much lower than 91 % in malting wastewater.

Table 5.3: Particle removal efficiency from the literature (Schwarzenbeck et al., 2004)

Particle size range, µm	COD removal efficiency, %
> 0.2	41
> 25-50	43
>1 and < 25-50	72
> 0.2 and < 1	98

As shown in Table 5.3, the COD removal efficiency (> 0.2 µm) was 41 %, which was similar to the result from the wastewater column experiment (43 %) shown in Figure 4.10. The COD removal efficiency decreased as increasing particle size, which was opposite to the plug-flow wastewater experiment result. It is likely due to the addition of aeration step, the applied oxygen bubble entered the reactor and loosed the aerobic granular sludge bed, resulting in release process of particle captured by filtering effect during anaerobic period. The release process of micro-sized particles captured by AGS bed due to resuspension of sludge bed was observed in the research of Ranzinger et al. (2020).

The COD removal efficiency for particles larger than 25-50 µm was 43 % (Table 5.3), which was much lower than 95% for 45 to 100 µm particles' capture efficiency from wastewater plug-flow experiment. For the particle size range of 1 to 25-50 µm, the COD removal efficiency was 72 %. This was a bit lower than the capture efficiency of 83 % for 10-45 µm particles. The differences can be due to several reasons. Firstly, the particle fractionation method of settlement used in Schwarzenbeck et al. (2004) result in the inaccurate particle classification of 25-50 µm. This leads to difficulties to make data comparison with thesis experiment. Secondly, some captured particles in these two size ranges were likely to be released during aeration period. The filtration efficiency increases by increasing particle size (Kim et al., 2018; Tiehm et al., 1999). But the particle removal efficiency of big size particles (>25-50 µm) was much lower than that of 1 to 25-50 µm particles after aeration period. Thus, the big size range particles (>25-50 µm) are likely to release more percentage of captured particles than particles in the size range of 1 to 25-50 µm. The deposited particles, which were not released during aeration, were possibly firstly transported to the granule surface by transport mechanism and then tightly stick on the surface by adsorption. So this is likely to indicate that the larger the particles, the harder for particles to stay on granules in aeration period. According to Ranzinger et al. (2020), the micrometer-sized particles accumulated on the granule surfaces layer by layer, resulting in the release process when the AGS bed

became loose. But the preference size for particle releasing after anaerobic feeding period was not studied in this research. For big particles, they are more possible to be captured by flocs in the AGS system than by granules in aeration phase (Pronk, De Kreuk, et al., 2015). Due to the lower settling velocity of flocs than granules, the loose flocs can be washed out by selection pressure. The waste AGS with captured big particles are potential for energy recovery in the form of biogas with the use of anaerobic digestion (Guo et al., 2020). Thirdly, the 1-10 µm particles were included in the range of 1 to 25-50 µm, which were hard to be treated. The involvement of 1-10 µm particles can give a negative impact on the removal efficiency of 1 to 25-50 µm particles.

The removal efficiency for 0.2 to 1 µm particles was 98 %. Such a high removal efficiency can be partly due to protozoans' activities in consuming organic particles during aeration. Additionally, the soluble substrate (0.2 to 0.45 µm) can easily enter the granules. The 0.45 to 1 µm particles can be captured by diffusion in anaerobic period. After that, adsorption might possibly take an important role to fix these small size range particles on granule surfaces, avoiding detachment in aeration phase. Besides, the influent filling period of 6 min was applied to feed the reactor with the volume exchange ratio of 66 %. Since the reactor volume (12 L) is much larger than that in the thesis reactor (1 L), the influent feeding rate is higher than the feeding rate (1 m/h) applied in wastewater plug-flow experiment. Kaminski et al. (1997) shows the capture efficiency with different size ranges in granular filtration bed changed with different up-flow velocities. In the research of Yu et al. (2018), the filtration efficiency in granular filtration bed decreased with increasing filtration velocity. Since the up-flow velocity in plug-flow experiment is lower than that in Schwarzenbeck et al. (2004), the capture efficiency in Schwarzenbeck et al. (2004) can possibly lower than that in plug-flow experiment if the feeding patterns are the same. However, the no mix anaerobic condition is likely to provide an environment for the interaction between granules and particles without interferes of flow. Sepúlveda-Mardones et al. (2019) reported that different feeding patterns and dissimilar wastewater composition and fractionation partly influenced the AGS particle treatment effectiveness. Besides, it is possible to lower the up-flow velocity for improving particle capture efficiency. Nevertheless, to treat the same amount of wastewater per cycle, lower the up-flow velocity means longer the anaerobic feeding duration. If the up-flow velocity is low but the anaerobic duration is fixed, less wastewater will be treated, which is not good for amount of wastewater treatment efficiency. Since only the particle captured by adsorption in anaerobic period can be removed in aeration phase, to what extent can up-flow velocity influence the particle adsorption efficiency in anaerobic phase should be explored.

Therefore, for domestic wastewater particles less than 100 μm, more attention should be paid to 1-10 μm particles on AGS research. For the real domestic wastewater, not only 1-10 μm particles need more focuses, but also the particles larger than 100 μm need to be studied. By comparing the anaerobic plug-flow experiment result, and the whole cycle result from Schwarzenbeck et al. (2004), there are many possible reasons leading to such distinctive results. This needs to be verified by further investigating the contribution of filtering effect and adsorption mechanism, and the influence of up-flow velocity on particle capture in anaerobic phase of AGS systems.

5.4 AGS AS A GRANULAR FILTRATION SYSTEM

As presented in Paragraph 2.1, the characteristics of granular filtration beds are similar to AGS systems. However, there are some differences.

Firstly, the filter media in the granular filtration bed is usually sands and in the AGS system is aerobic granular sludge. Although their shapes are spherical or relatively spherical, the inner characteristics are not the same. The sands or other inorganic solids in the granular filtration bed are physical material, and the aerobic granules are biological material. This dissimilarity is obvious when treating wastewater. For wastewater soluble organic pollutants (less than 0.45 μm), they are able to diffuse into the granules and be consumed by microorganisms growing in the aerobic granules (Pronk, Abbas, Al-Zuhairy, et al., 2015). For the sand or anthracite as filter media, the pollutants cannot enter grains' inner part. Thus, in the AGS system, the whole aerobic granules contribute to the wastewater treatment, while in the granular filtration bed, only the grain surface is effective for capturing pollutants.

The second difference is relevant with EPS contribution on particle capture in both systems. For the granular filtration bed, since the nutrient is likely to be captured in the first several layers in the filtration bed, this can benefit the growth of microorganisms and protozoa in these layers. But these small living creatures cannot be evenly distributed among the whole filtration bed. Then, the contribution of them and their secreted EPS on particle capture can possibly not be as efficient as that in AGS systems.

As stated in Paragraph 2.4, the surface interaction and bridge effect are the specified mechanism of adsorption by EPS. For the surface interaction including hydrophobic interaction and hydrophilic interaction, the effectiveness of them depends on the wastewater particles' characteristics. But the hydrophobic or hydrophilic characteristics of particles in the wastewater depend on their specific functional groups in their structures. For the bridge effect, the suspended solids in the

wastewater are mostly negatively charged (Lee et al., 2014). Since the charge and the zeta potential in EPS is generally negative (Esparza-Soto & Westerhoff, 2003; Liu & Fang, 2003; Subramanian et al., 2010; Wang et al., 2014), there is a repelling force between particles and aerobic granules if the surface interaction is neglected. This can negatively affect the particle efficiency. According to Wang et al. (2012), when the surface charge of aerobic granules was low and the hydrophobicity is high, the influence of hydrophobic interaction was greater than that of bridge effect. In this case, the repelling force can possibly be negligible. Besides, there are multivalent cations (Mg^{2+}, Ca^{2+}) exist in the wastewater (Bunani et al., 2015; Le Bonté et al., 2008), which can neutralize the negative charge of EPS and then improve the adsorption process (Boltz & La Motta, 2007; Wang et al., 2012). Therefore, the adsorption can contribute to particle capture in the wastewater plug-flow experiment, which is worth to be investigated in the future.

Thirdly, there is a difference about performance of captured particles among the whole operation cycle. Due to different operation process, the particles loosely captured by the filtering effect in anaerobic phase of AGS system can be released when the aeration phase starts. In the granular filtration beds, the particles captured in the bed are permanent removed and stayed in the bed until backwashing (Biskner & Young, 2000). Thus, the filtering effect is a permanent mechanism in granular filtration beds and a temporary mechanism in AGS systems when considering the whole operation cycle. But if only the anaerobic phase is considered, the filtering effect is a permanent mechanism in AGS system.

Since the main objective of thesis is to focus on the performance of AGS bed on particle capture in anaerobic period. The soluble pollutants' removal mentioned in the first aspect does not meet this objective. Thus, the difference in the inner part of filter media can be neglected. Towards to the second aspect about EPS and microorganisms' distribution, the EPS in the granular filtration bed has abilities to remove pollutants in the wastewater. This is like the performance of EPS in AGS systems, though the amount of EPS contribution on particle capture in these two systems is different. For the last difference about the filtering effect, since the investigation range is in anaerobic phase, the particle captured by filtering effect can stay in the AGS bed. Thus, the filtering effect can do contribution on particle capture in AGS, which is similar to granular filtration beds. Overall, the aerobic granular sludge in anaerobic phase can be regarded as granular filtration beds.

As aforementioned in Paragraph 5.3, particles need to be transported on the granule surfaces before being adsorbed. Hence, increasing the transport efficiency in anaerobic period seems can improve the adsorption efficiency and then the particle removal efficiency. However, Pronk, Abbas, Al-Zuhairy, et al. (2015) reported that the complex particulate substrate on granule surface led to finger type structure due

to low hydrolysis rate of complex substrate and lack of readily biodegradable compounds. Thus, even if the adsorption efficiency can increase, the granules are possibly hard to deal with so many particulate substrates, which can have a negative impact on granule morphology and worse the effluent quality. So not only the methods to improve the transport efficiency and the adsorption efficiency are important, the hydrolysis rate should also be paid attention. Besides, as presented in Paragraph 4.3.1.1.2, there was possibly no wormhole formation in AGS bed within one cycle. But after running several cycles, if the adsorption rate is higher than the hydrolysis rate or the influent particle concentration is high, the granule surfaces is likely to be filled up. Then, particles are possibly deposited on deposits and released during aeration period, leading to bad effluent quality. Therefore, the balance between adsorption and hydrolysis is necessary to be investigated for avoiding finger type structure and maintaining the performance of AGS system.

That balance can possibly reach by adjusting the operation conditions like up-flow velocity. Nevertheless, different wastewater such as domestic wastewater and industrial wastewater have different particulate substrate composition, and even same kind of wastewater have different components to some extent. It is inconvenient to optimize the operation condition for each AGS system in each WWTP. The model included whole AGS cycle is possible to predict the AGS performance on removing particulate substrate in different kinds of wastewater with different operation conditions. Hence, the thesis model is likely to be more applicable if not only the adsorption mechanism in anaerobic condition is involved as mentioned in Paragraph 5.5, but also the aeration phase in the AGS cycle and particle hydrolysis rate. After that, the model should be verified by experiments with different wastewater to make it flexible for future application.

5.5 THE USE OF FILTRATION MODELS IN AGS RESEARCH

The granular filtration models are important in AGS research especially in anaerobic period since the filtration process can also happen in AGS system.

The model described the particle capture process by specifying into three different mechanisms (settlement, interception and diffusion). The influence of particle deposition on the particle capture process was presented in the model by the participation of capture cross section areas as stated in Paragraph 4.3.1.2. The changes of capture cross section area did affect the interception capture process and then the total particle capture process. Although the granules' surface can probably be not affected a lot by the deposited particles in the experiment as presented in Paragraph 5.2, this was based on the condition of filtered wastewater. In the real domestic wastewater, the particle concentration must be higher than that applied in

the plug-flow experiment. In this case, the capture efficiency is possibly influenced by the changing of capture cross section area.

The other important phenomenon in granular filtration models was the wormhole formation (Paragraph 2.1) since the involvement of wormholes can show the detachment of the deposits and predict the backwash frequency (Ginn Jr et al., 1992). However, as described in Paragraph 4.3.1.1, it is likely that there was no wormhole formation in AGS bed. Thus, the influence of wormholes in AGS system can be not as vital as that in filtration system. However, the AGS system in anaerobic period worked like the initial phase of filtration bed before wormhole formation. The initial phase is still part of the filtration process, which can be simulated by the model.

All in all, the model can not only describe the particle capture process but can also give hints about the contribution of the transport mechanism on different particle size fractions.

Nevertheless, the model needs to be further improved in some ways.

Firstly, the estimation method for the capture cross section area needs to be revised. In the Paragraph 4.3.1.2.1, the capture cross section area was estimated only based on three data group. This inaccurate method caused inaccurate estimation on K_F, resulting in little influence of capture cross section area on particle capture. The other way was to estimate the area by a geometrical way (Paragraph 4.3.1.2.2), which was too complicated. Since the deposition position of each particle was unknown, the overlapped area between deposited particles in the same layer cannot be estimated. The intersection area between different layer deposited particles were calculated in an imprecise way. This method focused excessively on each deposited particle. Thus, one compromised method between these two methods needs to be come up with for the estimation of capture cross section areas. The method should describe the influence of the capture cross section area on particle capture process in a reasonable simplified way without taking each particle's condition into account.

Secondly, the time step set in the thesis model can be different from that in Stevenson (1997) model. This can be the other possible reason for the different results between the thesis model and the Stevenson model. The time step set in Stevenson (1997) was unclear. But based on the output figure (Figure 4.16) from Stevenson (1997), 15 min was possible to be its time step since there are four peaks in 1 hour. Also, it was said that the iteration was 15 min in the output table (Appendix C.5 Table C. 1). In addition, the paper was published in the end of 20th century, the computer technology was not as good as that in nowadays. It was mentioned in Stevenson (1997) that the model was limited by computer limitation. Thus, it can be possible that the author recorded the data with a frequency of 15 min. Within the first 15 min, the capture cross section area can be fixed as the initial grain

ring area. When the second 15 min started, the capture cross section area can rise a lot, starting to increase exponentially in DEP (Table 4.5). The long time step can give rise to the delayed in the calibration of capture cross section areas, which can also lead to less particle captured by interception and then less total particle capture efficiency in the beginning. This is likely to be the reason for the higher filtrate or lower capture efficiency in the initial stage of Stevenson model (Figure 4.16) than in thesis model (Figure 4.14). Thus, the capture efficiency was improved slowly in the beginning and increased in a high rate after 15 min in Stevenson model. In the thesis model, the capture cross section area was updated by every 8.64 seconds. The changes in capture cross section areas were much more frequent than that in the Stevenson model, attributing to immediate changes in capture efficiency. But the capture efficiency in the effective filtration stage in thesis model (Figure 4.14) was a bit lower than that in the Stevenson model (Figure 4.16). This is likely due to the underestimation the capture cross section area estimation since the deposition layer was assumed to be only two in the complex estimation method. For model verification, the time step should be modified to 15 min. But from the perspective of applicability, the short time step can be closer to the deposition process happens in the reactor compared to the long time step. The shorter the time step, the more accurate the result is. But the computation time will also increase. In the model, the outcome was not affected by shortening the time step less than 8.64 s.

Thirdly, Experiments are needed for improving the model. There was no calibration factor in the model, which also needs to be added and adjust by utilizing the experiment data.

Lastly, the model was based on the simplified filtration model which only contained transport mechanism. In the anaerobic phase of AGS system, adsorption is the other particle capture mechanism. Therefore, the model can be more applicable and complete in AGS research if the adsorption mechanism can be added in the model.

5.6 GENERAL DISCUSSION

In anaerobic period of AGS systems, protozoa are unlikely to consume particles due to the limitation of hydrogen partial pressure and the absence of methanogens on granule surfaces (Paragraph 5.1). The filtering effect, which was dependent on the transport mechanisms, can contribute on particle capture. The adsorption mechanism is dependent on the forces (surface interaction and bridge effect) between deposited particles and EPS on granule surfaces (Nouha et al., 2018; Wang et al., 2012). If the forces are balanced with or less than the high shear stress generated in aeration period, the particles are likely to be adsorbed and hydrolyzed on granules. But the particles captured by adsorption should be firstly transported

on the granules. Therefore, the transport efficiency can possibly determine the adsorption efficiency.

From the plug-flow experiment result, the capture efficiency of big particles was higher than that of small particles. According to the result from Schwarzenbeck et al. (2004) and the discussion in Paragraph 5.3, the big particles are probably harder to stick on the granule surfaces through adsorption compared to the small particles, and are mostly released to the bulk phase during aeration (Ranzinger et al., 2020). The small particles are likely to be easily adsorbed through EPS interaction. However, the small particles in the size range of 1 to 10 μm are hard to be captured. Thus, the big particles have both high capture and release efficiency and the small particles (1-10 μm) has high adsorption efficiency but low capture efficiency. These 1-10 μm particles can hardly interact with EPS on granule surface. The particles in the size range of 0.45 to 1 μm can be captured by diffusion mechanism. But due to the small size range and low composition among PCOD in domestic wastewater used in plug-flow experiment, 0.45-1 μm particles can contribute little to the particle removal process. Therefore, the anaerobic phase most likely contributes little to the particle removal over the whole AGS cycle. For verifying this conclusion, the fluidization experiment should be performed for investigating the capture efficiency of filtering effect mechanism and adsorption mechanism on different size particles.

Besides, from the wastewater plug-flow experiment, the capture efficiency for influent organic matter less than 0.45 μm was 73 %. In the research of Pronk, Abbas, Al-Zuhairy, et al. (2015) and Ranzinger et al. (2020), soluble organic matters or nanometer-sized pollutants diffused into granules with evenly distribution over the whole granules, and these compounds were consumed in aeration phase. Therefore, the anaerobic phase can play a more important role in treating soluble pollutants than particulate pollutants.

6 CONCLUSIONS & RECOMMENDATIONS

6.1 CONCLUSIONS

Based on the results and discussions stated in Paragraph 4 and 5, the conclusions drawn from this research are as follows:

1. The particle capture efficiency was 95 %, 84 %, and 23 % for particles in the range of 45-100 μm, 10-45 μm, and 0.45-10 μm, respectively. The 1-10 μm particles were hard to be captured.
2. The particle capture efficiency was constant with the duration of 2 hours. Anaerobic feeding duration will have limited influence on particle capture without negatively affecting the phosphorus and nitrogen removal.
3. It is unlikely that the protozoa can contribute on wastewater particle capture and removal in anaerobic period.
4. The AGS system in anaerobic phase can act as granular filtration system and the filtration model can be applicable in AGS research.
5. Anaerobic phase most likely contributes little on particle removal for whole AGS system, but it can be more important on the removal of soluble organic matters than particulate substances.

6.2 RECOMMENDATIONS

The following recommendations were listed below:

1. To verify the importance of anaerobic phase on particle removal, the fluidization should be applied after anaerobic duration. This is for releasing the particles captured by the filtering effect. The capture efficiency of filtering effect mechanism and adsorption mechanism on different size particles can be obtained by comparing the result from the plug-flow experiment with and without fluidization process.
2. The small particles with the size between 1 to 10 μm is worth to be explored since they are likely to be adsorbed through EPS interaction effects better than big particles. Besides, small particles take up high content of particulate substrate in domestic wastewater. But particles in these size range are hard to be captured. Since the final aim is to have a good wastewater treatment efficiency, methods should be applied to improve their capture efficiency.
3. The big particles also constitute high composition of particulate compounds in domestic wastewater with high capture efficiency and possibly relatively low

removal efficiency. Thus, the method for strengthening the EPS interaction effects with big particles should be investigated. This is for improving the contribution of anaerobic phase on particle removal and avoiding their releasing behavior while aeration.

4. The performance of AGS bed on particle removal in aeration phase should be evaluated due to the possibly little contribution of anaerobic feeding period on particle removal.
5. The filtration model in this study should be further improved to be more applicable in AGS research by addition of adsorption mechanism in anaerobic phase and even extending the model range to aerobic phase.

BIBLIOGRAPHY

Abdel-Shafy, H., El-Khateeb, M., & Shehata, M. J. D. a. W. T. (2014). Greywater treatment using different designs of sand filters. *52*(28-30), 5237-5242.

Adin, A. J. W. S. a. T. W. S. (2003). Slow granular filtration for water reuse. *3*(4), 123-130.

Alberty, R. A. (2005). *Thermodynamics of biochemical reactions*: John Wiley & Sons.

APHA. (2017). *Standard methods for the examination of water and wastewater. 23rd edition.*: Washington, D.C.: American Public Health Association.

Au, K. K. J. W. E. (2005). Granular bed and precoat filtration. *1*, 249-252.

Bernard, C., & Fenchel, T. J. E. J. o. P. (1996). Some microaerobic ciliates are facultative anaerobes. *32*(3), 293-297.

Bernardes, R., & Klapwijk, A. J. W. S. a. T. (1996). Biological nutrient removal in a sequencing batch reactor treating domestic wastewater. *33*(3), 29.

Bertrand, J.-C., Caumette, P., Lebaron, P., Matheron, R., Normand, P., & Sime-Ngando, T. (2015). *Environmental microbiology: Fundamentals and applications.*: Springer.

Beun, J., Hendriks, A., Van Loosdrecht, M., Morgenroth, E., Wilderer, P., & Heijnen, J. J. W. r. (1999). Aerobic granulation in a sequencing batch reactor. *33*(10), 2283-2290.

Beun, J., Van Loosdrecht, M., & Heijnen, J. J. W. R. (2002). Aerobic granulation in a sequencing batch airlift reactor. *36*(3), 702-712.

Biskner, C. D., & Young, J. C. (2000). Granular media filter including media settler assembly. In: Google Patents.

Boltz, J. P., & La Motta, E. J. J. W. e. r. (2007). Kinetics of particulate organic matter removal as a response to bioflocculation in aerobic biofilm reactors. *79*(7), 725-735.

Boumba, V. A., Ziavrou, K. S., & Vougiouklakis, T. J. F. s. i. (2008). Biochemical pathways generating post-mortem volatile compounds co-detected during forensic ethanol analyses. *174*(2-3), 133-151.

Bouwer, E. J. J. W. R. (1987). Theoretical investigation of particle deposition in biofilm systems. *21*(12), 1489-1498.

Britannica, E. (2019). Encyclopædia Britannica, Inc., 07 Feb. 2019. In.

Bunani, S., Yörükoğlu, E., Yüksel, Ü., Kabay, N., Yüksel, M., & Sert, G. J. D. (2015). Application of reverse osmosis for reuse of secondary treated urban wastewater in agricultural irrigation. *364*, 68-74.

Burdette, D., & Zeikus, J. J. B. J. (1994). Purification of acetaldehyde dehydrogenase and alcohol dehydrogenases from Thermoanaerobacter ethanolicus 39E and characterization of the secondary-alcohol dehydrogenase (2 Adh) as a bifunctional alcohol dehydrogenase-acetyl-CoA reductive thioesterase. *302*(1), 163-170.

Carlson, G., & Silverstein, J. J. W. R. (1998). Effect of molecular size and charge on biofilm sorption of organic matter. *32*(5), 1580-1592.

Carman, P. C. J. T. I. C. E. (1937). Fluid flow through granular beds. *15*, 150-166.

Čerkasovová, A., Čerkasov, J., & Kulda, J. J. M. b. p. (1984). Metabolic differences between metronidazole resistant and susceptible strains of Tritrichomonas foetus. *11*, 105-118.

Ciuk Karlsson, S. (2015). *Simulating water and pollutant transport in bark, charcoal and sand filters for greywater treatment* (Vol. 85).

Coleman, G. S. J. F. m. l. (1986). The metabolism of rumen ciliate protozoa. *39*(4), 321-344.

Corsino, S. F., di Biase, A., Devlin, T. R., Munz, G., Torregrossa, M., & Oleszkiewicz, J. A. J. B. t. (2017). Effect of extended famine conditions on aerobic granular sludge stability in the treatment of brewery wastewater. *226*, 150-157.

Coulson, J. M., Richardson, J. F., Backhurst, J. R., & Harker, J. H. (1996). *Coulson & Richardson's chemical engineering*: Butterworth-Heinemann.

De Kreuk, M., Heijnen, J., & Van Loosdrecht, M. J. B. a. b. (2005). Simultaneous COD, nitrogen, and phosphate removal by aerobic granular sludge. *90*(6), 761-769.

De Kreuk, M., Kishida, N., Tsuneda, S., & Van Loosdrecht, M. J. W. R. (2010). Behavior of polymeric substrates in an aerobic granular sludge system. *44*(20), 5929-5938.

De Kreuk, M., Kishida, N., & Van Loosdrecht, M. J. W. S. a. T. (2007). Aerobic granular sludge–state of the art. *55*(8-9), 75-81.

De Kreuk, M., McSwain, B., Bathe, S., Tay, S., Schwarzenbeck, N., & Wilderer, P. J. A. g. s. (2005). Discussion outcomes. 165-169.

De Kreuk, M., Pronk, M., & Van Loosdrecht, M. J. W. r. (2005). Formation of aerobic granules and conversion processes in an aerobic granular sludge reactor at moderate and low temperatures. *39*(18), 4476-4484.

De Kreuk, M., & van Loosdrecht, M. J. J. o. E. E. (2006). Formation of aerobic granules with domestic sewage. *132*(6), 694-697.

Dechsiri, C. J. U. M. C. G., University of Groningen. (2004). Particle Transport in Fluidized Beds.

Dignac, M.-F., Urbain, V., Rybacki, D., Bruchet, A., Snidaro, D., Scribe, P. J. W. S., & Technology. (1998). Chemical description of extracellular polymers: implication on activated sludge floc structure. *38*(8-9), 45-53.

Dong, J., Zhang, Z., Yu, Z., Dai, X., Xu, X., Alvarez, P. J., & Zhu, L. J. C. E. J. (2017). Evolution and functional analysis of extracellular polymeric substances during the granulation of aerobic sludge used to treat p-chloroaniline wastewater. *330*, 596-604.

Drury, W. J., Characklis, W. G., & Stewart, P. S. J. W. R. (1993). Interactions of 1 μm latex particles with Pseudomonas aeruginosa biofilms. *27*(7), 1119-1126.

Drzewicki, A., Cydzik-Kwiatkowska, A., & Mieczkowski, D. J. W. E. R. (2017). Impact of High-Nitrogen Leachate on Microfauna of Aerobic Granular Sludge. *89*(9), 890-895.

Eisenmann, H., Letsiou, I., Feuchtinger, A., Beisker, W., Mannweiler, E., Hutzler, P., & Arnz, P. J. A. E. M. (2001). Interception of small particles by flocculent structures, sessile ciliates, and the basic layer of a wastewater biofilm. *67*(9), 4286-4292.

Emelko, M. B., Huck, P. M., & Coffey, B. M. J. J. A. W. W. A. (2005). A review of Cryptosporidium removal by granular media filtration. *97*(12), 101-115.

Esparza-Soto, M., & Westerhoff, P. J. W. r. (2003). Biosorption of humic and fulvic acids to live activated sludge biomass. *37*(10), 2301-2310.

Fenchel, T. (2014). Protozoa and oxygen. *Acta Protozoologica*, *53*(1).

Fenchel, T., Finlay, B., & Gianni, A. J. A. f. P. (1989). Microaerophily in ciliates: responses of an Euplotes species (Hypotrichida) to oxygen tension. *137*(4), 317-330.

Fenchel, T., & Finlay, B. J. (1995). *Ecology and evolution in anoxic worlds*: Oxford; New York: Oxford University Press, 1995.

Fenchel, T., & Finlay, B. J. (2010). Free-living protozoa with endosymbiotic methanogens. In *(Endo) symbiotic methanogenic archaea* (pp. 1-11): Springer.

Fenchel, T., & Finlay, B. J. A. o. m. (1992). Production of methane and hydrogen by anaerobic ciliates containing symbiotic methanogens. *157*(6), 475-480.

Fenchel, T., & Finlay, B. J. J. E. j. o. p. (1991). The biology of free-living anaerobic ciliates. *26*(3-4), 201-215.

Fenchel, T., & Finlay, B. J. J. M. (1990). Oxygen toxicity, respiration and behavioural responses to oxygen in free-living anaerobic ciliates. *136*(10), 1953-1959.

Flamholz, A., Noor, E., Bar-Even, A., & Milo, R. J. N. a. r. (2012). eQuilibrator—the biochemical thermodynamics calculator. *40*(D1), D770-D775.

Flemming, H.-C., Wingender, J., Griegbe, T., & Mayer, C. J. B. r. a. i. t. s. a. c. A. H. A. P. (2000). Physico-chemical properties of biofilms. 19-34.

García-Mesa, J. J., Poyatos, J. M., Delgado, F., & Hontoria, E. J. W., Air, & Soil Pollution. (2010). The influence of biofilm treatment systems on particle size distribution in three wastewater treatment plants. *212*(1-4), 37-49.

Gieseke, A., Purkhold, U., Wagner, M., Amann, R., Schramm, A. J. A., & microbiology, e. (2001). Community structure and activity dynamics of nitrifying bacteria in a phosphate-removing biofilm. *67*(3), 1351-1362.

Ginn Jr, T. M., Amirtharajah, A., & Karr, P. R. J. J. A. W. W. A. (1992). Effects of particle detachment in granular-media filtration. *84*(2), 66-76.

Goosen, N. K., Horemans, A. M., Hillebrand, S. J., Stumm, C. K., & Vogels, G. D. J. A. o. m. (1988). Cultivation of the sapropelic ciliate Plagiopyla nasuta Stein and isolation of the endosymbiont Methanobacterium formicicum. *150*(2), 165-170.

Guo, H., van Lier, J. B., & de Kreuk, M. J. W. r. (2020). Digestibility of waste aerobic granular sludge from a full-scale municipal wastewater treatment system. *173*, 115617.

Guo, W., Ngo, H.-H., & Li, J. J. B. t. (2012). A mini-review on membrane fouling. *122*, 27-34.

Haan, C. T., Barfield, B. J., & Hayes, J. C. (1994). *Design hydrology and sedimentology for small catchments*: Elsevier.

Hamza, I. A., Jurzik, L., & Wilhelm, M. J. J. o. v. m. (2014). Development of a Luminex assay for the simultaneous detection of human enteric viruses in sewage and river water. *204*, 65-72.

Heijnen, J. J., & Kleerebezem, R. J. E. o. I. B. B., Bioseparation, Cell Technology. (2009). Bioenergetics of microbial growth. 1-66.

Hijnen, W. A., Schijven, J., Bonne, P., Visser, A., Medema, G. J. J. W. S., & Technology. (2004). Elimination of viruses, bacteria and protozoan oocysts by slow sand filtration. *50*(1), 147-154.

Hino, T. J. J. J. o. Z. S. (1983). Influence of hydrogen on the fermentation in rumen protozoa, Entodinium species.

Hogg, S. (2013). *Essential microbiology*: John Wiley & Sons.

Huang, W., She, Z., Gao, M., Wang, Q., Jin, C., Zhao, Y., & Guo, L. J. S. o. T. T. E. (2019). Effect of anaerobic/aerobic duration on nitrogen removal and microbial community in a simultaneous partial nitrification and denitrification system under low salinity. *651*, 859-870.

Ienne, S., Freschi, L., Vidotto, V. F., de Souza, T. A., Purgatto, E., & Zingales, B. J. P. (2014). Auxin production by the plant trypanosomatid Phytomonas serpens and auxin homoeostasis in infected tomato fruits. *141*(10), 1299-1310.

Ivanov, V., Tay, J.-H., Tay, S.-L., & Jiang, H.-L. J. W. S. a. T. (2004). Removal of micro-particles by microbial granules used for aerobic wastewater treatment. *50*(12), 147-154.

Ives, K. (1982). *Fundamentals of filtration.* Paper presented at the Proceedings of the 21st European Federation of Chemical Engineering Event Symposium on Water Filtration, Antwerp, Belgium.

Ives, K. J. W. R. (1970). Rapid filtration. *4*(3), 201-223.

Jegatheesan, V., & Vigneswaran, S. J. C. R. i. E. S. a. T. (2005). Deep bed filtration: mathematical models and observations. *35*(6), 515-569.

Jorand, F., Boue-Bigne, F., Block, J., & Urbain, V. J. W. S. a. T. (1998). Hydrophobic/hydrophilic properties of activated sludge exopolymeric substances. *37*(4-5), 307.

Kaminski, I., Vescan, N., & Adin, A. J. W. s. a. t. (1997). Particle size distribution and wastewater filter performance. *36*(4), 217-224.

Katznelson, R. (1989). Clogging of groundwater recharge basins by cyanobacterial mats. *FEMS Microbiology Ecology, 5*(4), 231-242.

Keir, G., Jegatheesan, V., Vigneswaran, S., & Saravanamuthu, V. J. W. a. w. t. t. (2009). Deep bed filtration: modeling theory and practice. 263-307.

Kengen, S. W., Goorissen, H. P., Verhaart, M., van Niel, E., Claassen, P., & Stams, A. J. B. J. W. a. S. (2009). Biological hydrogen production by anaerobic microorganisms.

Kim, Y., Nam, S. N., Jeong, S., & Oh, J. J. W. a. E. J. (2018). Characteristics of particle removals in a compressible media filter system. *32*(3), 341-350.

Kozeny, J. J. D. W. (1927). über kapillare Leitung des Wassers im Boden, Sitz. *136*, 271-306.

Kuehn, M., Mehl, M., Hausner, M., Bungartz, H.-J., & Wuertz, S. J. W. S. a. T. (2001). Time-resolved study of biofilm architecture and transport processes using experimental and simulation techniques: the role of EPS. *43*(6), 143-151.

Le Bonté, S., Pons, M.-N., Potier, O., & Rocklin, P. J. R. d. s. d. l. e. J. o. W. S. (2008). Relation between conductivity and ion content in urban wastewater. *21*(4), 429-438.

Lee, B., & Richards, F. M. J. J. o. m. b. (1971). The interpretation of protein structures: estimation of static accessibility. *55*(3), 379-IN374.

Lee, C. S., Robinson, J., Chong, M. F. J. P. s., & protection, e. (2014). A review on application of flocculants in wastewater treatment. *92*(6), 489-508.

Lew, B., Belavski, M., Admon, S., Tarre, S., & Green, M. J. W. S. a. T. (2003). Temperature effect on UASB reactor operation for domestic wastewater treatment in temperate climate regions. *48*(3), 25-30.

Li, J., Ma, L., Wei, S., & Horn, H. J. S. a. p. T. (2013). Aerobic granules dwelling vorticella and rotifers in an SBR fed with domestic wastewater. *110*, 127-131.

Liao, B., Allen, D., Droppo, I., Leppard, G., & Liss, S. J. W. r. (2001). Surface properties of sludge and their role in bioflocculation and settleability. *35*(2), 339-350.

Lin, D., Ma, W., Jin, Z., Wang, Y., Huang, Q., Cai, P. J. C., & Biointerfaces, S. B. (2016). Interactions of EPS with soil minerals: a combination study by ITC and CLSM. *138*, 10-16.

Lindmark, D. G., & Müller, M. J. J. o. B. C. (1973). Hydrogenosome, a cytoplasmic organelle of the anaerobic flagellate Tritrichomonas foetus, and its role in pyruvate metabolism. *248*(22), 7724-7728.

Liu, H., & Fang, H. H. J. J. o. b. (2002). Extraction of extracellular polymeric substances (EPS) of sludges. *95*(3), 249-256.

Liu, Y., & Fang, H. H. (2003). Influences of extracellular polymeric substances (EPS) on flocculation, settling, and dewatering of activated sludge.

Liu, Y., Lam, M., & Fang, H. J. W. S. a. T. (2001). Adsorption of heavy metals by EPS of activated sludge. *43*(6), 59-66.

Liu, Y., & Tay, J.-H. J. W. r. (2002). The essential role of hydrodynamic shear force in the formation of biofilm and granular sludge. *36*(7), 1653-1665.

Lloyd, D., Williams, J., Yarlett, N., & Williams, A. G. J. M. (1982). Oxygen affinities of the hydrogenosome-containing protozoa Tritrichomonas foetus and Dasytricha ruminantium, and two aerobic protozoa, determined by bacterial bioluminescence. *128*(5), 1019-1022.

Logsdon, G. S., Kohne, R., Abel, S., & LaBonde, S. J. J. o. E. E. a. S. (2002). Slow sand filtration for small water systems. *1*(5), 339-348.

Lucas, A., Arnaldos, J., Casal, J., Puigjaner, L. J. I., Design, E. C. P., & Development. (1986). Improved equation for the calculation of minimum fluidization velocity. *25*(2), 426-429.

Mack, S. R., & Müller, M. J. T. J. o. p. (1978). Effect of oxygen and carbon dioxide on the growth of Trichomonas vaginalis and Tritrichomonas foetus. *64*(5), 927-929.

Mackie, R. J. F. s. (1989). Rapid gravity filtration—Towards a deeper understanding. *26*(1), 32-35.

Madoni, P. J. I. J. o. Z. (2011). Protozoa in wastewater treatment processes: A minireview. *78*(1), 3-11.

Morgavi, D., Forano, E., Martin, C., & Newbold, C. J. A. (2010). Microbial ecosystem and methanogenesis in ruminants. *4*(7), 1024-1036.

Mosquera-Corral, A., De Kreuk, M., Heijnen, J., & Van Loosdrecht, M. J. W. R. (2005). Effects of oxygen concentration on N-removal in an aerobic granular sludge reactor. *39*(12), 2676-2686.

Mosquera-Corral, A., Montras, A., Heijnen, J., & Van Loosdrecht, M. C. J. W. R. (2003). Degradation of polymers in a biofilm airlift suspension reactor. *37*(3), 485-492.

Müller, H., & Geller, W. J. A. f. H. (1993). Maximum growth rates of aquatic ciliated protozoa: the dependence on body size and temperature reconsidered. *126*, 315-315.

Muller, M. J. A. R. i. M. (1988). Energy metabolism of protozoa without mitochondria. *42*(1), 465-488.

Neralla, S., Weaver, R. W., Lesikar, B. J., & Persyn, R. A. J. B. T. (2000). Improvement of domestic wastewater quality by subsurface flow constructed wetlands. *75*(1), 19-25.

Nielsen, L. T., Asadzadeh, S. S., Dölger, J., Walther, J. H., Kiørboe, T., & Andersen, A. J. P. o. t. N. A. o. S. (2017). Hydrodynamics of microbial filter feeding. *114*(35), 9373-9378.

Nielsen, P. H., & Jahn, A. (1999). Extraction of EPS. In *Microbial extracellular polymeric substances* (pp. 49-72): Springer.

Nouha, K., Kumar, R. S., Balasubramanian, S., & Tyagi, R. D. J. J. o. e. s. (2018). Critical review of EPS production, synthesis and composition for sludge flocculation. *66*, 225-245.

Panno, J. (2014). *The cell: evolution of the first organism*: Infobase Publishing.

Pattipati, R. R., Wen, C. J. I., Design, E. C. P., & Development. (1981). Minimum fluidization velocity at high temperatures. *20*(4), 705-707.

Peters, V., Conrad, R. J. A., & microbiology, e. (1995). Methanogenic and other strictly anaerobic bacteria in desert soil and other oxic soils. *61*(4), 1673-1676.

Plumb, J. A. (1997). Infectious diseases of striped bass. In *Developments in Aquaculture and Fisheries Science* (Vol. 30, pp. 271-313): Elsevier.

Pons, M., Spanjers, H., Baetens, D., Nowak, O., Gillot, S., Nouwen, J., & Schuttinga, N. J. E. W. M. O. (2004). Wastewater characteristics in Europe-A survey. *4*(10).

Prescott, L., Harley, J., & Klein, D. J. M. r. E. W. C. B. P., Chicago. (1996). Industrial microbiology and biotechnology. 923-927.

Priya, M., Haridas, A., & Manilal, V. J. B. (2008). Anaerobic protozoa and their growth in biomethanation systems. *19*(2), 179-185.

Priya, M., Shibuvardhan, Y., & Manilal, V. J. I. M. (2019). Response of Anaerobic Protozoa to Oxygen Tension in Anaerobic System. *22*(3), 355-361.

Pronk, M., Abbas, B., Al-Zuhairy, S., Kraan, R., Kleerebezem, R., Van Loosdrecht, M. J. A. m., & biotechnology. (2015). Effect and behaviour of different substrates in relation to the formation of aerobic granular sludge. *99*(12), 5257-5268.

Pronk, M., Abbas, B., Kleerebezem, R., & Van Loosdrecht, M. J. M. b. (2015). Effect of sludge age on methanogenic and glycogen accumulating organisms in an aerobic granular sludge process fed with methanol and acetate. *8*(5), 853-864.

Pronk, M., De Kreuk, M., De Bruin, B., Kamminga, P., Kleerebezem, R. v., & Van Loosdrecht, M. J. W. R. (2015). Full scale performance of the aerobic granular sludge process for sewage treatment. *84*, 207-217.

Ranzinger, F., Matern, M., Layer, M., Guthausen, G., Wagner, M., Derlon, N., & Horn, H. J. W. R. X. (2020). Transport and retention of artificial and real wastewater particles inside a bed of settled aerobic granular sludge assessed applying magnetic resonance imaging. 100050.

Ren, L.-y., Hong, Z.-n., Qian, W., Li, J.-y., & Xu, R.-k. J. E. P. (2018). Adsorption mechanism of extracellular polymeric substances from two bacteria on Ultisol and Alfisol. *237*, 39-49.

Rose, J. M., Caron, D. A. J. L., & Oceanography. (2007). Does low temperature constrain the growth rates of heterotrophic protists? Evidence and implications for algal blooms in cold waters. *52*(2), 886-895.

Ryan, E. T., Hill, D. R., Solomon, T., Endy, T. P., & Aronson, N. (2019). *Hunter's Tropical Medicine and Emerging Infectious Diseases E-Book*: Elsevier Health Sciences.

Sander, R. J. A. C. P. (2015). Compilation of Henry's law constants (version 4.0) for water as solvent. *15*(8), 4399-4981.

Schwarzenbeck, N., Erley, R., & Wilderer, P. J. W. S. (2004). Aerobic granular sludge in an SBR-system treating wastewater rich in particulate matter. *49*(11-12), 41-46.

Sepúlveda-Mardones, M., Campos, J. L., Magrí, A., Vidal, G. J. R. i. E. S., & Bio/Technology. (2019). Moving forward in the use of aerobic granular sludge for municipal wastewater treatment: an overview. 1-29.

Seviour, T., Pijuan, M., Nicholson, T., Keller, J., & Yuan, Z. J. W. r. (2009). Gel-forming exopolysaccharides explain basic differences between structures of aerobic sludge granules and floccular sludges. *43*(18), 4469-4478.

Sheng, G.-P., Yu, H.-Q., & Li, X.-Y. J. B. a. (2010). Extracellular polymeric substances (EPS) of microbial aggregates in biological wastewater treatment systems: a review. *28*(6), 882-894.

Sheng, G.-P., Zhang, M.-L., & Yu, H.-Q. J. C. a. S. B. B. (2008). Characterization of adsorption properties of extracellular polymeric substances (EPS) extracted from sludge. *62*(1), 83-90.

Sleigh, M. J. J. o. C. S. (1964). Flagellar movement of the sessile flagellates Actinomonas, Codonosiga, Monas, and Poteriodendron. *3*(72), 405-414.

Smith, F. L., & Harvey, A. H. J. C. e. p. (2007). Avoid common pitfalls when using Henry's law. *103*(9), 33-39.

Snowdon, C., & Turner, J. (1967). *Mass transfer in liquid-fluidized beds of ion exchange resin beads.* Paper presented at the Proceedings of the International Symposium on Fluidization, Netherlands University Press, Amsterdam.

Späth, R., Flemming, H.-C., & Wuertz, S. J. W. S. a. T. (1998). Sorption properties of biofilms. *37*(4-5), 207-210.

Staudt, C., Horn, H., Hempel, D., & Neu, T. J. B. a. b. (2004). Volumetric measurements of bacterial cells and extracellular polymeric substance glycoconjugates in biofilms. *88*(5), 585-592.

Stevenson, D. J. W. R. (1997). Flow and filtration through granular media—the effect of grain and particle size dispersion. *31*(2), 310-322.

Subramanian, S. B., Yan, S., Tyagi, R. D., & Surampalli, R. J. W. r. (2010). Extracellular polymeric substances (EPS) producing bacterial strains of municipal wastewater sludge: isolation, molecular identification, EPS characterization and performance for sludge settling and dewatering. *44*(7), 2253-2266.

Sun, P., Clamp, J. C., Xu, D., Kusuoka, Y., Hori, M. J. I. j. o. s., & microbiology, e. (2011). Molecular phylogeny of the family Vorticellidae (Ciliophora, Peritrichia) using combined datasets with a special emphasis on the three morphologically similar genera Carchesium, Epicarchesium and Apocarchesium. *61*(4), 1001-1010.

Tang, Z., Butkus, M. A., & Xie, Y. F. J. M. e. r. (2006). Crumb rubber filtration: a potential technology for ballast water treatment. *61*(4), 410-423.

Tay, J. H., Ivanov, V., Pan, S., & Tay, S. L. J. L. i. A. M. (2002). Specific layers in aerobically grown microbial granules. *34*(4), 254-257.

Tay, J. H., Liu, Q. S., & Liu, Y. J. L. i. A. M. (2001). The role of cellular polysaccharides in the formation and stability of aerobic granules. *33*(3), 222-226.

Tiehm, A., Herwig, V., & Neis, U. J. W. s. a. t. (1999). Particle size analysis for improved sedimentation and filtration in waste water treatment. *39*(8), 99-106.

Tien, C., & Ramarao, B. V. (2011). *Granular filtration of aerosols and hydrosols*: Elsevier.

Tijhuis, L., Van Benthum, W., Van Loosdrecht, M., & Heijnen, J. J. B. a. b. (1994). Solids retention time in spherical biofilms in a biofilm airlift suspension reactor. *44*(8), 867-879.

TUDelft. Granular filtration. Retrieved from https://ocw.tudelft.nl/wp-content/uploads/Granular-filtration-1.pdf

Uhlinger, D. J., & White, D. C. J. A. a. E. M. (1983). Relationship between physiological status and formation of extracellular polysaccharide glycocalyx in Pseudomonas atlantica. *45*(1), 64-70.

Van Benthum, W., Van Loosdrecht, M., Tijhuis, L., & Heijnen, J. (1995). Solids retention time in heterotrophic and nitrifying biofilms in a biofilm airlift suspension reactor. In: Elsevier.

Van Bruggen, J., Zwart, K., Hermans, J., Van Hove, E., Stumm, C., & Vogels, G. J. A. o. m. (1986). Isolation and characterization of Methanoplanus endosymbiosus sp. nov., an endosymbiont of the marine sapropelic ciliate Metopus contortus Quennerstedt. *144*(4), 367-374.

Vigneswaran, S., Chang, J. S., & Janssens, J. J. W. R. (1990). Experimental investigation of size distribution of suspended particles in granular bed filtration. *24*(7), 927-930.

Vlyssides, A., Karlis, P., Rori, N., & Zorpas, A. J. J. o. H. M. (2002). Electrochemical treatment in relation to pH of domestic wastewater using Ti/Pt electrodes. *95*(1-2), 215-226.

Wagner, J., Weissbrodt, D. G., Manguin, V., da Costa, R. H. R., Morgenroth, E., & Derlon, N. J. W. r. (2015). Effect of particulate organic substrate on aerobic granulation and operating conditions of sequencing batch reactors. *85*, 158-166.

Wang, B., Peng, D., Hou, Y., Li, H., Pei, L., & Yu, L. J. w. r. (2014). The important implications of particulate substrate in determining the physicochemical characteristics of extracellular polymeric substances (EPS) in activated sludge. *58*, 1-8.

Wang, Y., Geng, J., Ren, Z., He, W., Xing, M., Wu, M., & Chen, S. J. B. T. (2011). Effect of anaerobic reaction time on denitrifying phosphorus removal and N2O production. *102*(10), 5674-5684.

Wang, Y., Guo, G., Wang, H., Stephenson, T., Guo, J., & Ye, L. J. W. r. (2013). Long-term impact of anaerobic reaction time on the performance and granular characteristics of granular denitrifying biological phosphorus removal systems. *47*(14), 5326-5337.

Wang, Z., Hessler, C. M., Xue, Z., & Seo, Y. J. W. r. (2012). The role of extracellular polymeric substances on the sorption of natural organic matter. *46*(4), 1052-1060.

Weissbrodt, D. G., Holliger, C., & Morgenroth, E. J. B. a. b. (2017). Modeling hydraulic transport and anaerobic uptake by PAOs and GAOs during wastewater feeding in EBPR granular sludge reactors. *114*(8), 1688-1702.

Winkler, M. H., Kleerebezem, R., Strous, M., Chandran, K., Van Loosdrecht, M. J. A. m., & biotechnology. (2013). Factors influencing the density of aerobic granular sludge. *97*(16), 7459-7468.

Winkler, M. K., Kleerebezem, R., Khunjar, W. O., de Bruin, B., & van Loosdrecht, M. C. J. W. r. (2012). Evaluating the solid retention time of bacteria in flocculent and granular sludge. *46*(16), 4973-4980.

Worm, P., Müller, N., Plugge, C. M., Stams, A. J., & Schink, B. (2010). Syntrophy in methanogenic degradation. In *(Endo) symbiotic methanogenic archaea* (pp. 143-173): Springer.

Xiong, Y., & Liu, Y. J. C. a. S. B. B. (2013). Importance of extracellular proteins in maintaining structural integrity of aerobic granules. *112*, 435-440.

Yan, L., Yu, L., Liu, Q., Zhang, X., Liu, Y., Zhang, M., . . . Quarterly, B. E. (2019). Effects of phosphorus on loosely bound and tightly bound extracellular polymer substances in aerobic granular sludge. *33*(1), 59-68.

Yan, Z., Zhu, Y., Meng, H., Wang, S., Gan, L., Li, X., . . . Zhang, W. J. S. o. T. T. E. (2019). Insights into thermodynamic mechanisms driving bisphenol A (BPA) binding to extracellular polymeric substances (EPS) of activated sludge. *677*, 502-510.

Yao, K.-M., Habibian, M. T., O'Melia, C. R. J. E. s., & technology. (1971). Water and waste water filtration. Concepts and applications. *5*(11), 1105-1112.

Yu, Y., Tao, Y., Ma, Z., & He, Y.-L. J. P. T. (2018). Experimental study and optimization on filtration and fluid flow performance of a granular bed filter. *333*, 449-457.

Zamani, A., & Maini, B. J. J. o. P. S. a. E. (2009). Flow of dispersed particles through porous media—deep bed filtration. *69*(1-2), 71-88.

Zhu, L., Dai, X., Yu, Y.-w., Qi, H.-y., & Xu, X.-y. J. B. T. (2012). Role and significance of extracellular polymeric substances on the property of aerobic granule. *107*, 46-54.

APPENDIX A: PROTOZOA CONTRIBUTION

Table A. 1: Standard Gibbs free energy and enthalpy values of formation for each component (Alberty, 2005)

Substrate/Product	ΔG_f^0, kJ/mol	ΔH_f^0, kJ/mol
$C_6H_{12}O_6$(Glucose)	-915.9	-1262.9
H_2O	-237.19	-285.83
CH_3COO^-(Acetate)	-369.31	-486.01
HCO_3^-	-586.77	-691.99
H^+	0	0
H_2(aq)	17.6	-4.2
H_2(g)	0	0
NADH	22.65	-31.94
NAD^+	0	0
$Fd_{red}(Fe^{2+})$	38.07	-
$Fd_{ox}(Fe^{3+})$	0	-
CH_3COCOO^-(Pyruvate)	-472.27	-596.22
Acetyl-CoA	-188.52	-
CoA	-47.83	-

Table A. 2: Standard Gibbs free energy and enthalpy change for hydrogen production pathway

No.	Reactions	ΔG^0, kJ/mol	ΔH^0, kJ/mol
(1)	$C_6H_{12}O_6+4H_2O \rightarrow 2CH_3COO^- + 2HCO_3^- + 4H^+ + 4H_2$	22.9	33.42
(2)	$C_6H_{12}O_6 + 2NAD^+ \rightarrow 2CH_3COCOO^- + 2NADH + 4H^+$	16.66	6.58
(3)	$CH_3COCOO^- + CoA + 2Fd(ox)+H_2O \rightarrow Acetyl-CoA + HCO_3^- + 2Fd(red) + 2H^+$	58.14	-
(4)	$2Fd_{red} + 2H^+ \rightarrow 2Fd_{ox} + H_2$	-58.54	-
(5)	$Acetyl-CoA + H_2O \rightarrow CH_3COO^- + CoA + H^+$	8.57	-

Table A. 3: ΔG^0 under different temperature for Reaction (4)

Reaction	ΔG^0, kJ/reaction (283 K)	ΔG^0, kJ/reaction (288 K)	ΔG^0, kJ/reaction (293 K)
$2Fd_{red} + 2H^+ \rightarrow 2Fd_{ox} + H_2$	-53.02	-53.89	-54.75

Table A. 4: ΔG^1 under different temperature for Reaction (4)

Reaction	ΔG^1, kJ/reaction (283K)	ΔG^1, kJ/reaction (288 K)	ΔG^1, kJ/reaction (293 K)
$2Fd_{red} + 2H^+ \rightarrow 2Fd_{ox} + H_2$	$-53.02 + \frac{8.314}{1000} \times 283 \times \ln(P_{H2} \times (10^{-7})^{-2})$	$-53.89 + \frac{8.314}{1000} \times 288 \times \ln(P_{H2} \times (10^{-7})^{-2})$	$-54.75 + \frac{8.314}{1000} \times 293 \times \ln(P_{H2} \times (10^{-7})^{-2})$

Table A. 5: ΔG^1 under different temperature and P_{H2} for ferredoxin reaction (4)

$-\lg P_{H2}$	ΔG^1, kJ/reaction (283K)	ΔG^1, kJ/reaction (288 K)	ΔG^1, kJ/reaction (293 K)
0	22.82	23.30	23.78
1	17.41	17.79	18.17
2	11.99	12.27	12.56
3	6.57	6.76	6.95
4	1.15	1.25	1.34
5	-4.26	-4.27	-4.27
6	-9.68	-9.78	-9.88
7	-15.10	-15.29	-15.49
8	-20.52	-20.81	-21.09
9	-25.94	-26.32	-26.70
10	-31.35	-31.83	-32.31

APPENDIX B: EXPERIMENT

B.1 PUMP CALIBRATION

To reach the target up-flow velocity by adjusting RPM, both the influent pump and the fluidization pump were calibrated and shown in Figure B. 1 and

Figure B. **2**. It is obvious that there was a linear relationship between RPM and up-flow velocity. During calibration process, the influent used was tap water. Under each RPM, the effluent was collected in a tank and the effluent weight was measured by a balance. For each RPM, the duration was 2 min. The up-flow velocity was acquired by using the flow rate divided by the reactor's surface area.

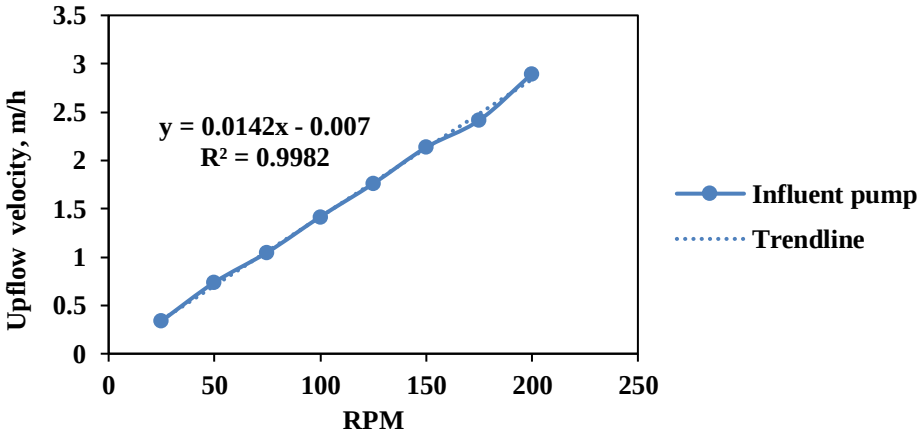

Figure B. 1: Influent pump calibration

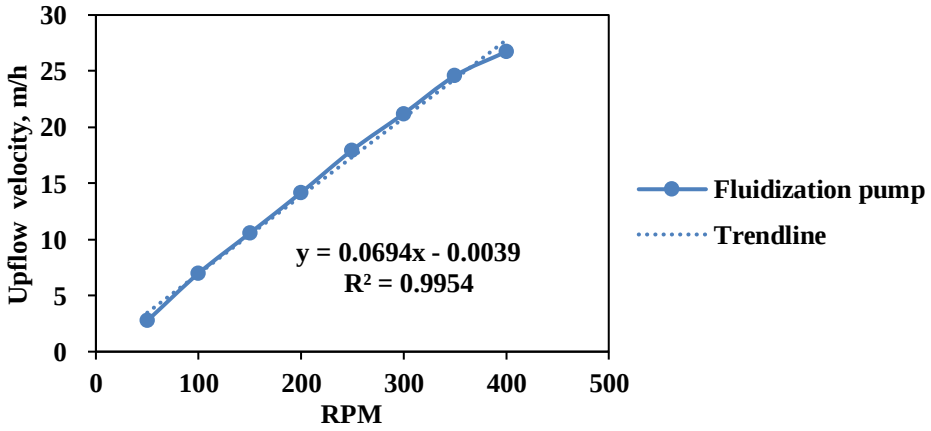

Figure B. 2: Fluidization pump calibration

B.2 MINIMUM FLUIDIZATION VELOCITY

The minimum fluidization velocity is applied during fluidization process in order to investigate the contribution of filtering effect mechanisms on particle removal. The flow is applied from downside of the reactor to the upside. Under the minimum fluidization state, the drag force imparted by the influent flow is equal to the weight of the granules in the reactor, leading to a bit increase in porosity (Dechsiri, 2004). The Equations (B 1) to (B 5) were used to calculate the minimum fluidization velocity (Lucas et al., 1986; Pattipati et al., 1981). The sphericity of aerobic granules was assumed to be 1 and the density of granules was assumed to be 1.035 kg/m^3 (Winkler et al., 2013). Since the porosity of granular bed was 0.46 (Weissbrodt et al., 2017) and it can be increased a bit at minimum fluidization, the voidage at minimum fluidization was assumed to be 0.5. The calculation result shows that the minimum fluidization velocity was 20 m/h, which can be reached under RPM 300 by the use of the fluidization pump. The RPM 300 for the fluidization pump was verified in the experimental set-up and the granular bed in the reactor expanded and mixed with the influent.

$$Re_{mf} = [\left(42.857\frac{C_1}{C_2}\right)^2 + \frac{Ar}{1.75C_1}]^{\frac{1}{2}} - 42.857\frac{C_1}{C_2} \quad \text{(B 1)}$$

$$C_1 = \frac{1}{\Phi^3 \varepsilon_{mf}} \quad \text{(B 2)}$$

$$C_2 = \frac{1-\varepsilon_{mf}}{\Phi^2 \varepsilon_{mf}^3} \quad \text{(B 3)}$$

$$Ar = \frac{d_p^3 \rho(\rho_s - \rho_L)g}{\mu^2} \quad \text{(B 4)}$$

$$Re = \frac{v d_p \rho}{\mu} \quad \text{(B 5)}$$

B.3 SIZE RANGES AND CONCENTRATION OF FMBS

The fluorescent microbeads (FMBs) are from Polysciences and Cospheric. Four size (ranges) of FMBs were chosen to stand for the divided four size ranges of the Delft influent PSD. The chosen FMBs size ranges and the demand concentration (weight and number) for each size range are shown in Table B. 1. The FMBs with 6 µm diameter is from Polysciences. The rest three kinds of FMBs are from Cospheric. The only difference between these FMBs from two companies is the density. The density of the 6 µm FMBs are a bit higher than the rest FMBs. Due to its quite small size, the settling velocity calculated by the Stoke's Law (Equation (B 6)) is 10^{-7} m/s

which can flow with the influent. Since the density of the rest FMBs is the same to the density of water, all the chosen FMBs have the same flow behavior.

$$v_s(m/s) = \frac{1}{18}\frac{g}{\mu}(\rho_p - \rho_f){d_p}^2 \qquad \text{(B 6)}$$

The weight for each size range of FMBs per L was calculated by using particles' volume for each size range shown in Table 4.4 to multiply the corresponded density. The influent microbeads concentration per size range of FMBs was calculated by using particles volume (Table 4.4) divided by the volume of each particle. Per particle volume for each size range was calculated via the average radius per size range.

The influent microbeads concentration used in the literature is between 10^{11} and 10^{14} beads/m^3 (Drury et al., 1993; Hamza et al., 2014; Ivanov et al., 2004; Kuehn et al., 2001; Van Benthum et al., 1995). The concentration shown in Table B. 1 is lower than this range. It is because that the microbeads used in the above references are all submicron FMBs. But the FMBs used in this case are not only submicron FMBs but also microbeads with lager sizes. Under the same volume, smaller the FMBs are, higher microbeads concentration is. Therefore, it is reasonable that the influent FMBs concentration is lower than the average concentration range.

Table B. 1: Information of FMBs in each fraction.

Size range in PSD, µm	Size range of FMBs, µm	Density, g/L	Weight, g/L	Number, beads/L	Influent FMBs concentration, beads/m^{-3}
0.45-10	6	1.05	0.01	1.32E+08	1.34E+08
10-45	27-32	1	0.02	1.66E+06	
45-100	75-90	1	0.02	7.57E+04	

However, the chosen FMBs only take organic particles in domestic wastewater into account. In reality, both the organic and inorganic particles are applied to the reactor. The inorganic particle can influence the capture process of organic particles. Therefore, there should be extra particles to stand for the inorganic particles in wastewater. To distinguish the particles standing for organic and inorganic particles, the magnetic beads can be used for simulating inorganic particles in domestic wastewater. After taking effluent samples, the magnet can be put in the bottom of the sample bottle. Then, the FMBs in the solution can be measured without the influence of magnetic beads.

B.4 DILUTION FACTOR CALCULATION

The dilution ratio should be calculated by the Equation (B 7). V_{in} is calculated via Equation (B 8). V_f is calculated via Equation (B 9). The relevant parameters for fluidization calculation are displayed in Table B. 2.

$$\text{Dilution factor} = \frac{V_f + V_{in}}{V_{in}} \tag{B 7}$$

$$V_{in} = (h_b \times \varepsilon + (h_o - h_b)) \times \pi \times (\frac{d_r}{2})^2 \tag{B 8}$$

$$V_f = t_f \times \pi \times (\frac{d_r}{2})^2 \times v_f \tag{B 9}$$

Table B. 2: Relevant parameters for fluidization calculation

Parameter	Symbol	Unit	Values
Bed height	h_b	m	0.3
Outlet height	h_o	m	0.34
Bed porosity	ε	-	0.46
Reactor diameter	d	m	0.0625
Fluidization velocity	v_f	m/h	20
Fluidization time	t_f	s	10

APPENDIX C: MODEL

C.1 INTERCEPTION MECHANISM

The number of particles (N) and the total capture cross section area (A_h) in a bed unit area were obtained by Equation (C 1) and (C 2), respectively.

$$N = \frac{V_{tp}}{V_p} = \frac{6}{\pi D^3} \cdot (1 - e_0) \cdot h \qquad \text{(C 1)}$$

$$A_h = NA_c = 3\frac{d}{D^2} \cdot (1 - e_0) \cdot h \qquad \text{(C 2)}$$

The fluid velocity (u_y) around the grains increases linearly with distance (y) from the surface of grains when the distance is short (Equation (C 3)). The average velocity through the capture cross section area is half of Equation (C 3). The distance (y) is d/2, at which the streamline passing through the grain equator with a distance of d/2. The flow passing through the capture cross section areas around grains for a bed unit area (Q_c) was calculated (Equation (C 4)) by combining the Equation (1), (C 1) to (C 3). The way to calculate the surface shear stress ($R^{'}$) and headloss (ΔH) is introduced in Paragraph 3.3.4 and 3.3.6.

$$u_y = R' \cdot \frac{y}{\mu} \qquad \text{(C 3)}$$

$$Q_c = \frac{3}{4} \cdot \frac{d^2}{D^2} \cdot (1 - e_0) \cdot \frac{R'}{\mu} \cdot h \qquad \text{(C 4)}$$

The ratio (C/C_0) of effluent concentration over influent concentration (Equation (C 5)) was obtained by the exponent of the ratio of the flow passing through the capture cross section area over the total flow for a unit area (v). After combining Equation (C 4), the filtration coefficient for interception can be derived with the addition of correction factors K_F and K_M as shown in Equation (2).

$$\frac{C}{C_0} = \exp\left(-\frac{Q_c}{v}\right) \qquad \text{(C 5)}$$

C.2 SETTLEMENT MECHANISM

In the settlement tank, an area (Equation (C 6)) is needed for particle settlement process. Similar to settlement tanks, one grain in granular filter can be regarded as a settlement tank. The projected area for a bed unit area (A_p) was calculated by Equation (C 7). Since the effective settlement area is affected by the angle of repose (α), the projected area is calibrated by multiplying $\sin^2\alpha$ (Equation (3)).

$$A = \frac{Q}{v_s} \tag{C 6}$$

$$A_p = NA_s = \frac{\pi D^2}{4} \cdot \frac{6}{\pi D^3} \cdot (1 - e_0) = 1.5\frac{(1 - e_0)}{D} \tag{C 7}$$

Only part of particles can be captured due to limited settling area. The settling process is also influenced by particle settling velocity (v_s), which was obtained by Equation (C 8). The ratio of C/C_0 is defined as Equation (C 9). This is relevant with the ratio of the flow between which particles are captured by settlement and the total flow for the unit area (v). The overall particle captured by settlement was acquired by Equation (4) after combining Equation (C 7) to (C 9).

$$v_s = (\rho_s - \rho_L) \cdot \frac{gd^2}{18\mu} \tag{C 8}$$

$$\frac{C}{C_0} = \exp\left(-A_p \cdot \frac{v_s}{v_{cm}}\right) \tag{C 9}$$

C.3 DIFFUSION MECHANISM

Equation (C 11) and (C 12) are used for ion exchange kinetics (Snowdon & Turner, 1967), which are applied in diffusion mechanism in filtration beds. The relation between mass transfer coefficient K_L and the Sherwood number (Sh) is shown in Equation (C 13).

$$K_D = \frac{K_B T}{3\pi\mu d} \tag{C 10}$$

$$K_L = Sh \cdot \frac{K_D}{D} \tag{C 11}$$

$$Sh = \frac{0.81}{e} \cdot Re^{1/2} \cdot Sc^{1/3} \tag{C 12}$$

$$Sc = \frac{\mu}{\rho K_D} \tag{C 13}$$

$$Re = \frac{v_{cm}\rho}{S(1-e_0)\mu} \quad \text{(C 14)}$$

$$S = \frac{6}{D} \quad \text{(C 15)}$$

C.4 GEOMETRICAL METHOD FOR A_C ESTIMATION

After one particle deposition, the capture cross section area is changed. The area is not as simple as equal to the summation of two ring areas, which is expressed as blue area and green area in Figure C. 1 (a). There is an overlap area, which is highlighted in Figure C. 1 (b). Thus, the capture cross section area after one particle deposition is the summation of two ring areas subtracted the overlap area, which is the yellow part shown in Figure C. 1 (c).

Since the width of both ring area is the radius of the arriving particle shown as purple circle in Figure C. 1, the two interception points expressed as black points in Figure C. 1 (c) are the circle centers of the particle with the diameter of d_2. Then, the green, purple and blue circles are tangent to each other.

For calculating the intersection area, the four circle centers are connected as shown in Figure 4.13 (d). The half of the intersection area is the summation of yellow sector area in Figure C. 1 (e) and green sector area in Figure C. 1 (f) deducted by the black triangle area.

The Law of Cosines method was applied for central angle calculation for both yellow and green sector areas. The yellow and green sector areas were acquired by the use of central angles. For calculating the triangle area, the Law of Cosines was also used for obtaining the side length of the triangle. The triangle area was calculated by using the side lengths and angles.

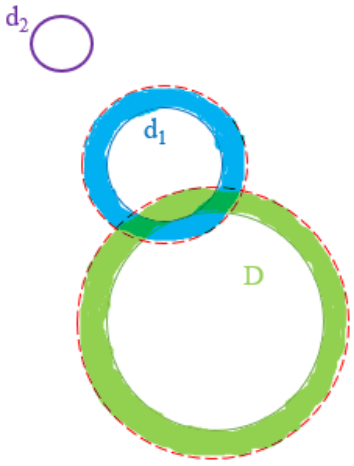

(a)

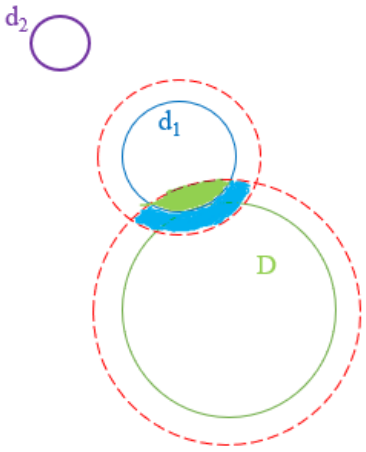

(b)

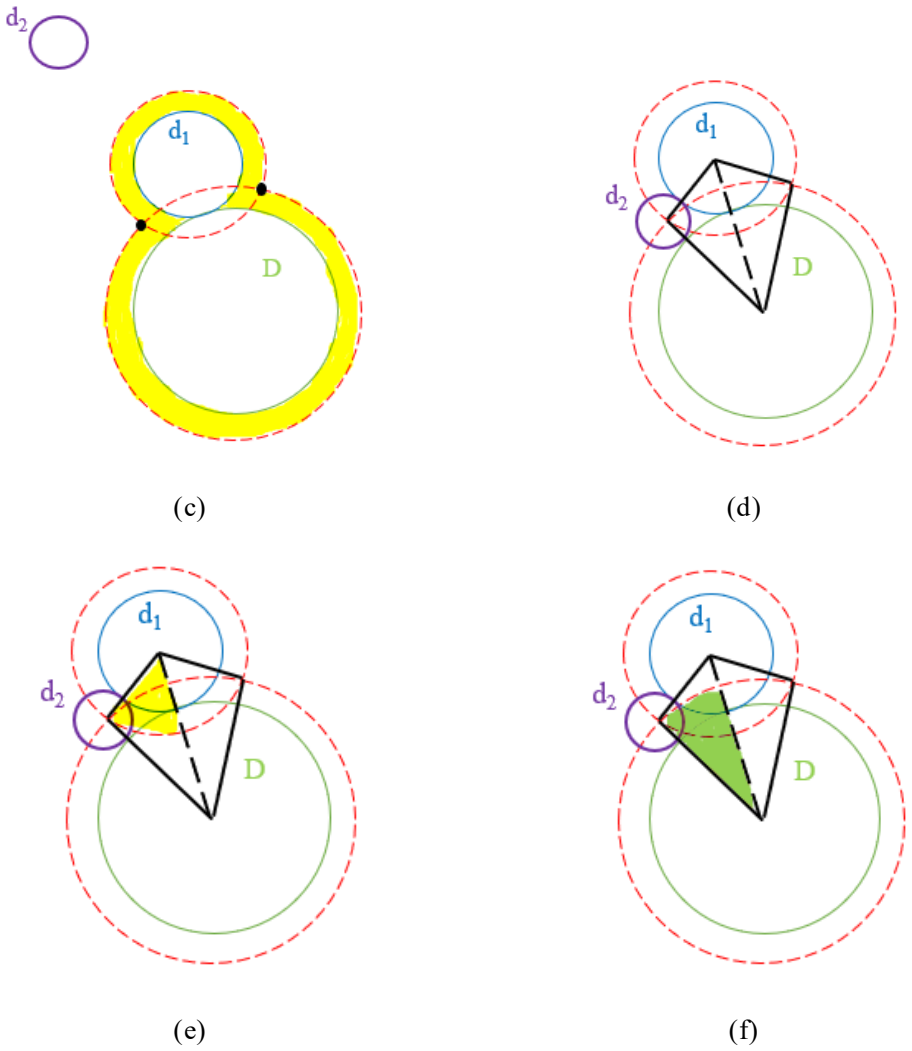

Figure C. 1: Capture cross section area after one particle deposition

C.5 OUTPUT TABLE FROM STEVENSON

The filtration velocity in 0.25 h was 7.5 m/h instead of 5 m/h (Table C. 1).

Table C. 1: Model result of cell velocities and DEP in the first layer (Stevenson, 1997).

First iteration 0.25 h, 5 m/h									
DEP	U	DEP	U	DEP	U	DEP	U	DEP	U
0.009	1.69	0.008	2.54	0.008	3.01	0.007	4.34	0.006	6.77
0.010	2.33	0.010	3.52	0.009	4.16	0.008	6.00	0.006	9.35
0.012	3.18	0.011	4.81	0.010	5.69	0.009	8.20	0.007	12.72
0.014	4.31	0.012	6.51	0.011	7.70	0.010	11.08	0.008	17.11
0.015	5.79	0.013	8.75	0.013	10.34	0.011	14.84	0.009	22.79
After 1 h									
DEP	U	DEP	U	DEP	U	DEP	U	DEP	U
0.116	3.41	0.133	4.16	0.139	4.55	0.149	5.73	0.152	8.43
0.141	3.99	0.159	4.84	0.165	5.30	0.173	6.77	0.174	10.35
0.168	4.57	0.186	5.54	0.192	6.09	0.199	7.95	0.196	12.65
0.197	5.14	0.215	6.25	0.220	6.92	0.225	9.28	0.218	14.43
0.228	5.70	0.245	6.99	0.249	7.81	0.251	10.81	0.240	18.84
After 1.5 h									
0.223	0.96	0.243	0.92	0.250	0.91	0.265	0.89	0.279	0.90
0.256	0.98	0.277	0.93	0.284	0.92	0.298	0.90	0.278	2.38
0.291	0.98	0.311	0.93	0.318	0.92	0.332	0.89	0.311	2.46
0.326	0.98	0.345	0.92	0.352	0.90	0.329	2.35	0.321	4.25
0.362	0.96	0.380	0.91	0.347	2.37	0.364	2.35	**0.000**	**154.6**
After 2.5 h, flow raised to 15 m/h									
DEP	U	DEP	U	DEP	U	DEP	U	DEP	U
0.279	0.20	0.294	0.17	0.299	0.17	0.259	0.92	0.276	0.86
0.312	0.19	0.301	0.42	0.308	0.40	0.291	0.95	0.298	1.21
0.346	0.19	0.334	0.42	0.308	1.04	0.324	0.97	**0.062**	**53.47**
0.350	0.48	0.333	1.09	0.341	1.05	0.347	1.30	**0.000**	**109.3**
0.346	1.20	0.368	1.09	0.365	1.39	**0.090**	**55.79**	**0.000**	**140.8**